To the Graduate Council:

I am submitting herewith a dissertation written by Atin Kumar Sinha entitled "A Study of Lift Characteristics of an Upper Surface Blown Jetwing with a Rectangular Nozzle." I have examined the final copy of this dissertation for form and content and recommend that it be accepted in partial fulfillment of the requirements for the degree of Doctor of Philosophy, with a major in Aerospace Engineering.

Jain Ming Wu, Major Professor

We have read this dissertation
and recommend its acceptance:

Accepted for the Council:

The Graduate School

A STUDY OF LIFT CHARACTERISTICS OF AN UPPER SURFACE BLOWN JETWING WITH A RECTANGULAR NOZZLE

A Dissertation

Presented for the

Doctor of Philosophy

Degree

The University of Tennessee, Knoxville

Atin Kumar Sinha

June 1984

ACKNOWLEDGMENTS

The author wishes to express his sincere appreciation to Dr. J. M. Wu, Director, Gas Dynamics Division and Professor, Aerospace Engineering, for his thoughtful guidance, invaluable suggestions and constant encouragement during the course of this study.

The author is deeply grateful to Dr. W. F. Jacobs for introducing him to the exciting subject of Powered Lift Technology and sharing with him the results of a lifetime of research work.

Special acknowledgments are due to Professor R. D. Kimberlin for always being available to share his experience, offer helpful suggestions, extend support and encouragement, without which compilation of this work would never have been possible.

The author likes to take this opportunity to thank the Space Institute's librarians, Mrs. Helen Mason, Mrs. Marjorie Joseph and Mrs. Mary Lo, for their eagerness in spending time and effort in obtaining numerous references required for this work.

Special thanks are due to upper E wing secretaries, Mrs. Sandra Shankle and Mrs. Linda Hall, for typing the draft in a very short notice.

The author would like to express his deep appreciation to Mrs. Madge Gibson for her patience and dedication in typing the dissertation so carefully.

The author likes to express his gratitude for the love and companionship of his wife, Shukla, during the difficult days of conducting this research.

The work reported herein is partially supported by the Naval Air Systems Command Advanced Aircraft Development and Systems Objectives Offices (AIR-03PA) under Naval Air Systems Command Contract No. N00019-81-C-0506.

ABSTRACT

A study was conducted to determine the lift characteristics of an upper surface blown (USB) jet-flapped aircraft with rectangular nozzle. An empirical criterion was used to replace the jet sheet leaving the trailing edge with an equivalent mechanical flap extension. Lifting line analysis was used to obtain the spanwise load and induced angle of attack distribution. Additional supercirculation, because of the presence of a high energy jet on the wing upper surface, was obtained from momentum considerations. The predicted values of lift and pitching moment coefficient (C_L and C_M) were compared with full scale wind tunnel and flight test data on the Ball-Bartoe JETWING USB aircraft and show good agreement in C_L. However, theoretical C_M values did not compare favorably with wind tunnel data though the slope (dC_M/dC_L) agreed fairly well. The semi-empirical model developed here, can handle a part span flap with variable jet momentum distribution and chordwise location of the nozzle. This simple method is considered to be a valuable tool for the preliminary design of an USB aircraft with a rectangular nozzle.

TABLE OF CONTENTS

CHAPTER		PAGE
I.	INTRODUCTION	1
	The Need for STOL Aircraft	1
	Various Means of Achieving STOL	4
	Upper Surface Blowing--An Efficient Powered Lift Concept	16
	Advantages and Disadvantages of the USB Concept	16
	Technology Demonstration Vehicle: Ball-Bartoe JETWING	21
II.	PREDICTION OF AERODYNAMIC CHARACTERISTICS	25
	A Review of Some of the Methods	25
	Motivation--The Need for a Simplified Theory for Preliminary Design	29
	Scope of the Present Work	30
III.	EQUIVALENT FLAP THEORY: A NEW METHOD	31
	Description of the Method	31
	Calculation of Lift	32
	Calculation of Pitching Moment	39
	Results and Discussion	42
IV.	THEORY OF TURBULENT JETS	56
	Turbulent Wall Jets	56
	Previous Work on Wall Jets	58
	Formulation of the Problem	60

CHAPTER PAGE

IV. (Continued)

Mixing Zone of a Two-Dimensional Jet of Finite Thickness in a Coflowing External Stream in an Adverse Pressure Gradient 62

Initial Region of a Wall Jet 68

Main Region of a Wall Jet 70

V. DETERMINATION OF ADDITIONAL SUPERCIRCULATION LIFT 76

An Analytical Method of Obtaining the Jet Velocity 76

Jet Induced Momentum--A Measure of Jet Induced Circulation 79

Results and Discussion 81

VI. CONCLUSIONS AND RECOMMENDATIONS 88

BIBLIOGRAPHY 90

APPENDIXES 96

APPENDIX I EVALUATION OF THE INTEGRAL IN EQUATION (3.4) 97

APPENDIX II EVALUATION OF SECTIONAL BLOWING COEFFICIENT (C_j) . . 109

APPENDIX III EVALUATION OF THE INTEGRALS IN EQUATION (3.11) . . 111

APPENDIX IV EVALUATION OF THE INTEGRALS IN EQUATION (4.19) . . . 125

VITA 127

LIST OF FIGURES

FIGURE		PAGE
1.1	Typical V/STOL port proposal	3
1.2	Comparison of near-airport noise contours	3
1.3	Speed vs. risk in landing	4
1.4	Demonstrated $C_{L_{max}}$ levels	5
1.5	$C_{L_{max}}$ trends	6
1.6	Mechanical high lift devices	6
1.7	Variable camber Kruger flaps on the Boeing YC-14	7
1.8	Blowing BLC concepts	8
1.9	Suction BLC concepts	8
1.10	Powered lift concepts	9
1.11	Jet flap aircraft	10
1.12	Some jet flap schemes	10
1.13	Jacobs-Hurkamp jet flap wing	12
1.14	The Hunting H.126 jet flap research airplane	13
1.15	Components of lift on a jet flap aircraft	15
1.16	Circulation control wing modes of operation	15
1.17	CCW/USB thrust deflector and lift augmentation concept . .	15
1.18	Processes affecting USB jet turning performance	17

FIGURE PAGE

1.19 Three view drawing of NASA-Boeing Quiet Short-Haul Research Aircraft (QSRA) 17

1.20 Noise levels for powered lift concepts 19

1.21 USB flow characteristics 19

1.22 Spanwise exhaust spreading on an externally blown flap . . 20

1.23 Spanwise normal-force distribution for two-engine straight-wing USB configuration ($\delta_F = 60^\circ$, $\alpha = 0^\circ$) . . . 20

1.24 Three view drawing of Ball-Bartoe JETWING JW-1 experimental USB aircraft 22

1.25 JETWING ducting arrangement 22

1.26 Two-dimensional view of "Jetwing" concept 24

1.27 Two-dimensional view of "Jetwing" concept with thrust reverser deployed 24

3.1 Geometry of airfoil with jet augmented flap 33

3.2 Circulation distribution over the basic and equivalent airfoil 35

3.3 Comparison of Equivalent Flap Theory with full scale data for $\delta_F = 0^\circ$ (upper wing removed) 43

3.4 Comparison of Equivalent Flap Theory with full scale data for $\delta_F = 15^\circ$ (upper wing removed) 44

3.5 Comparison of Equivalent Flap Theory with full scale data for $\delta_F = 30^\circ$ (upper wing removed) 45

FIGURE PAGE

3.6 Comparison of Equivalent Flap Theory with full scale data for $\delta_F = 45^\circ$ (upper wing removed) 46

3.7 Comparison of Equivalent Flap Theory with full scale data for $\delta_F = 0^\circ$ (upper wing and horizontal tail removed) 47

3.8 Comparison of Equivalent Flap Theory with full scale data for $\delta_F = 30^\circ$ (upper wing and horizontal tail removed) 48

3.9 Spanwise distribution of C_ℓ for $\alpha = 10^\circ$ and $\delta_F = 0^\circ$ 50

3.10 Spanwise distribution of C_ℓ for $\alpha = 10^\circ$ and $\delta_F = 15^\circ$ 51

3.11 Spanwise distribution of C_ℓ for $\alpha = 10^\circ$ and $\delta_F = 30^\circ$ 52

3.12 Spanwise distribution of C_ℓ for $\alpha = 10^\circ$ and $\delta_F = 45^\circ$ 53

3.13 Spanwise distribution of C_m for $\alpha = 10^\circ$ and $\delta_F = 15^\circ$ 54

4.1 Velocity profile for a "Simple" wall jet 57

4.2 Velocity profile for a blown boundary layer 57

4.3 Idealized flow produced by a turbulent wall jet in a coflowing external stream in adverse pressure gradient 61

4.4 Boundary layer of a jet in a coflowing stream ($u_2>0$) 62

5.1 Comparison of Modified Equivalent Flap Theory with flight and full scale wind tunnel data for $\delta_F = 0^\circ$ (upper wing removed) 82

FIGURE PAGE

5.2 Comparison of Modified Equivalent Flap Theory with flight and full scale wind tunnel data for $\delta_F = 15^\circ$ (upper wing removed) 84

5.3 Comparison of Modified Equivalent Flap Theory with flight and full scale wind tunnel data for $\delta_F = 30^\circ$ (upper wing removed) 86

5.4 Comparison of Modified Equivalent Flap Theory with full scale wind tunnel data for $\delta_F = 30^\circ$ (upper wing and horizontal tail removed) 87

LIST OF SYMBOLS

a_1	Nondimensionalized pressure gradient parameter
A_j	Area of the jet exhaust
A_o	Engine inlet area
b	Jet thickness
b_o	Jet thickness at the nozzle exit, i.e., nozzle height
c	Projected airfoil chord length
c'	Projected equivalent airfoil chord length
c_f	Projected mechanical flap chord length
c'_f	Projected total equivalent flap chord length
c_{fj}	Projected equivalent jet flap length
C_j	Jet blowing coefficient based on actual airfoil chord
C'_j	Jet blowing coefficient based on equivalent airfoil chord
C_J	Three-dimensional jet blowing coefficient
C_ℓ	Lift coefficient based on actual airfoil chord
C_L	Overall lift coefficient generated by the wing
$C_{L_{max}}$	Maximum lift coefficient generated by the wing
C_m	Pitching moment coefficient based on actual airfoil chord
C'_m	Pitching moment coefficient based on equivalent airfoil chord
C_M	Overall moment coefficient generated by the wing
C_{T_N}	Net thrust coefficient
F_{net}	Net thrust
j	Jet momentum per unit span, i.e., $\dot{M}_j V_j$
k	Ratio of specific heats for air, i.e., c_p/c_v
L_{fj}	Lift generated by the two-dimensional jet flap alone

m	Ratio of velocities of external stream to jet
m_o	Ratio of velocities of external stream to jet at nozzle exit
M	Pitching moment of an airfoil section
M_{Fu}	Pitching moment of fuselage
$\dot{M}_j$	Rate of mass flow of the jet per unit span
M_∞	Freestream Mach number
p	Static pressure
p'	z/c'
p_1, p_2	Static pressure in the jet and external stream respectively
p_a	Ambient static pressure
p_o	Static pressure at the nozzle exit
p_1^*, p_2^*	Total pressure in the jet and external stream respectively
p_{o1}^*, p_{o2}^*	Total pressure in the boundaries of the mixing zone
q	Freestream dynamic pressure
R	Gas constant for air
S	Wing reference area
T_j	Mean temperature of the jet
u, u_j	Velocity in the wall boundary layer as well as mixing layer
u_1, u_2	Velocities of the jet and external stream
u_{1max}, u_{2max}	Maximum possible velocities of the jet and external stream
u_{o1}, u_{o2}	Velocities on the boundaries of the mixing zone
u_m	Velocity at the edge of the wall boundary layer
v_1, v_2	Transverse velocities on the boundaries of the mixing zone
V	True airspeed, i.e., freestream velocity
V_j	Mean velocity of the jet at the trailing edge
x	Distance from the leading edge along the airfoil chord

x_H	Length of the initial region
y	Transverse distance
y'	Cos ψ_1
y_1, y_2	Transverse coordinate of the boundaries of the mixing zone in the initial region
z	Distance of the leading edge of the airfoil from the datum line about which pitching moment is desired

Greek Symbols

α	Overall angle of attack of the airfoil section (angle between zero lift line and freestream velocity)
α_e	Effective angle of attack of the airfoil section
α_i	Induced angle of attack for the airfoil section
β	$\sqrt{1-M_\infty^2}$
γ	Circulation on chordwise elements of the airfoil section
γ_Δ	Additional supercirculation on chordwise elements of the airfoil section
δ	Wall boundary layer thickness
δ_F	Trailing edge mechanical flap deflection angle in radians
δ_H	Wall boundary layer thickness at x_H
δ_j	Angle of jet with respect to trailing edge flap chord in radians
δ_n	Leading edge flap deflection angle in radians
ψ	Angular coordinate in radians of the elements of the airfoil section including mechanical and jet flap
ψ_1	Trailing edge mechanical flap trailing edge coordinate in radians
ψ_0	Trailing edge mechanical flap hinge line coordinate in radians
ψ_n	Leading edge flap hinge line coordinate in radians

λ_F	c_f'/c'
μ	dynamic viscosity
π	Ratio of circumference to diameter of a circle
ρ, ρ_∞	Freestream air density
ρ_j	Mean density of the jet
ξ, η	Nondimensionalized transverse distance

CHAPTER I

INTRODUCTION

The Need for STOL Aircraft

From the early days of aviation, air transport has played a crucial role in the spectacular progress achieved by mankind, particularly in the later half of this century. Air travel has shortened the commuting time for businessmen, thereby spuring economic growth. Transport of mail and cargo by air has helped in achieving better communication and understanding between people of various lands. In many countries, air travel is primarily, if not solely, responsible for the booming tourist industry. Also, in countries with a large land mass, an extensive air transport network can help bring the people of remote mountainous regions or distant islands into the main stream of national life. Not surprisingly, governments around the world have considered air transport as a vital instrument of achieving social and economic progress.

While the airplane is an efficient and an economical vehicle for transportation over moderate to long distances, its need to operate from rather large airports reduces its effectiveness for short range operations. A number of significant social benefits can be achieved from a viable STOL (Short Takeoff and Landing) transportation system. Economy of land usage is probably the most obvious. While jet airports around the world have grown to enormous size over the last few decades, one can readily envision compact STOL airports with only a 2000 ft. runway. The benefits are both social and economic, because the small land

requirements will prevent large segments of the population from having to be relocated. Also, STOL airports can be constructed near the city center (over existing railroad yards or major highways) which will greatly reduce the ground transportation time. A typical proposal is shown in Figure 1.1 [1].[1]

In spite of increased airframe noise, basically due to lift increasing devices, STOL aircraft expose a smaller ground area to high noise levels than do conventional aircraft. This noise reduction is primarily due to their capability to have steep climbout and approach paths (see Figure 1.2 [2]). Thus STOL airports have minimum noise impact on the adjoining communities. Also, from an operational standpoint, increased safety is inversely proportional to the relative speed between the airplane and the ground. Landings can be easier and safer when they occur at lower speeds. This direct link between landing speed and safety is well illustrated by both commercial and military operational experience as shown in Figure 1.3 [2].

Apart from the reasons mentioned above for STOL transports for commercial uses, one important reason for military STOL application is that it enables the air force mission planners to deploy the forces in diverse sites with short, semi-prepared runways closer to the battle lines. The STOL aircraft also can be operated effectively at sea from smaller, less costly ships decreasing the dependence on large carrier battle groups which are becoming vulnerable to increasingly sophisticated anti-ship missiles. Missions having combined needs for high altitude, long range,

---

[1]Numbers in brackets refer to similarly numbered references in the Bibliography.

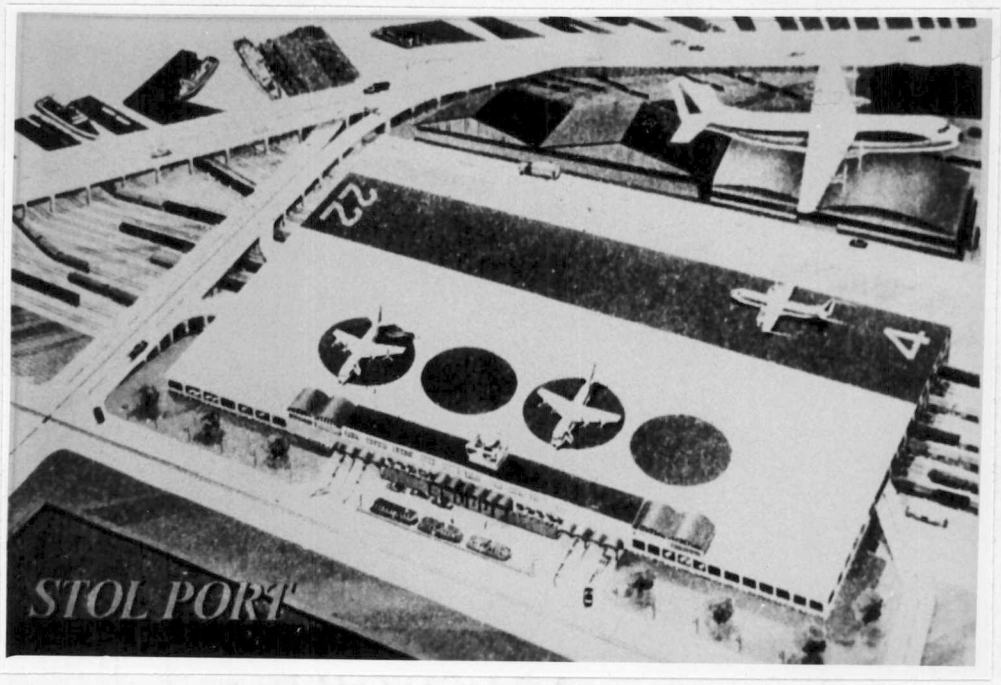


Figure 1.1 Typical V/STOL port proposal

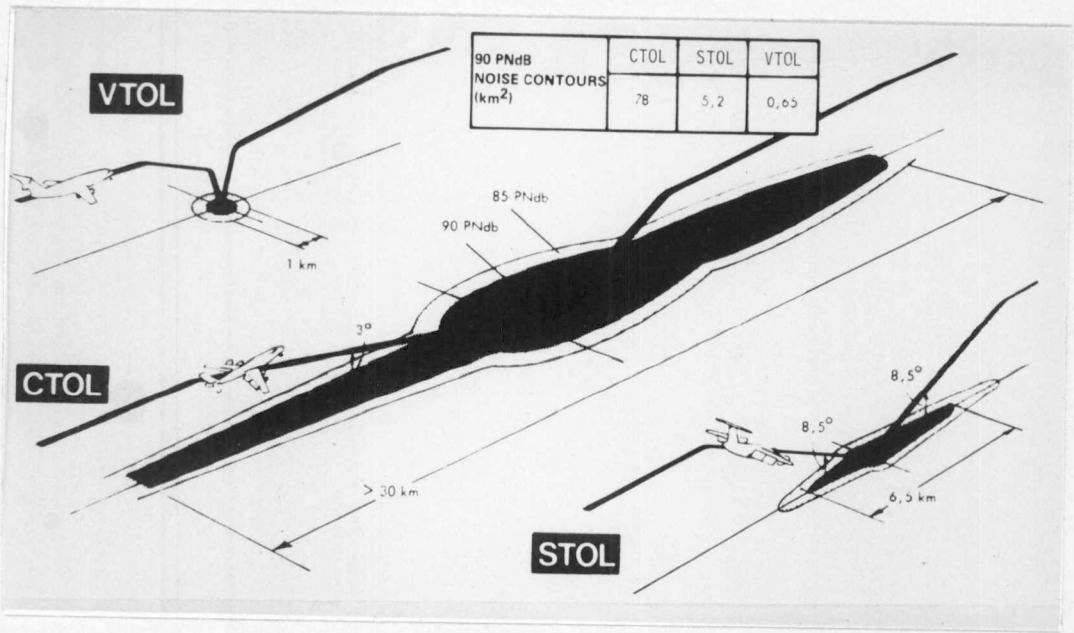


Figure 1.2 Comparison of near-airport noise contours

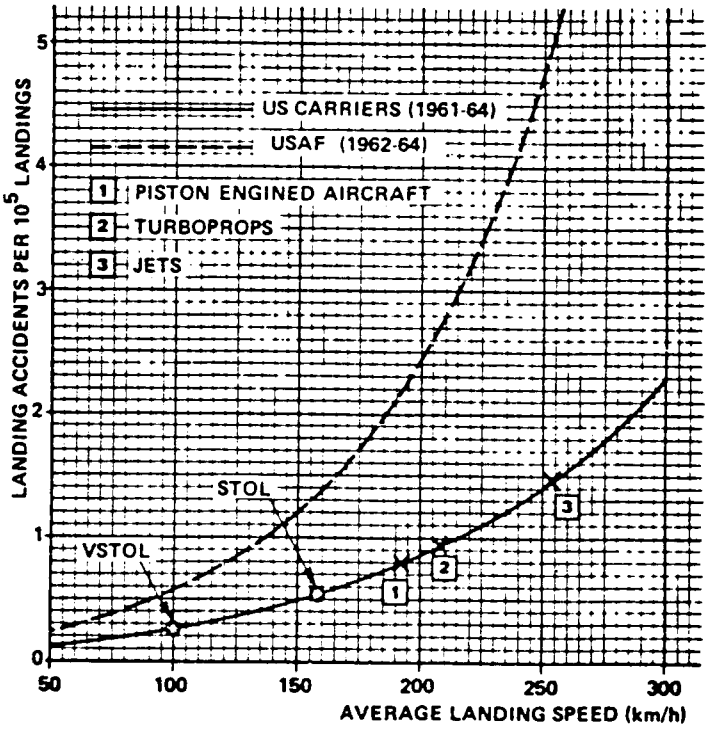


Figure 1.3 Speed vs. risk in landing

low speed maneuverability, and flexible basing will be prime candidates for STOL aircraft. Potential STOL missions include close air support, fleet air defense, surveillance, air superiority, strike and strategic-missile launch [3].

Various Means of Achieving STOL

To achieve STOL performance without excessive deceleration and with a wing loading compatible with a smooth ride at a high cruise speed (>70 psf), a very high maximum lift coefficient is required. A high lift coefficient also enhances the level of safety besides decreasing the required field length. The design of a high lift system should also consider lift/drag (L/D) ratio, as the drag penalty associated with high lift coefficient may be prohibitive in terms of climb performance after

an engine failure. Figure 1.4 [4] shows the demonstrated $C_{L_{max}}$ levels of some contemporary commercial and military transport aircraft. Figure 1.5 [4] depicts the trend of $C_{L_{max}}$ over the years.

Wing planform and airfoil profile normally are designed based upon the cruise condition. Once these are fixed, there is only a limited way of increasing wing $C_{L_{max}}$. The most widely used methods are by employing geometry changes or by boundary layer control. The geometry change can be achieved by mechanical means such as flaps or variable camber devices that increases circulation, hence $C_{L_{max}}$, by increasing wing camber, area and angle of attack in various combinations. Figure 1.6 describes various mechanical high lift devices. Of these double and triple slotted Fowler flaps are the most effective in increasing $C_{L_{max}}$. Figure 1.7 shows the leading edge device employed in the Boeing YC-14.

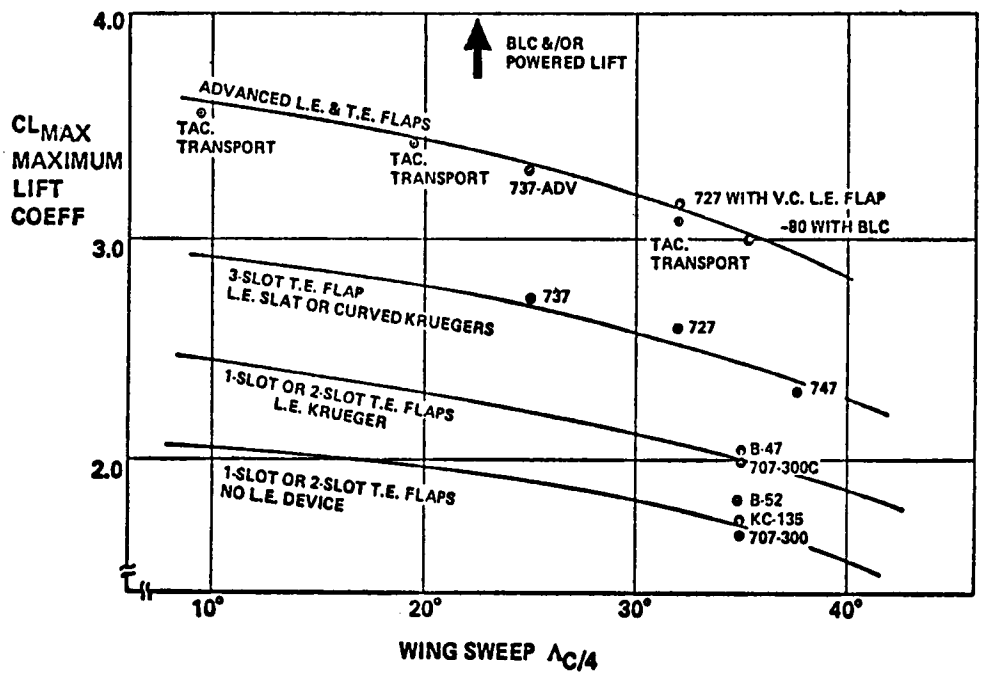


Figure 1.4 Demonstrated $C_{L_{max}}$ levels

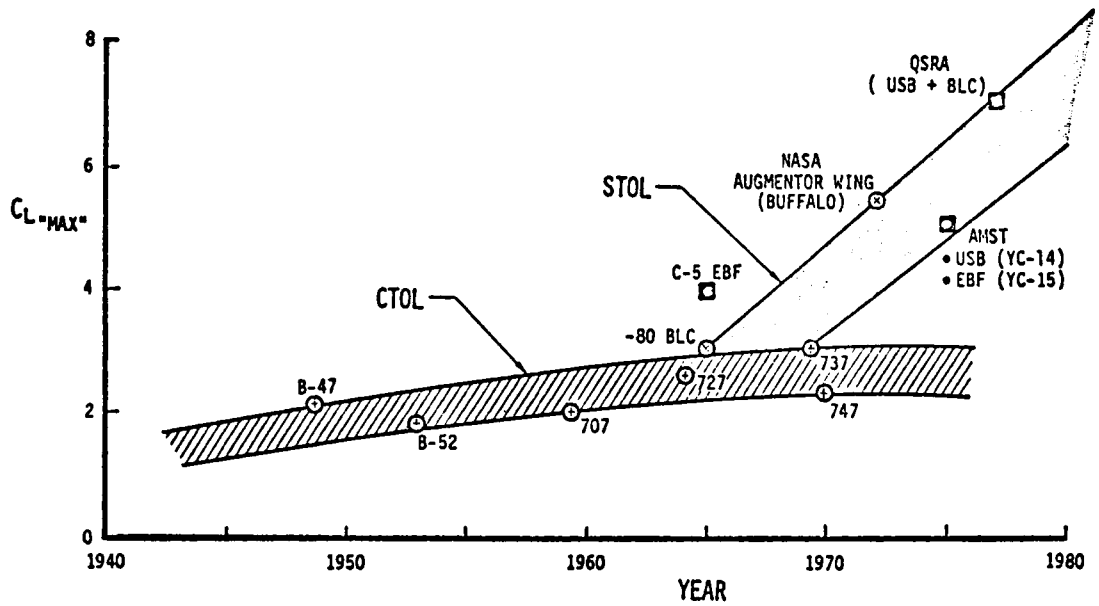


Figure 1.5 $C_{L_{max}}$ trends

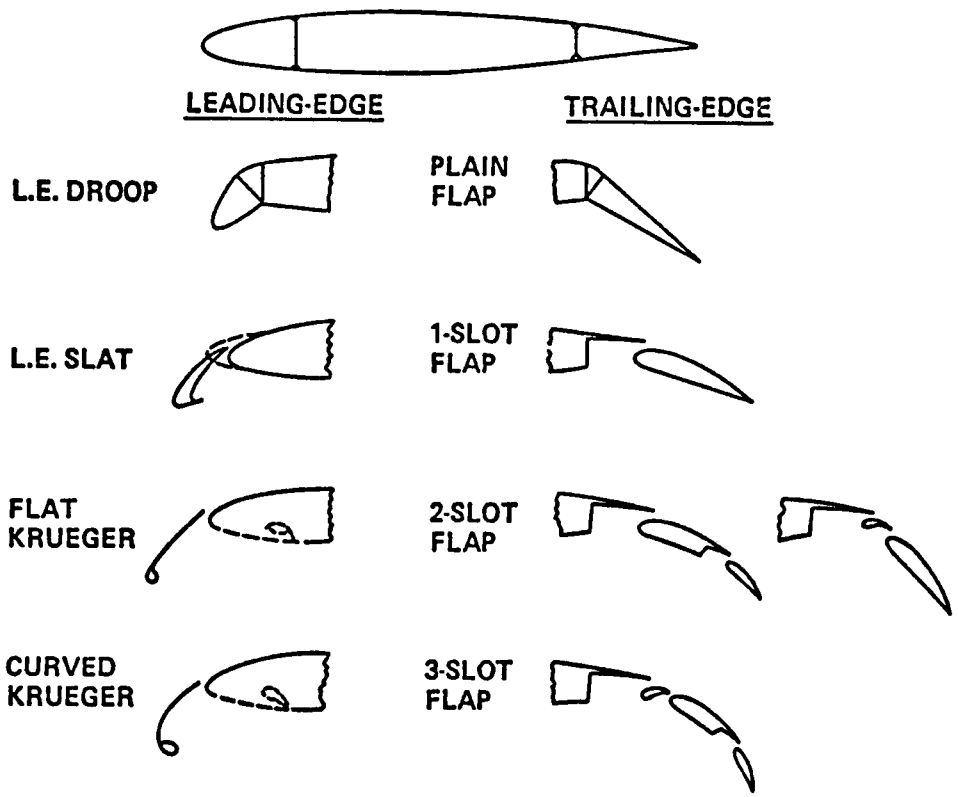


Figure 1.6 Mechanical high lift devices

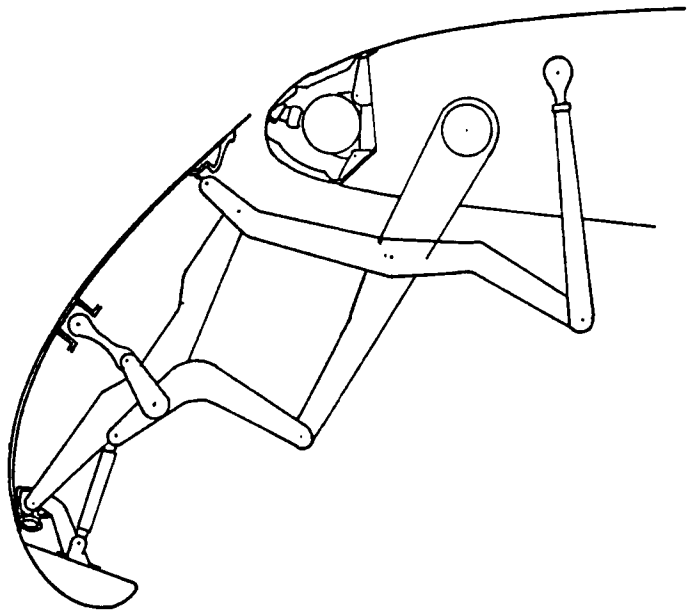


Figure 1.7 Variable camber Kruger flaps on the Boeing YC-14

The boundary layer control (BLC) devices are used to delay flow separation on the wing upper surface, caused by an adverse pressure gradient, thereby increasing $C_{L_{max}}$. Figure 1.8 shows several practical methods of applying blowing BLC to the leading and trailing edge of a wing. Maximum effectiveness can be obtained for a leading edge blowing BLC concept when used in conjunction with a curved Kruger Flap. At the trailing edge, blowing from the shroud over a simple flap is an effective way to increase the lift capability of the wing. Figure 1.9 describes several suction BLC concepts. These are based on the principle of removing low energy boundary layer through porous surfaces.

The lift augmenting devices described above are all dependent upon circulation to generate lift. If the $C_{L_{max}}$ has to be increased beyond the value imposed by circulation, either a vertical component of thrust

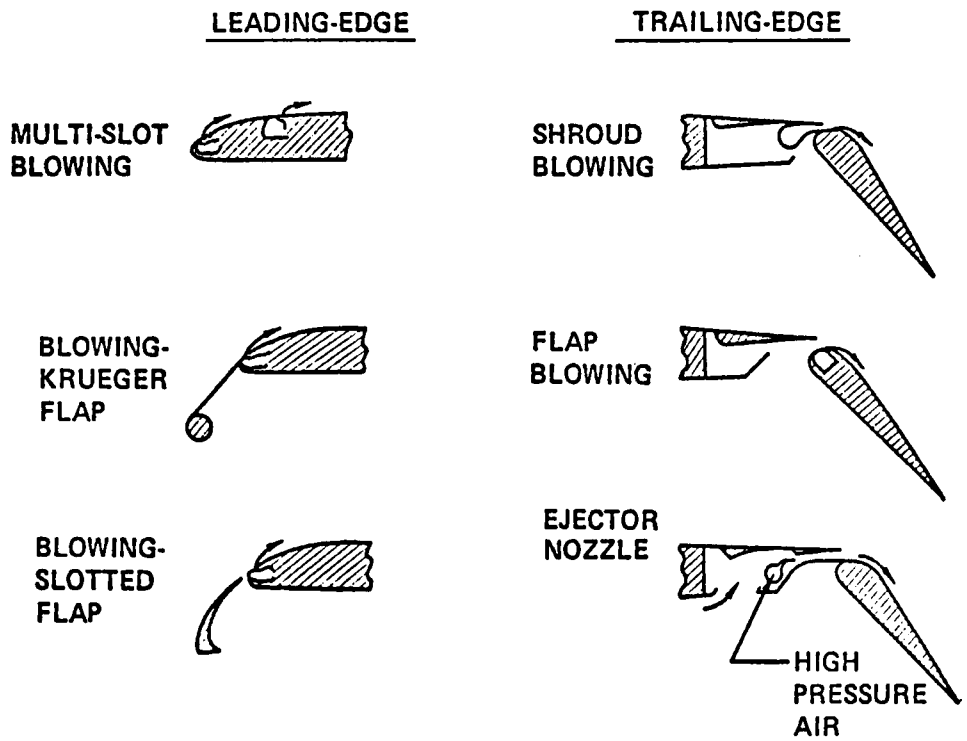


Figure 1.8 Blowing BLC concepts

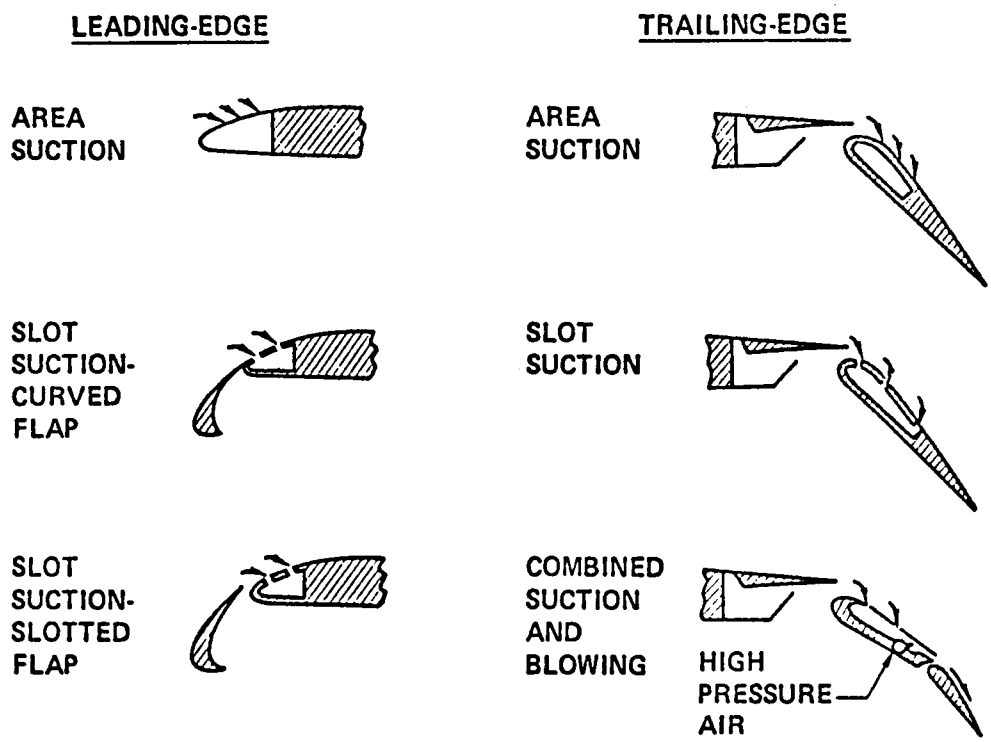


Figure 1.9 Suction BLC concepts

has to be employed or one can adopt a propulsive lift system such that the process of vectoring the thrust also increases circulation. The last approach, which started as the jet flap concept, has been developed in recent years into several propulsive lift systems which were adopted on actual prototype or research airplanes. Figure 1.10 depicts several of these powered lift concepts [5].

Figure 1.11 [6] illustrates the fundamental concept of the jet flap. A thin high energy jet is directed downward at some angle with respect to the freestream. It is usually combined with a mechanical lift system but may consist of only a high energy jet sheet emanating from the trailing edge. Figure 1.12 [6] describes jet flap scheme used alone or in conjunction with other mechanical lift enhancing devices.

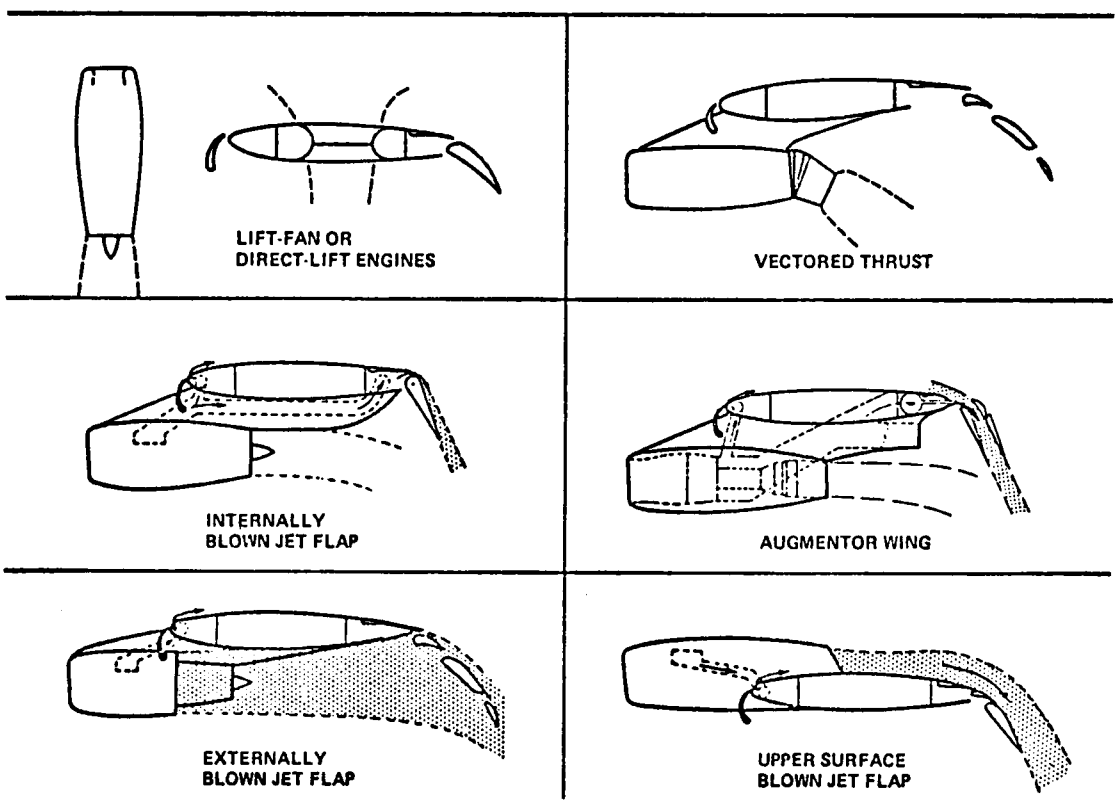


Figure 1.10 Powered lift concepts

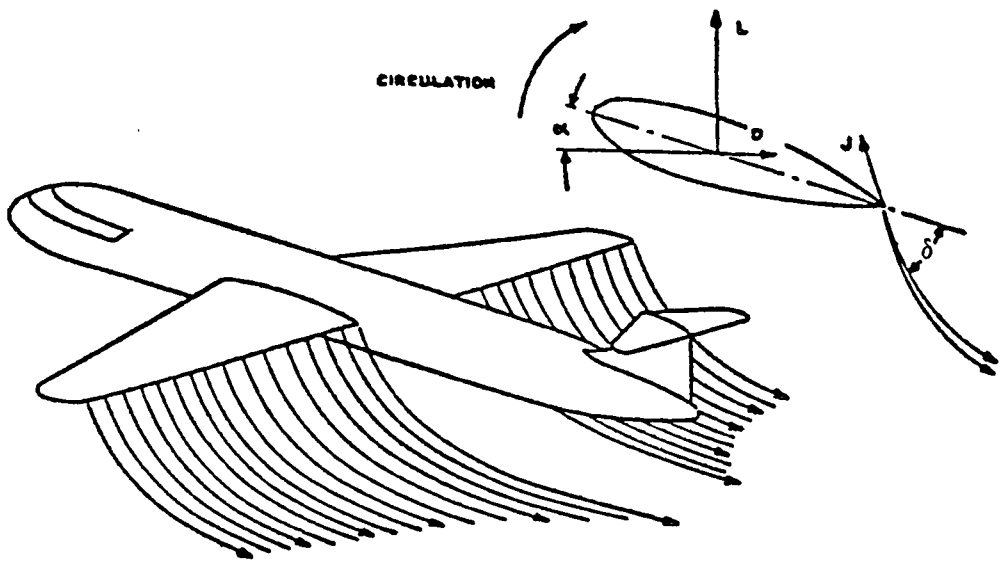


Figure 1.11 Jet flap aircraft

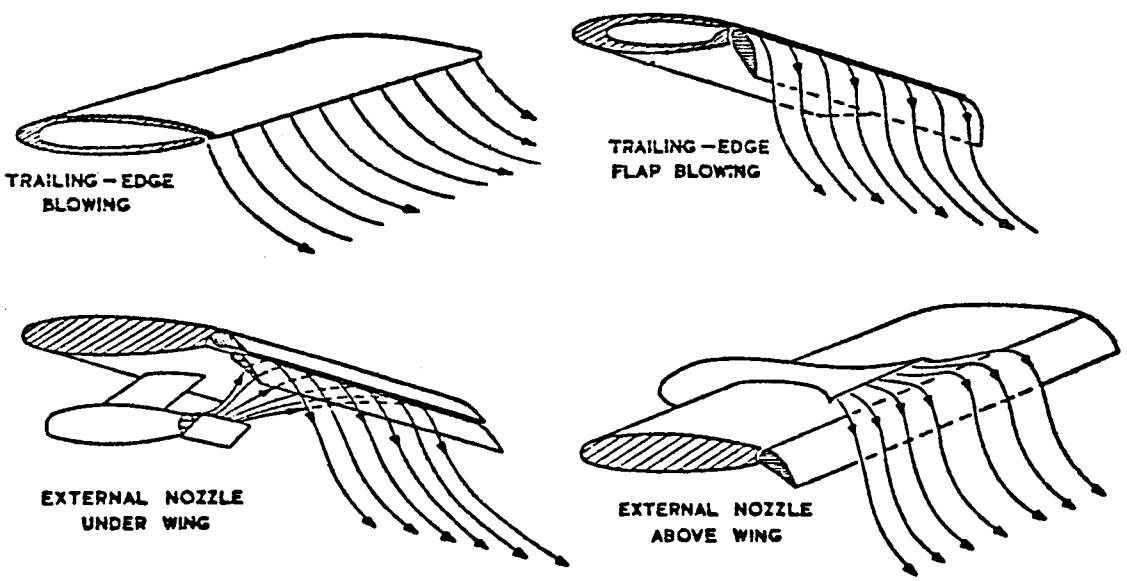


Figure 1.12 Some jet flap schemes

Figure 1.13 is another example of the application of the jet flap concept which incorporates features of a mechanical flap and blowing BLC. This concept, called the advanced internally blown flap, was developed and patented by Jacobs and Hurkamp of Lockheed-Georgia Company in 1971. The system includes a mechanical flap with an upper and lower surface that split when deflected to provide a variable-geometry cavity that serves as an air distribution duct for the wing. This avoids the necessity for ducting in the wing thereby increasing fuel storage space. Air is ejected from the flap trailing edge, in the manner of a pure jet flap. But, in the event of air cut-off, the mechanical flap continues to provide some lift. In addition, a small amount of air is blown from the knee slot of the trailing edge flap to provide boundary layer control. A small auxiliary flap is attached at the trailing edge of the flap system, near the jet flap exit. A small change in deflection can be used to produce substantial change in drag, particularly during landing maneuver. Also, differential deflection can be used for lateral control.

The idea of a jet flap is quite old though it has not been used in a practical aircraft configuration until recently because of nonavailability of a large source of high energy air. Schubauer [7] proposed and investigated the jet flap in 1932. In 1938, Hagedorn and Ruden [8] in Germany showed that a jet sheet blown over the upper surface of a wing produced higher lift coefficients than could be explained by the jet reaction thrust plus the original circulation lift. Hence, they concluded correctly that the jet sheet behaved similar to a rigid flap extension from the wing inducing additional circulation, i.e.,

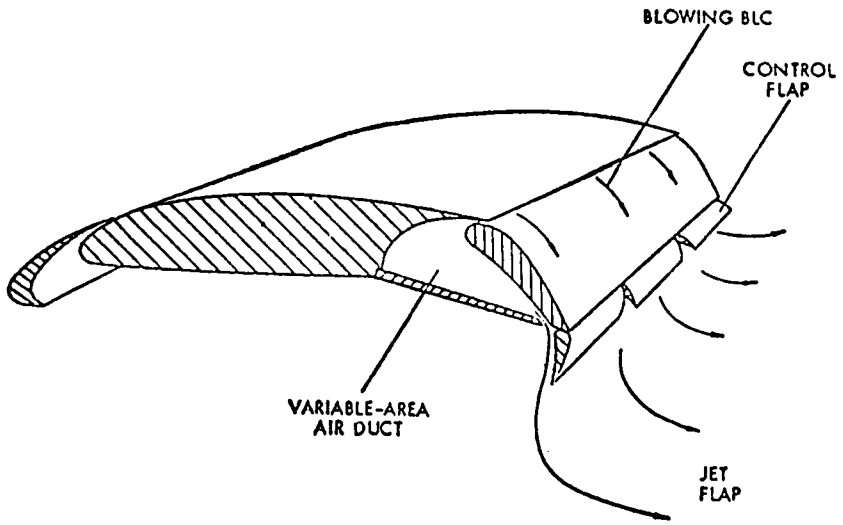


Figure 1.13 Jacobs-Hurkamp jet flap wing

additional lift, which nowadays has come to be known as supercirculation lift. This idea of replacing the jet sheet with an equivalent mechanical flap would be propounded into a full theory of predicting the aerodynamic characteristics of a jet-flapped wing later. However, after numerous research studies undertaken in the United States, Germany, France and England, the first jet flap research airplane, the Hunting H.126, shown in Figure 1.14 [9], first flew in March 1963.

The jet flap causes several important phenomena which makes an aircraft equipped with it different from the conventional aircraft:

i) There is a reaction lift created by the vertical component of jet momentum. This is affected by scrubbing loss on the flap and entrainment of the surrounding air.

ii) The apparent increase in flap area due to the jet sheet increases the circulation (i.e., creates supercirculation) and aerodynamic lift on the airfoil.

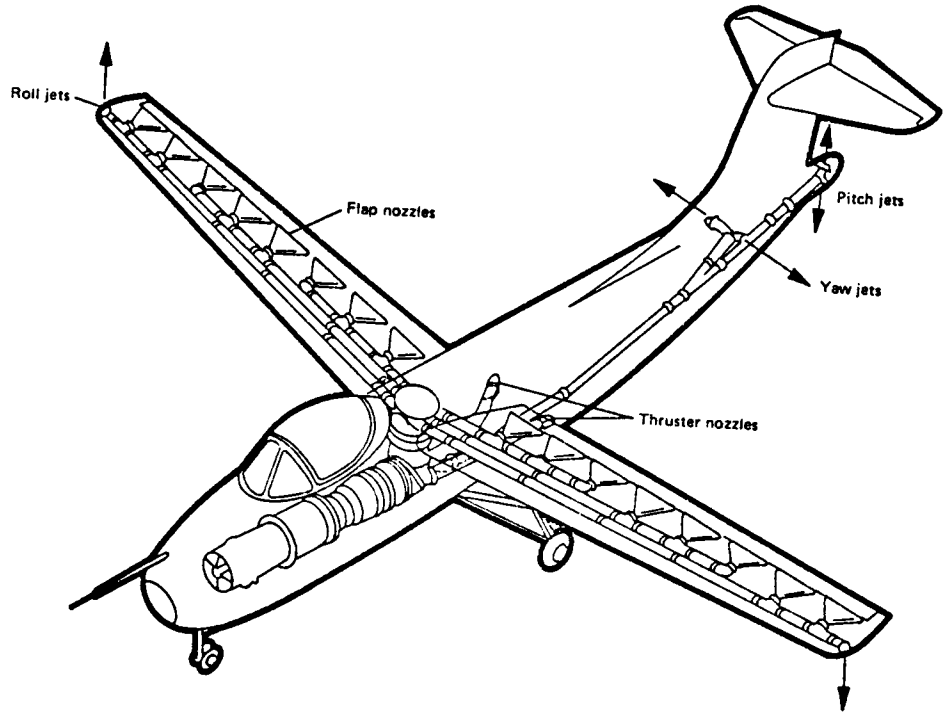


Figure 1.14 The Hunting H.126 jet flap research airplane

iii) Boundary layer separation is prevented on the flap because of the favorable pressure gradient over much of the main airfoil. Thus stall is delayed until a high angle of attack and high C_L is reached.

iv) The freestream flow eventually turns the jet sheet almost parallel to the remote velocity. Since the final momentum vector is nearly opposite to the direction of the flight path, almost the entire reaction force of the jet is recovered as thrust without sacrificing the vertical component of thrust which acts at the jet flap nozzle.

The presence of the jet on the wing creates an additional pressure drop over the one generated due to wing geometry and angle of attack. This pressure difference, highest at the trailing edge, causes the jet sheet to follow a curved path of gradually increasing radius until the sheet is parallel with the remote airflow and the pressure difference is

zero. It is equivalent to a vortex sheet with a strength directly related to the momentum flux and curvature of the jet sheet. The net effect is a greatly increased total circulation strength contained within the wing and jet flap system. This increased circulation strength increases the lift generated by the wing.

The components of the total lift generated by a jet flapped aircraft is shown in Figure 1.15.

Another rather recent powered lift concept is the circulation control wing (CCW), which is mechanically simple and has significant potential for providing high lift coefficients and STOL performance for high performance airplanes with relatively low blowing coefficients. In the CCW concept the sharp trailing edge of a conventional airfoil is replaced by a circular trailing edge over which a thin jet of air is blown tangentially as shown in Figure 1.16 [10]. This eliminates the usual Kutta condition that determines the level of circulation. Instead, the aft stagnation point moves into the lower surface, resulting in a considerable increase in circulation and lift coefficient. The position of the stagnation point and hence the value of the circulation is controlled by the plenum chamber pressure. A major flight test program of the CCW concept, carried out by U.S. Navy using a modified Grumman A-6A airplane [11,12], demonstrated substantial performance enhancement. A combination of upper surface blowing and the circulation control wing (USB/CCW) was incorporated in the NASA Quiet Short-Haul Research Aircraft (QSRA) to employ the flow entrainment properties of CCW to pneumatically deflect engine thrust in lieu of the mechanical USB flap system (see Figure 1.17 [13]).

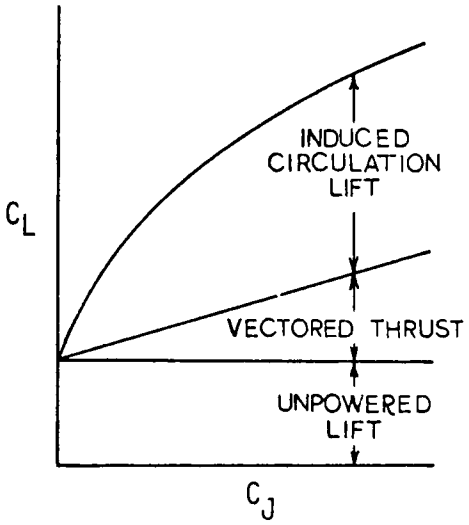


Figure 1.15 Components of lift on a jet flap aircraft

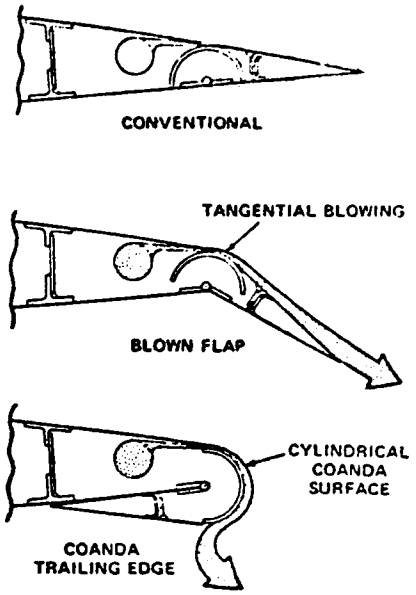


Figure 1.16 Circulation control wing modes of operation

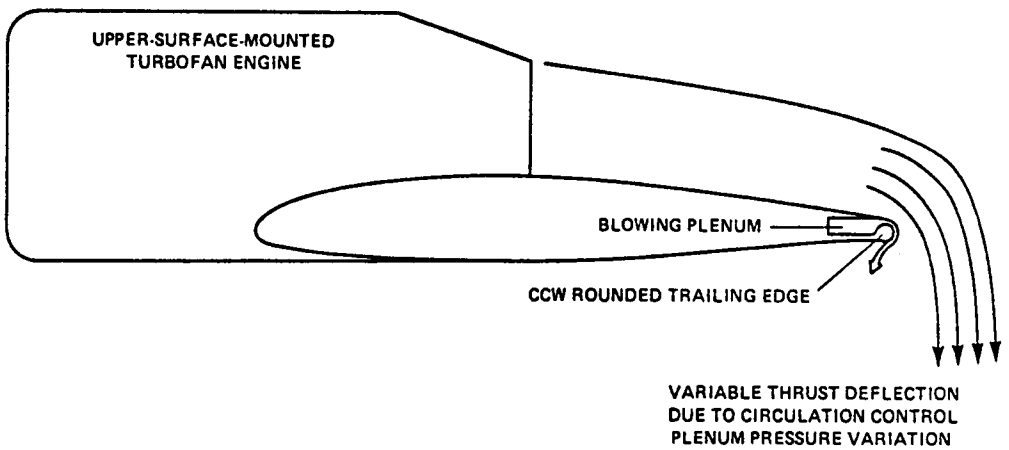


Figure 1.17 CCW/USB thrust deflector and lift augmentation concept

Upper Surface Blowing--An Efficient Powered Lift Concept

One of the most promising and widely studied powered lift concepts is the upper surface blown (USB) jet flap which has been applied in several experimental or research airplanes. In the USB concept, the exhaust of a turbofan engine is either ducted through the wing or directly blown over the upper surface of the wing through a rectangular or semi-circular nozzle. The flow is then deflected downward by a trailing edge flap and Coanda effect (i.e., the property of airflow adhering to the surface). Figure 1.18 shows the flow turning mechanism of a USB concept [14]. As described earlier, high momentum air on the upper surface creates additional circulation, hence lift, in addition to the basic aerodynamic lift and jet reaction lift.

The Boeing YC-14 is probably the earliest USB configuration which attained flight status as Boeing's entry to AMST competition [15]. The YC-14 is a twin-engine airplane with carefully optimized USB flaps and nozzles that vary their geometry for each flight condition. Leading edge blowing is used because of the strong upwash created by the jet flap induced circulation. A similar four-engine USB airplane has been built by Boeing for the NASA Quiet Short-Haul Research Aircraft (QSRA) program, Figure 1.19 [16]. The Soviet Union has produced a twin-engine USB airplane which is quite similar in appearance to the YC-14.

Advantages and Disadvantages of the USB Concept

The most important advantage of the USB concept is that the jet follows the upper surface of the wing uncluttered by the hinge and struts of the mechanical flap articulation mechanism keeping the loss to

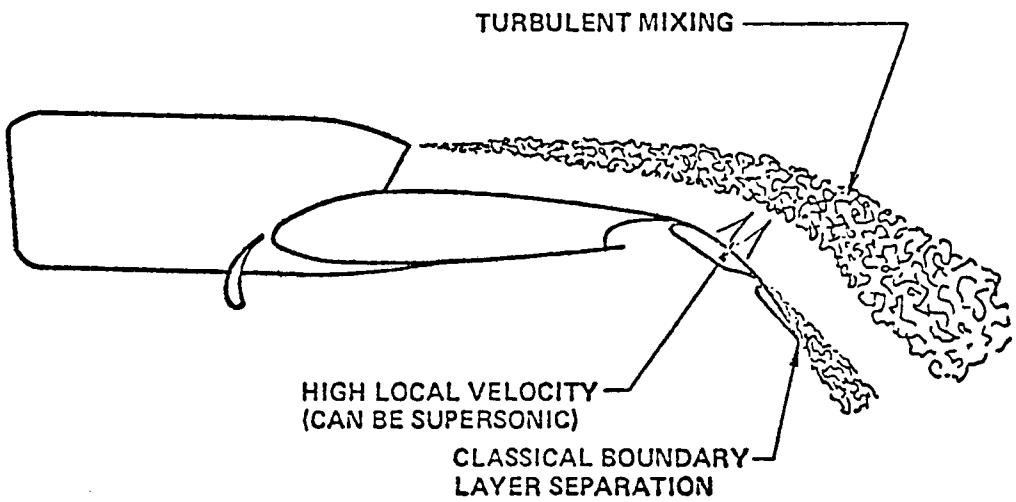


Figure 1.18 Processes affecting USB jet turning performance

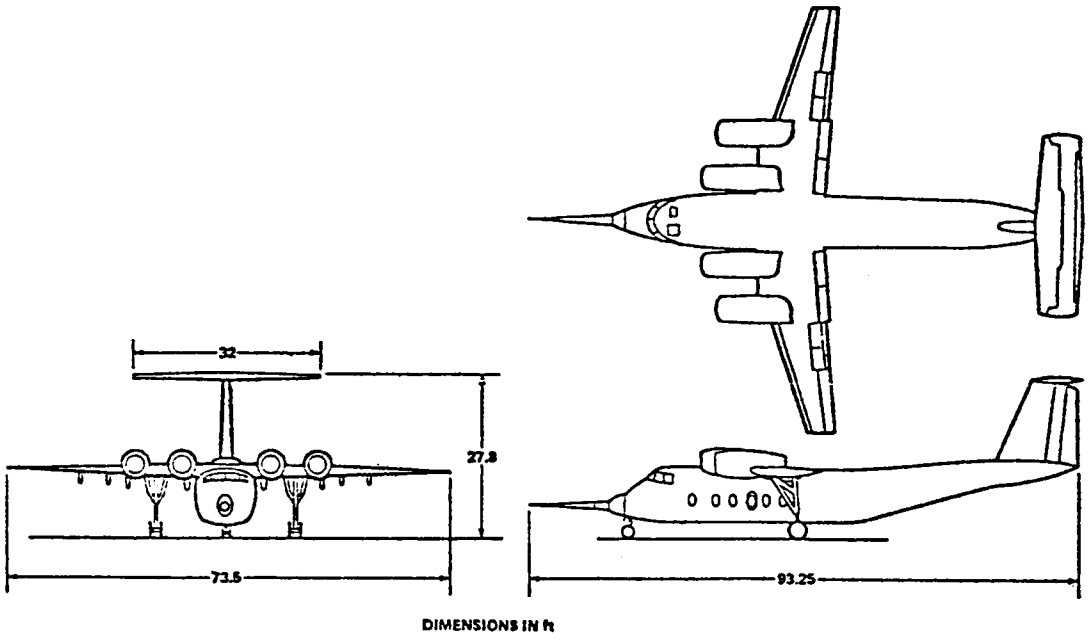


Figure 1.19 Three view drawing of NASA-Boeing Quiet Short-Haul Research Aircraft (QSRA)

a minimum. Also, it has been observed that the turning efficiency of the USB jet, as per the Coanda principle, is much higher than it is for the externally blown flap (EBF) concept as long as the jet is thin and the jet velocity is evenly distributed spanwise. Perhaps the most dramatic feature of the USB jet is that it causes the lift vector to cant forward thereby reducing induced drag. This reduction of induced drag is directly proportional to the blowing coefficient which makes it all the more attractive for a tight maneuvering combat aircraft in a dogfight. With exception of the augmentor wing, an USB aircraft will produce less noise than any other powered lift aircraft (see Figure 1.20 [5]). This noise reduction characteristic has implications for civilian as well as military applications.

When USB is effected by the engine exhaust being directly blown over the wing upper surface through semi-circular or elliptical (instead of rectangular) nozzles (thick jet as opposed to thin jet), the spanwise flow is more restricted, as shown in Figure 1.21 [1]. This restriction confines the jet flap effect to less span than the equivalent EBF system, shown in Figure 1.22 [1]. The thick jet USB like EBF, creates large peaks in lift behind the engines, as shown in Figure 1.23 [1]. Outboard of the engines, the flow and the resulting loads are almost independent of power level. This rather large increase in aerodynamic load is almost entirely created in the rear portion of wing section, causing the center of lift and aerodynamic center to both move rearward with increasing blowing. The net result is an increasing nose down pitching moment and very high downwash velocity. Both of these effects

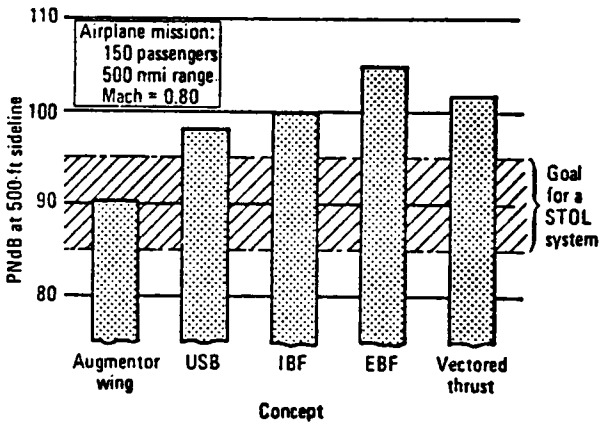


Figure 1.20 Noise levels for powered lift concepts

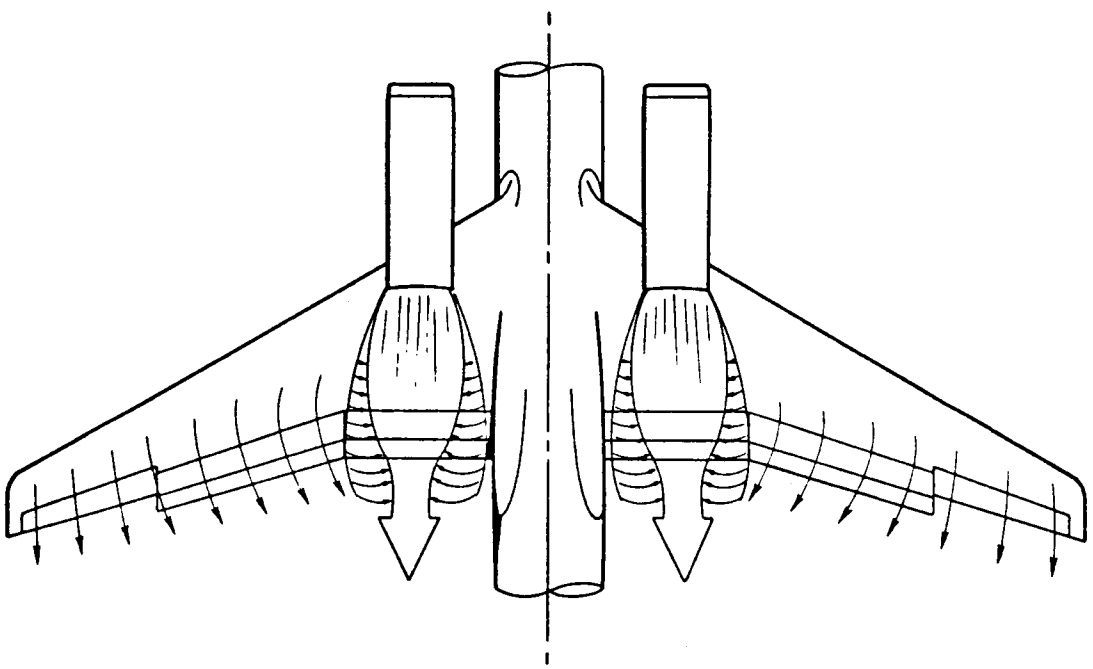


Figure 1.21 USB flow characteristics

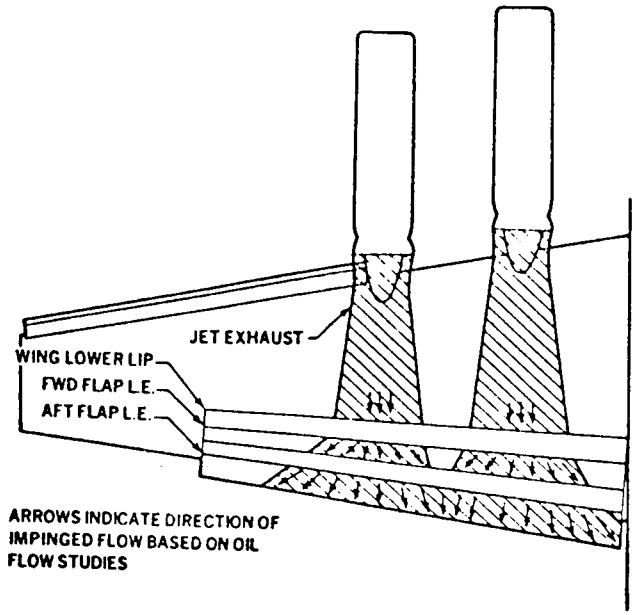


Figure 1.22 Spanwise exhaust spreading on an externally blown flap

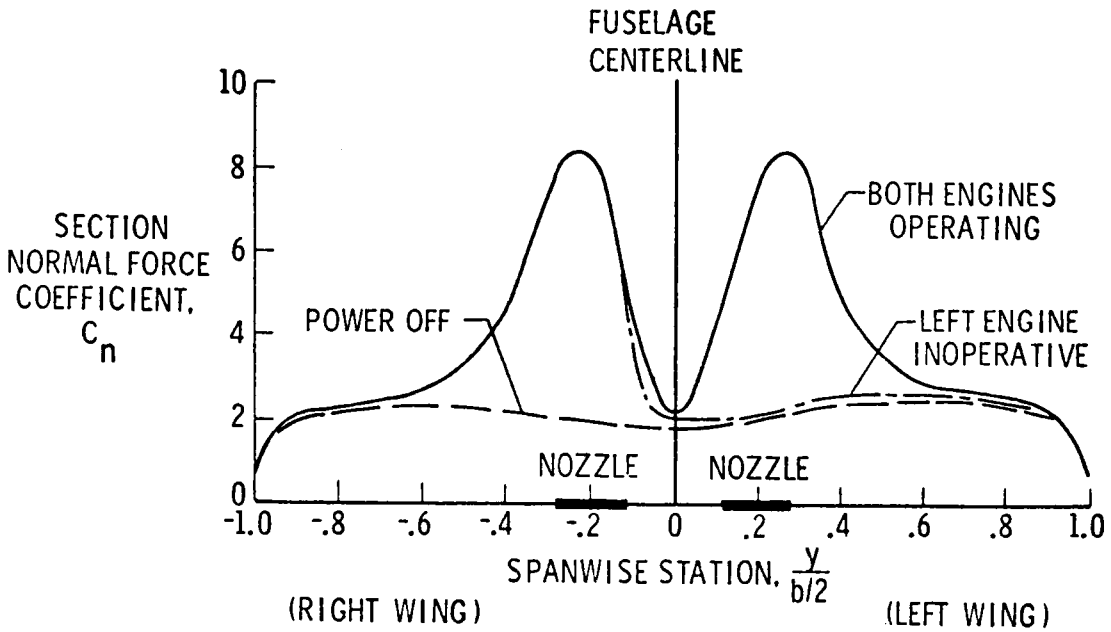


Figure 1.23 Spanwise normal-force distribution for two-engine Straight-wing USB configuration ($\delta_F = 60^\circ$, $\alpha = 0^\circ$)

have to be accounted for while designing the horizontal tail. One way of solving this problem is to have a T-tail aircraft or a canard configuration. If a rectangular nozzle is used and implemented by ducting the engine exhaust through the wing, the wing weight and ducting losses will increase. These losses can be minimized by careful laying out of the exhaust duct.

Technology Demonstration Vehicle: Ball-Bartoe JETWING

In 1976, the Ball-Bartoe Aircraft Company of Colorado developed an experimental single engine, single seat, USB aircraft, JETWING JW-1, as a proof of concept vehicle for powered lift [17,18,19]. Figure 1.24 [17] is a three view drawing of the aircraft showing its general arrangement. This is the first, and to date only, single engine USB aircraft to be built anywhere. In the "Jetwing" concept, USB is achieved from a single JT15D-1 turbofan engine by ducting all engine air (both from by-pass and core exhaust) through the wing leading edge and ejecting it over the upper surface of the wing through a slot nozzle. The nozzle is located at approximately 33% of the wing chord and extends about 70% of the wing span. By-pass air is ducted to the outboard portion of the wing while the core exhaust is ducted to the inboard portion of the wing as shown in Figure 1.25 [17]. Located above the nozzle is a separate, and much smaller wing surface. The purpose of this surface is to act as an ejector or thrust augmentor. A Coanda type, single element flap is located at the trailing edge of the wing along the blown portion of the wing span. A two dimensional sketch of the arrangement is shown

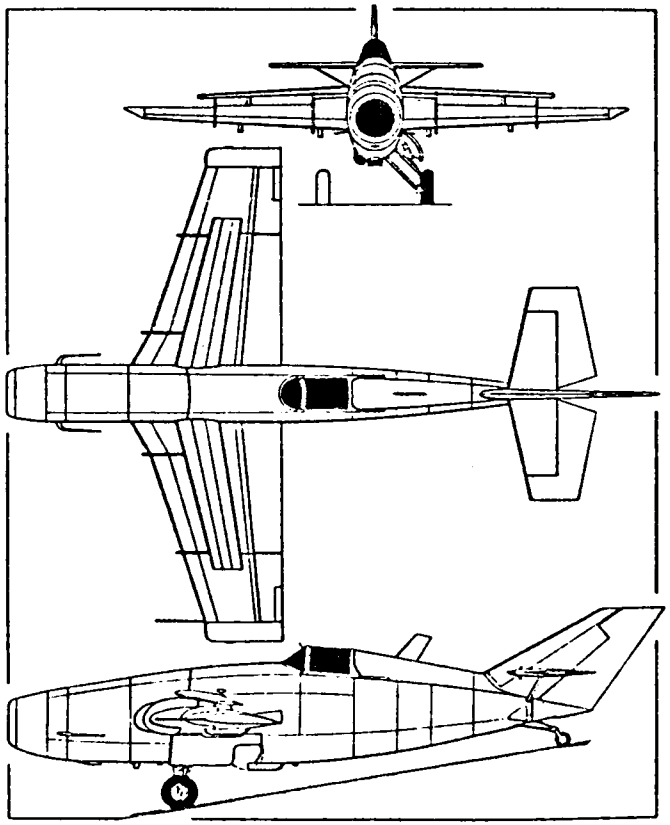


Figure 1.24 Three view drawing of Ball-Bartoe JETWING JW-1 experimental USB aircraft

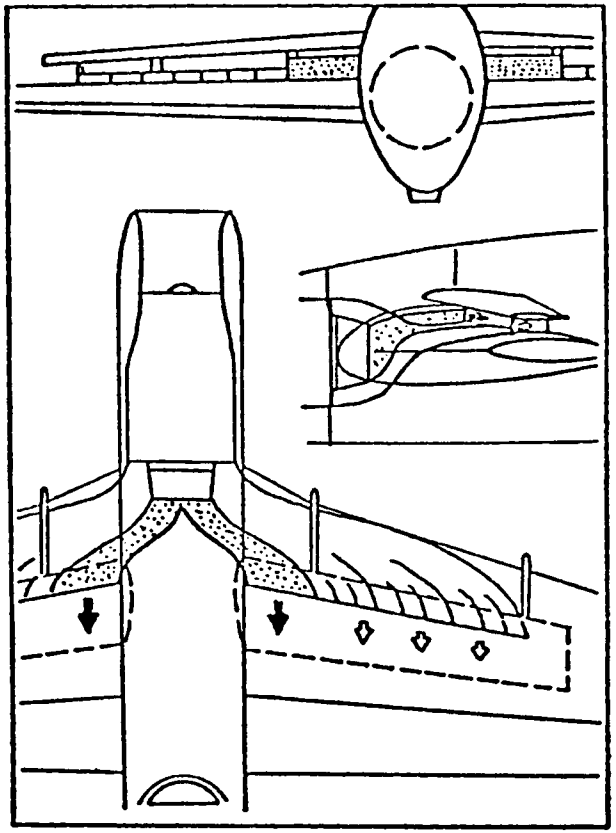


Figure 1.25 JETWING ducting arrangement

in Figure 1.26. The top of the by-pass air nozzle can be rotated to act as a thrust reverser as shown in Figure 1.27. The JETWING research aircraft, now owned by The University of Tennessee, has undergone extensive full scale wind tunnel test at NASA Ames Research Center 40' X 80' wind tunnel and flight test, with and without the upper wing, at The University of Tennessee Space Institute. These tests and concurrent analytical study [20,21] confirmed the low speed, high angle of attack flight and STOL capability. Full potential in these regards could not be realized because of longitudinal instability. Also, the horizontal tail stalls prior to the main wing preventing the maximum lift capability of the wing ever being achieved. Both these features are the result of poor airframe design rather than an inherent flaw in the concept.

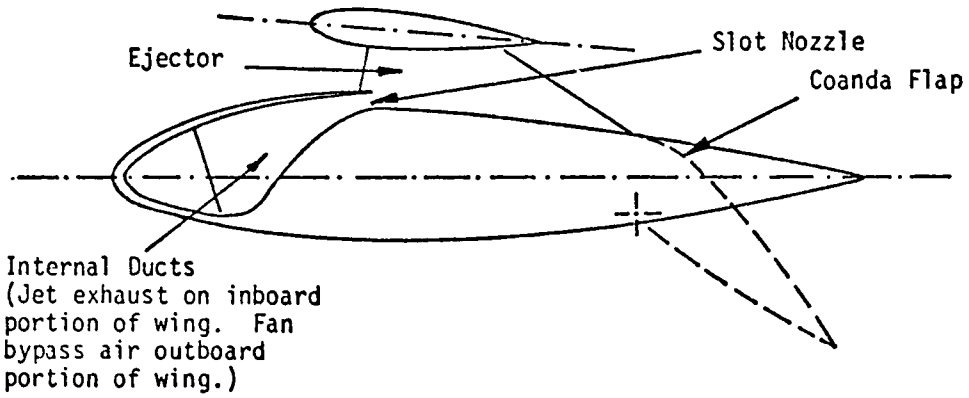


Figure 1.26 Two-dimensional view of "Jetwing" concept

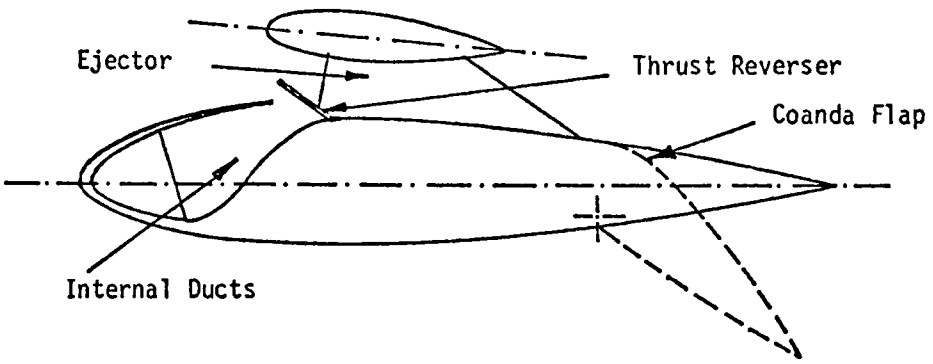


Figure 1.27 Two-dimensional view of "Jetwing" concept
with thrust reverser deployed

CHAPTER II

PREDICTION OF AERODYNAMIC CHARACTERISTICS

A Review of Some of the Methods

To undertake the design of a jet-flapped aircraft, a large number of analytical methods for predicting the aerodynamic characteristics have been developed over the years in various countries. They include simple handbook type methods relying purely on empirical formulae as well as very sophisticated methods that employ rational analytical modeling of the real aerodynamics. A few of the methods of both types are discussed here.

The basic theoretical properties of a thin two-dimensional jet in inviscid flow were formulated by Maskell and Gates [22], together with the overall momentum relations satisfied by the two-dimensional jet-flapped airfoil. Subsequently, jet flap theories were developed for the case of the thin wing and jet in inviscid incompressible flow, excluding mixing between the mainstream and the jet. The two-dimensional problem was solved by Spence using a treatment similar to the classical "Prandtl's Lifting Line Theory," both for ejection from the trailing edge [23] and over a plain (hinged) flap [24]. This lifting line analysis was extended to the case of a finite aspect ratio full span "jet-flapped elliptic wing" by Maskell and Spence [25]. A "jet-flapped elliptic wing" or a blown elliptic wing, is defined as a wing having an elliptic planform, an elliptic span loading, and an elliptic spanwise distribution of blowing momentum with constant jet angle over the span.

Analogous to an unblown elliptic wing, the spanwise distribution of the section lift coefficient, C_ℓ, section blowing coefficient, C_j, and the downwash angle for a blown elliptic wing are constant. Additionally, the section and total lift coefficient, C_ℓ and C_L, are equal and the section and total blowing coefficients, C_j and C_J, are equal. Other lifting line theories were developed by Hartunian [26], Kerney [27] and Tokuda [28]. This type of analysis was further developed for the estimation of the associated wing pressure distribution, downwash and jet path by Ross [29], as well as for damping in roll by Thomas and Ross [30] and longitudinal stability derivatives by Taylor [31]. One of the most simple methods based on the linerized inviscid flow theory of Spence was given by Williams, et.al. [6]. In general, these theories yield the result that the power-on to power-off lift curve slope ratio, K_π, is a function of the Spence [23] two-dimensional lift curve slope ratio, k_π, the three dimensional momentum coefficient, C_J, and the wing aspect ratio, A; i.e., $K_\pi = f(k_\pi, C_J, A)$. The specific form of the function "f" depends upon which of the aforementioned theoretical methods is employed. The method of Williams, et. al. [6] also gives a simple expression for excess thrust coefficient which has been found to agree very well with experimental data.

Among the more rigorous treatment of the aerodynamics of a jet-flapped wing, and perhaps the earliest, was the lifting surface theory given by Das [32]. A loading function technique was adopted along with the use of certain jet flap characteristics derived from Spence's [23] two-dimensional jet flap solution. The boundary conditions are satisfied at only three points in a chordwise section, namely, the

quarter-chord and the three-quarter-chord points, and downstream at infinity. Because of this limitation, the method is not normally regarded as satisfactory when there is a variation of chordwise geometry of the wing, such as camber and flap deflection.

One of the most sophisticated and comprehensive analytical methods for prediction of aerodynamic characteristics of a jet-flapped wing was developed by Shen, Lopez and Wasson [33] of Douglas Aircraft Company. This work was sponsored by the Air Force Flight Dynamics Laboratory [34]. This method consists of a lifting surface theory for jet-flapped wings based on a finite element method which is identified as the method of Elementary Vortex Distribution or the EVD method. The method utilizes a set of independent, but overlapped, elementary horseshoe vortex distributions to represent the wing and jet sheet. It satisfies a set of mixed-type boundary conditions on both the wing and jet sheet. The solution includes chordwise and spanwise loading distributions, from which sectional and total aerodynamic quantities, such as, lift, pitching moment, induced drag, etc., are derived. In view of the finite element approach, the method can, in general, be applied to jet-flapped wings of arbitrary planform, camber, twist, partial-span flaps, arbitrary trailing edge jet momentum, and jet deflection angle distribution. The method reduces to a conventional lifting surface theory when the jet momentum is zero. The EVD method had been implemented by means of a relatively large size digital computer program. Within the framework of a linearized model, the EVD method represents one of the most general and most exact solutions available for jet-flapped finite span wings.

As such, the method not only serves as a useful analysis and design tool, but also provides a convenient basis of comparison for other approximate methods of analysis.

Chen and Wu [35] developed a nonlinear vortex lattice theory for jet-flapped wing. Their method utilizes the system of bound vortices and free vortices with vortex lattice to represent wing, jet wake and tip vortices. They considered the interaction among the vortices. Nonlinear jet wake and tip vortices are determined simultaneously. Results obtained by this method compare well with those obtained by other methods. This method can also handle arbitrary wing planform, camber, twist, partial-span flaps, and trailing edge jet momentum distribution.

Another detailed analytical method was developed by Mendenhall and Spangler [36] for prediction of longitudinal aerodynamic characteristics of wing-flap configurations with upper surface blowing. Two potential flow models were incorporated into the prediction method: a wing and flap lifting surface model and a jet wake model. The wing-flap model uses a vortex-lattice to represent the wing and flaps. The wing may have an arbitrary planform, camber and twist. The flap system may be made up of a Coanda flap and other flap segments of arbitrary size. The jet wake model consists of a series of closely spaced rectangular vortex rings, which are positioned a priori tangent to the wing and flap upper surface where it induces an interference velocity field on the lifting surface. The wake model has a rectangular cross section over its entire length, and the wake can be specified such that the mass, momentum, and

spreading rates are similar to actual USB jet wakes. The flow tangency condition satisfied at the wing and flap control points results in a total loading which represents the aerodynamic loading, the jet reaction force, and the additional loading, known as supercirculation. The method is also capable of computing the total induced velocity at a field point off the lifting surface.

Motivation--The Need for a Simplified Theory for Preliminary Design

The theoretical aerodynamics of basic jet-flapped wing is by now reasonably well established. But, the analytical methods discussed earlier are one of two varieties. Either they rely heavily on empiricism, or are very complex and hence consume excessive computer time. It is believed that there is a need for both handbook and sophisticated computer-program-type methods in STOL aircraft aerodynamic prediction methodology. In particular, there is a need for handbook-type methods based upon rational analytical modeling with appropriate empirical modification as opposed to total reliance upon empiricism, since the former has more growth potential than the latter. Another problem that a potential user of a purely empirical method has to face is that the condition under which the empirical formulae were derived may not be valid for the configuration which he is interested in.

From the standpoint of the preliminary design of jet-flapped aircraft, where the design team must evaluate many configurations before selecting one, a simple but rational method, which considers a basic understanding of the flow phenomena, has to be made available to the designer. Preferably, this will be based on a lifting line theory,

which can treat arbitrary wings with arbitrary jet momentum and angle of jet deflection distribution spanwise. In the following pages one such method is developed and applied to an actual STOL aircraft configuration.

Scope of the Present Work

The method developed in the following chapters considers the two-dimensional airfoil sectional characteristics, wing planform, fuselage geometry (which is considered as slender body), chordwise location of the nozzle, spanwise extent and distribution of jet blowing velocity, and nozzle area as input. The method can handle part span blowing, part span single element trailing edge flaps with variable jet momentum, and variable jet and flap deflection spanwise. The method can also easily be extended to include a leading edge flap. Blowing can be effected at any chordwise station and not necessarily at the trailing edge flap hinge line. The method uses an empirical criterion to modify sectional geometry and then uses the lifting line theory. The method predicts the spanwise distribution of local lift coefficient, C_ℓ, and local pitching momentum coefficient, C_m, as well as total lift coefficient, C_L, and total pitching moment coefficient, C_M. It is also possible to isolate various components of lift into basic aerodynamic lift, jet reaction lift, and supercirculation lift.

CHAPTER III

EQUIVALENT FLAP THEORY: A NEW METHOD

Description of the Method

The criterion of obtaining the length of the equivalent mechanical flap for a pure jet-flapped airfoil was first given by Stratford [37]. Jacobs [38, 39] expanded this criterion to include an airfoil with a mechanical flap and a jet issuing at the trailing edge of the flap. He also gave the expression for pitching moment induced by an airfoil with jet augmented flap.

Jacobs proposed to replace the airfoil with a jet issuing at the trailing edge of the mechanical flap by the original airfoil and an extension of the flap itself. The jet may form any angle with respect to the flap or the free stream. For a two-dimensional airfoil, the length of the equivalent mechanical flap extension was determined by equating the lift generated by it with the vertical component of jet reaction. In the case of a three-dimensional wing, the effect of the induced downwash field was considered in the form of a decrease in effective angle of attack distribution. Hence, jet reaction lift would decrease, which in turn would reduce the length of the equivalent mechanical flap, as both the jet reaction lift and the lift on the equivalent flap extension have to be the same. The method described here employed the equivalent flap theory of Jacobs to calculate the equivalent mechanical flap extension of every spanwise section of the jet-flapped wing knowing the corresponding jet blowing velocity and then used the well known Multhopp's lifting line theory [40] to predict the

spanwise load and induced angle of attack distribution. The approach adopted here called for an iteration on induced angle of attack distribution, starting with zero throughout the span. Using this distribution, the equivalent wing shape was determined. Then by going through the lifting line theory, the load and new induced angle of attack distribution was obtained for that shape. The equivalent wing shape was then recalculated along with corresponding load, and induced angle of attack distribution, until the process converges. Once the equivalent wing shape and the load distribution on it was known, pitching moment could easily be obtained as the integrated (spanwise and chordwise) result of the product of density, velocity, circulation and distance from the moment center. Pitching moment of the fuselage was also calculated from an empirical formula. The method has the capability of handling leading edge flap along with the more conventional trailing edge flap.

Calculation of Lift

From geometric considerations and Figure 3.1, the following relations can be derived.

$$x = \frac{c'}{2}(1 + \cos\psi)$$

$$c_{fj} = c' - c = c' - \frac{c'}{2}(1 + \cos\psi_1) = \frac{c'}{2}(1 - \cos\psi_1)$$

$$c = c' - c_{fj} = c' - \frac{c'}{2}(1 - \cos\psi_1) = \frac{c'}{2}(1 + \cos\psi_1)$$

$$\frac{c_{fj}}{c} = \frac{1 - \cos\psi_1}{1 + \cos\psi_1}$$

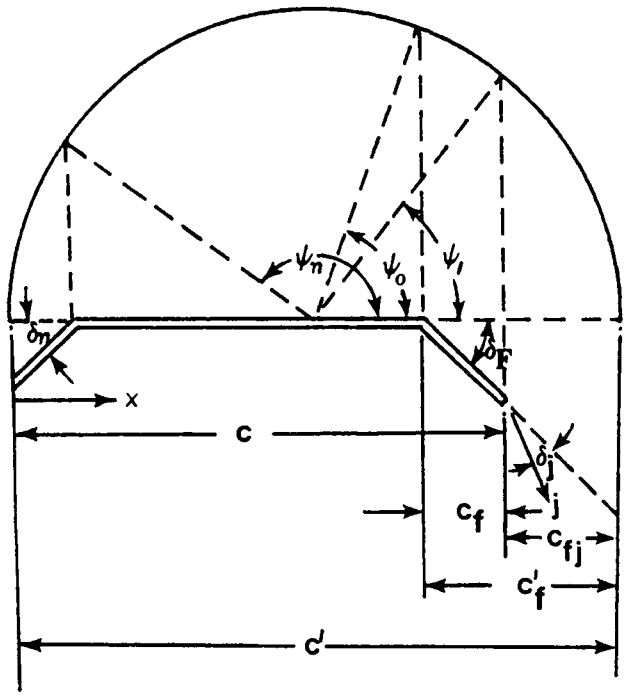


Figure 3.1 Geometry of airfoil with jet augmented flap

Again,

$$c'_f = c' - \frac{c'}{2}(1 + \cos\psi_o) = \frac{c'}{2}(1 - \cos\psi_o)$$

$$c_f = c'_f - c_{fj} = \frac{c'}{2}(1 - \cos\psi_o) - \frac{c'}{2}(1 - \cos\psi_1)$$

$$= \frac{c'}{2}(\cos\psi_1 - \cos\psi_o)$$

$$\frac{c_f}{c} = \frac{\cos\psi_1 - \cos\psi_o}{1 + \cos\psi_1}$$

$$\frac{c_f}{c}(1 + \cos\psi_1) = \cos\psi_1 - \cos\psi_o$$

$$\cos\psi_o = \cos\psi_1 - \frac{c_f}{c}(1 + \cos\psi_1) \qquad (3.1)$$

The circulation distribution $\gamma(\psi)$ over a thin airfoil with leading edge flap deflection δ_n, trailing edge flap deflection δ_F, and overall angle of attack α is given by Glauert as,

$$\gamma(\psi) = \frac{2V}{\pi}\left[- \delta_n\left\{(\pi - \psi_n)\tan\frac{\psi}{2} - \ln\left|\frac{\sin\frac{\psi + \psi_n}{2}}{\sin\frac{\psi - \psi_n}{2}}\right|\right\}\right.$$

$$+ \delta_F\left\{\psi_o \tan\frac{\psi}{2} + \ln\left|\frac{\sin\frac{\psi + \psi_o}{2}}{\sin\frac{\psi - \psi_o}{2}}\right|\right\}$$

$$\left. + \alpha\left\{\pi \tan\frac{\psi}{2} + \ln\left|\frac{\sin\frac{\psi + \pi}{2}}{\sin\frac{\psi - \pi}{2}}\right|\right\}\right] \qquad (3.2)$$

By the equivalent flap theory, the length of the equivalent flap extension can be calculated by equating the integrated lift over its length with the vertical component of jet reaction lift.

$$L_{fj} = \rho V \int_C^{C'} \gamma(x)dx = \dot{M}_j V_j \sin(\delta_F + \delta_j + \alpha) \qquad (3.3)$$

Figure (3.2) shows a typical circulation distribution over the basic and the equivalent airfoil. The hatched area is equal to the vertical component of jet reaction lift. Substituting $\gamma(x)$ from equation (3.2) into equation (3.3) and setting leading edge flap deflection δ_n to be zero, we get,

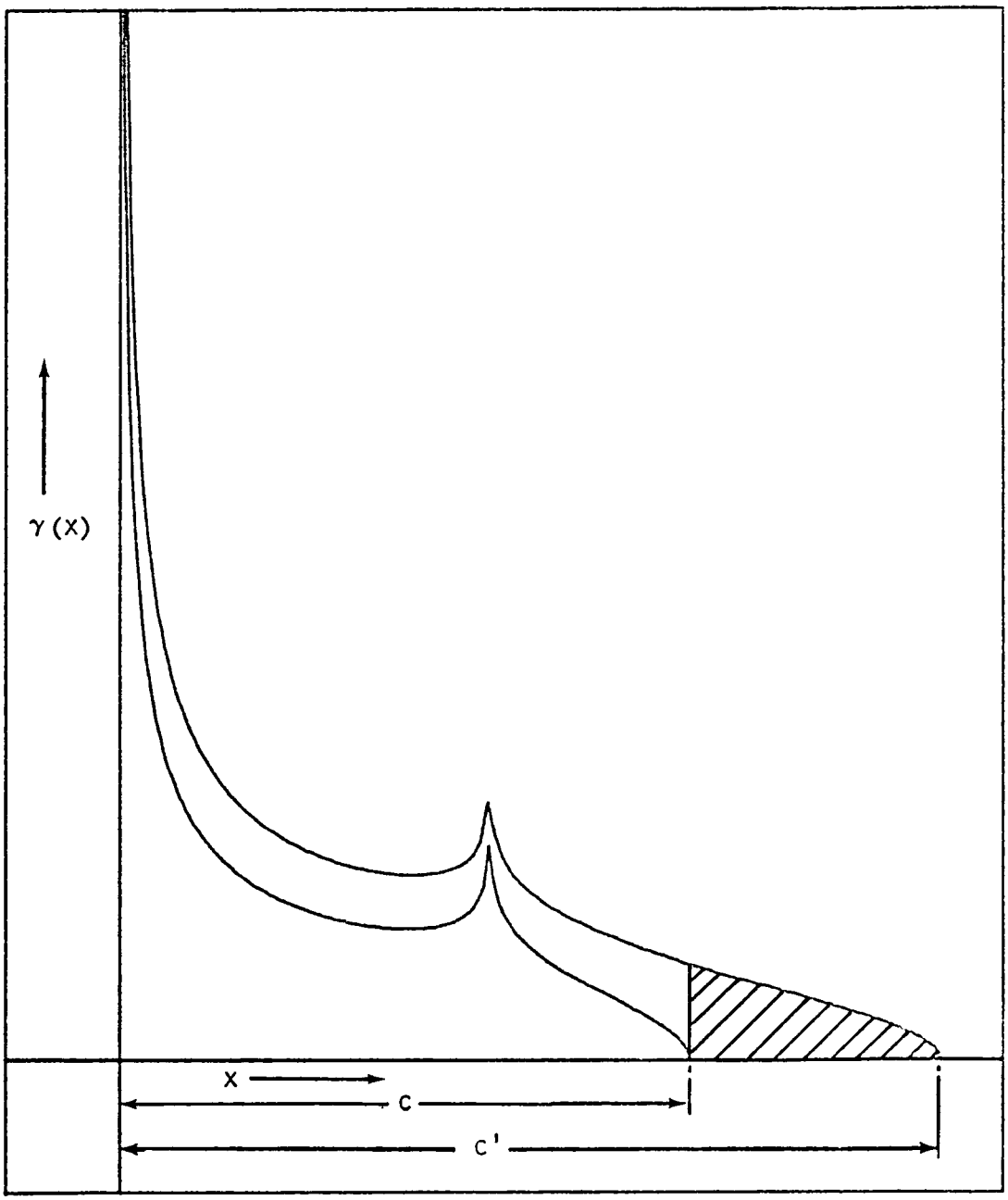


Figure 3.2 Circulation distribution over the basic and equivalent airfoil

$$\frac{\dot{M}_j V_j}{\frac{1}{2}\rho V^2 c'} \sin(\delta_F + \delta_j + \alpha) = \frac{2}{\pi} \int_0^{\psi_1} \left[\delta_F \left\{ \psi_0 \tan\frac{\psi}{2} + \ln\left| \frac{\sin\frac{\psi + \psi_0}{2}}{\sin\frac{\psi - \psi_0}{2}} \right| \right\} \right.$$

$$\left. + \alpha \left\{ \pi \tan\frac{\psi}{2} + \ln\left| \frac{\sin\frac{\psi + \pi}{2}}{\sin\frac{\psi - \pi}{2}} \right| \right\} \right] \sin\psi \, d\psi \qquad (3.4)$$

The integral on the right hand side of equation (3.4) has been evaluated in Appendix I.

Defining the blowing coefficient with respect to the equivalent chord c' as,

$$C_j' = \frac{\dot{M}_j V_j}{\frac{1}{2}\rho V^2 c'},$$

we can rewrite equation (3.4) as:

$$C_j' \sin(\delta_F + \delta_j + \alpha) = \frac{2}{\pi} \left[(\delta_F \psi_0 + \alpha\pi)(\psi_1 - \sin\psi_1) + \delta_F \left\{ \psi_1 \sin\psi_0 \right.\right.$$

$$\left.\left. + (\cos\psi_1 - \cos\psi_0) \cdot \ln\frac{\sin\frac{\psi_0 - \psi_1}{2}}{\sin\frac{\psi_0 + \psi_1}{2}} \right\} \right] \qquad (3.5)$$

Knowing the relation between c and c', we can write

$$C_j' = C_j \frac{1 + \cos\psi_1}{2} \qquad (3.6)$$

where C_j is obtained by the procedure given in Appendix II. Hence, equation (3.5) transforms to:

$$C_j \frac{1 + \cos \psi_1}{2} \sin (\delta_F + \delta_j + \alpha) = \frac{2}{\pi} \left[(\delta_F \psi_0 + \alpha\pi)(\psi_1 - \sin \psi_1) + \delta_F \left\{ \psi_1 \sin \psi_0 + (\cos \psi_1 - \cos \psi_0) \ln \frac{\sin \frac{\psi_0 - \psi_1}{2}}{\sin \frac{\psi_0 + \psi_1}{2}} \right\} \right] \tag{3.7}$$

Equation (3.7) is valid for a 2-D airfoil. The three-dimensional effects express themselves only in changes of angle of attack. For a 3-D wing, equation (3.7) should be modified as:

$$C_j \frac{1 + \cos \psi_1}{2} \cdot \left\{ \sin(\delta_F + \alpha + \delta_j - \alpha_i) - \sin \alpha_i \right\} = \frac{2}{\pi} \left[(\delta_F \psi_0 + \alpha\pi)(\psi_1 - \sin \psi_1) + \delta_F \left\{ \psi_1 \sin \psi_0 + (\cos \psi_1 - \cos \psi_0) \ln \frac{\sin \frac{\psi_0 - \psi_1}{2}}{\sin \frac{\psi_0 + \psi_1}{2}} \right\} \right] \tag{3.8}$$

Equations (3.1) and (3.8) must be solved simultaneously for the two unknowns ψ_0 and ψ_1. This problem is transformed into finding one unknown in one equation as described below.

Let $\cos \psi_1 = y'$, then $\sin \psi_1 = \sqrt{1 - y'^2}$

From equation (3.1),

$$\cos \psi_0 = y' - \frac{c_f}{c} (1 + y')$$

and

$$\sin \psi_0 = \sqrt{1 - \left\{ y' - \frac{c_f}{c} (1 + y') \right\}^2}$$

$$\text{Also, } \sin\left(\frac{\psi_0}{2} - \frac{\psi_1}{2}\right) = \sin\frac{\psi_0}{2} \cdot \cos\frac{\psi_1}{2} - \cos\frac{\psi_0}{2} \cdot \sin\frac{\psi_1}{2}$$

$$= \sqrt{\frac{1 - \cos\psi_0}{2}} \cdot \sqrt{\frac{1 + \cos\psi_1}{2}} - \sqrt{\frac{1 + \cos\psi_0}{2}} \cdot \sqrt{\frac{1 - \cos\psi_1}{2}}$$

$$\text{and, } \sin\left(\frac{\psi_0}{2} + \frac{\psi_1}{2}\right) = \sin\frac{\psi_0}{2} \cdot \cos\frac{\psi_1}{2} + \cos\frac{\psi_0}{2} \cdot \sin\frac{\psi_1}{2}$$

$$= \sqrt{\frac{1 - \cos\psi_0}{2}} \cdot \sqrt{\frac{1 + \cos\psi_1}{2}} + \sqrt{\frac{1 + \cos\psi_0}{2}} \cdot \sqrt{\frac{1 - \cos\psi_1}{2}}$$

Substituting these in Equation (3.8) we get,

$$C_j \left(\frac{1 + y'}{2}\right) \{\sin(\delta_F + \delta_j + \alpha - \alpha_i) - \sin\alpha_i\}$$

$$= \frac{2}{\pi}\left[\left\{\delta_F \cdot \cos^{-1}\left(y' - \frac{c_f}{c}(1 + y')\right) + \alpha\pi\right\} \cdot (\cos^{-1}y' - \sqrt{1 - y'^2}\,)\right.$$

$$+ \delta_F \cdot \left\{\cos^{-1}y' \cdot \sqrt{1 - \left(y' - \frac{c_f}{c}(1 + y')\right)^2} + \frac{c_f}{c}(1 + y') \cdot \right.$$

$$\left.\left. \ln \frac{\sqrt{\frac{1-y'+(c_f/c)(1+y')}{2}}\sqrt{\frac{1+y'}{2}} - \sqrt{\frac{1+y'-(c_f/c)(1+y')}{2}}\sqrt{\frac{1-y'}{2}}}{\sqrt{\frac{1-y'+(c_f/c)(1+y')}{2}}\sqrt{\frac{1+y'}{2}} + \sqrt{\frac{1+y'-(c_f/c)(1+y')}{2}}\sqrt{\frac{1-y'}{2}}} \right\}\right] \quad (3.9)$$

This is a transcendental equation in one variable y'. Initially we assume induced angle of attack α_i to be zero throughout the span. Then knowing C_j, δ_F, δ_j, α, c, c_f for each and every spanwise section, equation (3.9) is solved for y' by a multivariate search program [41] for error minimization. Once y' has been obtained, ψ_1, ψ_0, and c' can be determined from the relations developed earlier. That means, we can replace our jet-flapped wing by the actual hard wing and a hypothetical extension of the mechanical flap in the same plane as the actual flap. Now, the spanwise lift distribution, lift curve slope and overall C_L can be calculated by the well known Multhopp's Lifting Line Theory [40].

The input for the Lifting Line Theory will need the local chord and effective angle of attack (α_e) for each spanwise section. The last term, according to Glauert, can easily be obtained as

$$\alpha_e = \alpha + \frac{\partial \alpha}{\partial \delta_F} \delta_F$$

where

$$\frac{\partial \alpha}{\partial \delta_F} = \frac{2}{\pi} \left[\sqrt{\lambda_F(1-\lambda_F)} + \sin^{-1} \sqrt{\lambda_F} \right], \quad \lambda_F = \frac{c_f'}{c'}$$

The output of Multhopp's program will contain spanwise variation of induced angles of attack which then can be fed in equation (3.9) to obtain a new set of y', i.e., a new equivalent wing, which will produce another set of induced angles of attack. This process is continued until the induced angles of attack in two successive iterations matches within the desired accuracy.

Calculation of Pitching Moment

The pitching moment of an airfoil with a jet augmented flap can be written as:

$$M = -\rho V \int_0^{c'} \gamma(x)(x + z)dx + \rho V \int_c^{c'} \gamma(x)(x + z)dx$$

$$- j \sin(\delta_F + \delta_j) \cdot (c + z) \qquad (3.10)$$

Hence,

$$M = -\rho V \int_0^{\pi} \gamma(\psi) \left\{\frac{c'}{2}(1 + \cos\psi) + p'c'\right\}\frac{c'}{2} \sin\psi \, d\psi$$

$$+ \rho V \int_0^{\psi_1} \gamma(\psi) \left\{\frac{c'}{2}(1 + \cos\psi) + p'c'\right\}\frac{c'}{2} \sin\psi \, d\psi$$

$$- j \sin(\delta_F + \delta_j) \cdot \left\{\frac{c'}{2}(1 + \cos\psi_1) + p'c'\right\}$$

$$M = -\rho V \frac{c'^2}{4} \int_0^{\pi} \gamma(\psi)(1 + \cos\psi + 2p') \sin\psi \, d\psi$$

$$+ \rho V \frac{c'^2}{4} \int_0^{\psi_1} \gamma(\psi)(1 + \cos\psi + 2p') \sin\psi \, d\psi$$

$$- j \sin(\delta_F + \delta_j) \cdot \frac{c'}{2}(1 + \cos\psi_1 + 2p') \qquad (3.11)$$

In non-dimensional form equation (3.11) can be written as:

$$C_m' = \frac{M}{\frac{1}{2}\rho V^2 c'^2} = -\frac{1}{2V} \int_0^{\pi} \gamma(\psi)(1 + \cos\psi + 2p') \sin\psi \, d\psi$$

$$+ \frac{1}{2V} \int_0^{\psi_1} \gamma(\psi)(1 + \cos\psi + 2p') \sin\psi \, d\psi$$

$$- C_j' \sin(\delta_F + \delta_j) \cdot \left(\frac{1 + \cos\psi_1 + 2p'}{2}\right) \qquad (3.12)$$

The integrals in equation (3.11) have been evaluated in Appendix III.

The pitching moment coefficient based on the actual airfoil chord is then

$$C_m = C_m' \left(\frac{2}{1 + \cos\psi_1}\right)^2 \qquad (3.13)$$

Rewriting equation (3.11) we obtain:

$$M = -\frac{\rho V^2 c'^2}{4}\left[(1 + 4p')(\delta_F\psi_0 + \alpha\pi) + \delta_F \sin\psi_0\left\{2(1 + 2p') + \cos\psi_0\right\}\right]$$

$$+ \frac{\rho V^2 c'^2}{4\pi}\left[(\delta_F\psi_0 + \alpha\pi)\left\{(\psi_1 - \sin\psi_1\cos\psi_1) + 4p'(\psi_1 - \sin\psi_1)\right\}\right.$$

$$+ \delta_F \ln\frac{\sin\frac{\psi_0 + \psi_1}{2}}{\sin\frac{\psi_0 - \psi_1}{2}} \cdot\left\{2(1 + 2p')(\cos\psi_0 - \cos\psi_1)\right.$$

$$\left.\left. + \frac{1}{2}(\cos 2\psi_0 - \cos 2\psi_1)\right\} + 2(1 + 2p')\delta_F\psi_1 \sin\psi_0\right.$$

$$- \frac{\delta_F}{2}\left\{\cos 2\psi_0(2\sin\psi_0\sin\psi_1 + \frac{1}{2}\sin 2\psi_1 \sin 2\psi_0)\right.$$

$$- \sin 2\psi_0\left(\psi_1 + 2\sin\psi_1\cos\psi_0\right.$$

$$\left.\left.\left. + \frac{1}{4}\cdot(\cos 2\psi_0 - \sin 2\psi_0)\cdot(\cos 2\psi_1 + \sin 2\psi_1 - 1)\right)\right\}\right]$$

$$- \dot{M}_j V_j \sin(\delta_F + \delta_j)\frac{c'}{2}(1 + \cos\psi_1 + 2p') \qquad (3.14)$$

Equation (3.14) is the expression for the pitching moment for a unit spanwise length. First two terms of the right hand side have to be multiplied by unit length in order to get consistency in units. In the last term, $\dot{M}_j$ denotes mass flow rate per unit span. All the terms in right hand side have to be divided by gc (i.e., 32.174 lbm-ft/lbf-sec^2) if the final result is desired in English Engineering Unit, i.e., ft-lbf.

The contribution of the fuselage to the pitching moment can be estimated as follows. According to Munk [42], for a very slender body of revolution, the variation of the pitching moment with angle of attack in degrees is a function of the fuselage volume and dynamic pressure.

$$\frac{dM}{d\alpha} = \frac{\text{Volume}}{28.7} \cdot q \tag{3.15}$$

This expression is corrected by a factor $(K_2 - K_1)$, which is a function of fuselage fineness ratio.

Hence,

$$\frac{dM}{d\alpha} = \frac{\text{Volume}}{28.7} \cdot q \cdot (K_2 - K_1) \tag{3.16}$$

For the JETWING aircraft the fineness ratio is 10. Correspondingly, $K_2 - K_1 = 0.95$. Hence, equation (3.16) can be written as:

$$\frac{dM}{d\alpha} = 0.033101 \cdot \text{Volume} \cdot q \tag{3.17}$$

Therefore, the pitching moment contribution of the fuselage is

$$M_{FU} = 0.033101 \cdot \text{Volume} \cdot q \cdot \alpha \tag{3.18}$$

The overall pitching moment coefficient can be calculated by summing up individual moments for all spanwise sections of the wing, adding them to the fuselage pitching moment, and then dividing by the product of the dynamic pressure, actual gross wing area and mean aerodynamic chord.

Results and Discussion

The method described here has been coded in FORTRAN. The code comprises about 700 instructions and occupies a core memory of nearly 40 blocks (1 block = 512 bytes). The computer time required in a VAX-11/780 system for each combination of C_J, δ_F, and α (with α varying between 0° and 30° in steps of 5°) does not exceed 5 minutes for the cases shown in the results. Figure (3.3) through Figure (3.8) show the comparison of predicted values of C_L vs. α and C_L vs. C_M with that of

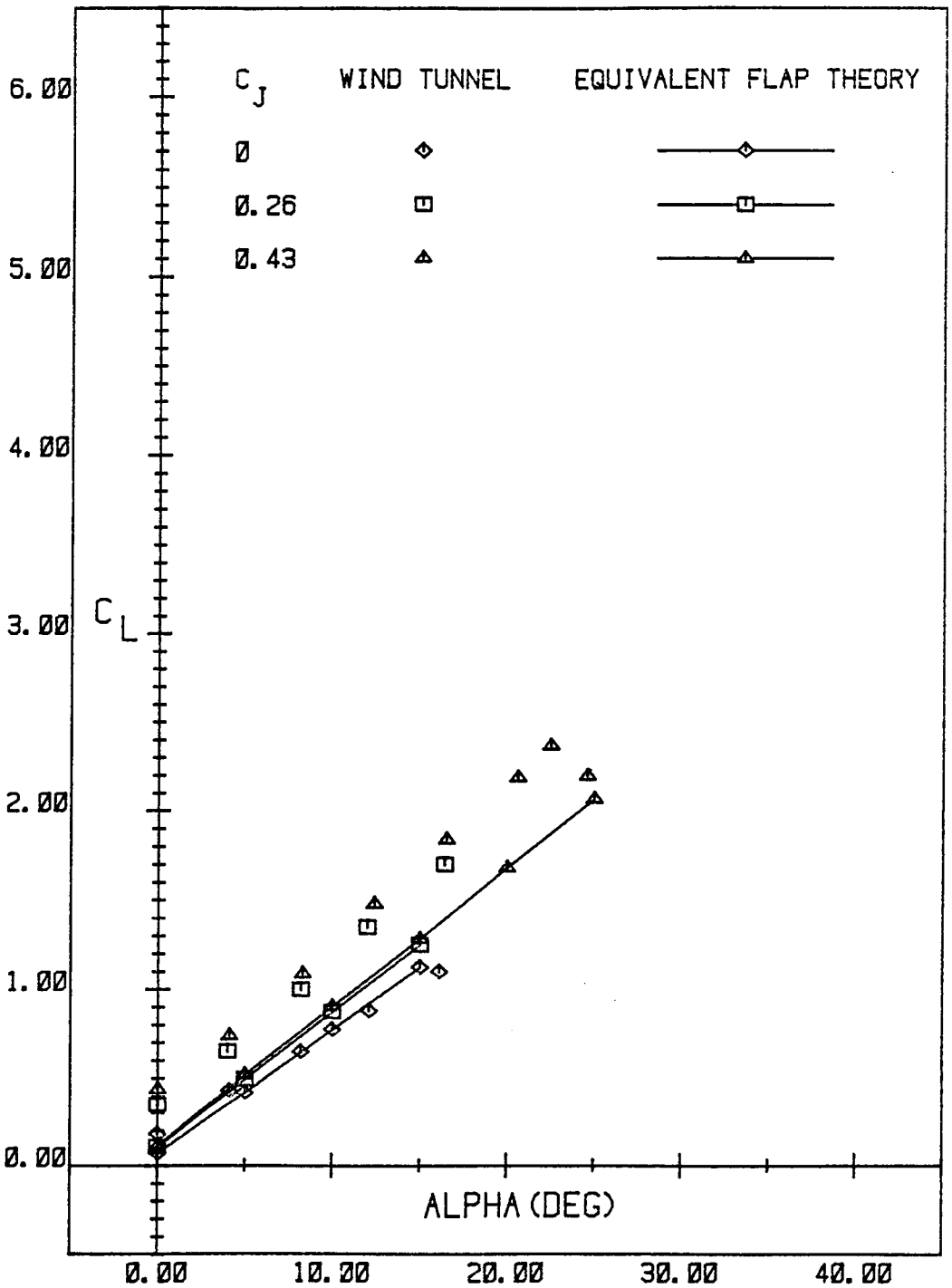


Figure 3.3 Comparison of Equivalent Flap Theory with full scale data for $\delta_F = 0^\circ$ (upper wing removed)

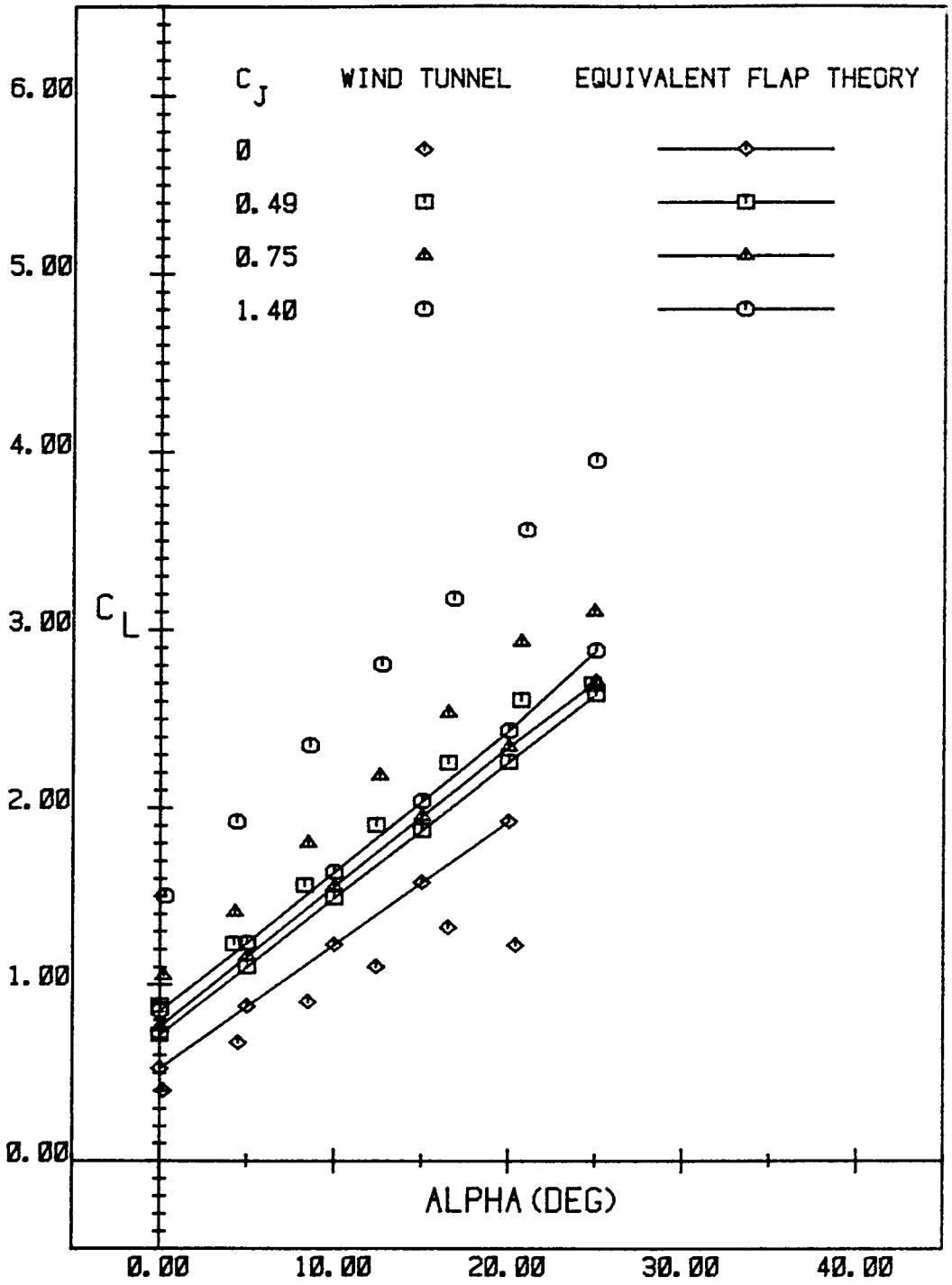


Figure 3.4 Comparison of Equivalent Flap Theory with full scale data for $\delta_F = 15^\circ$ (upper wing removed)

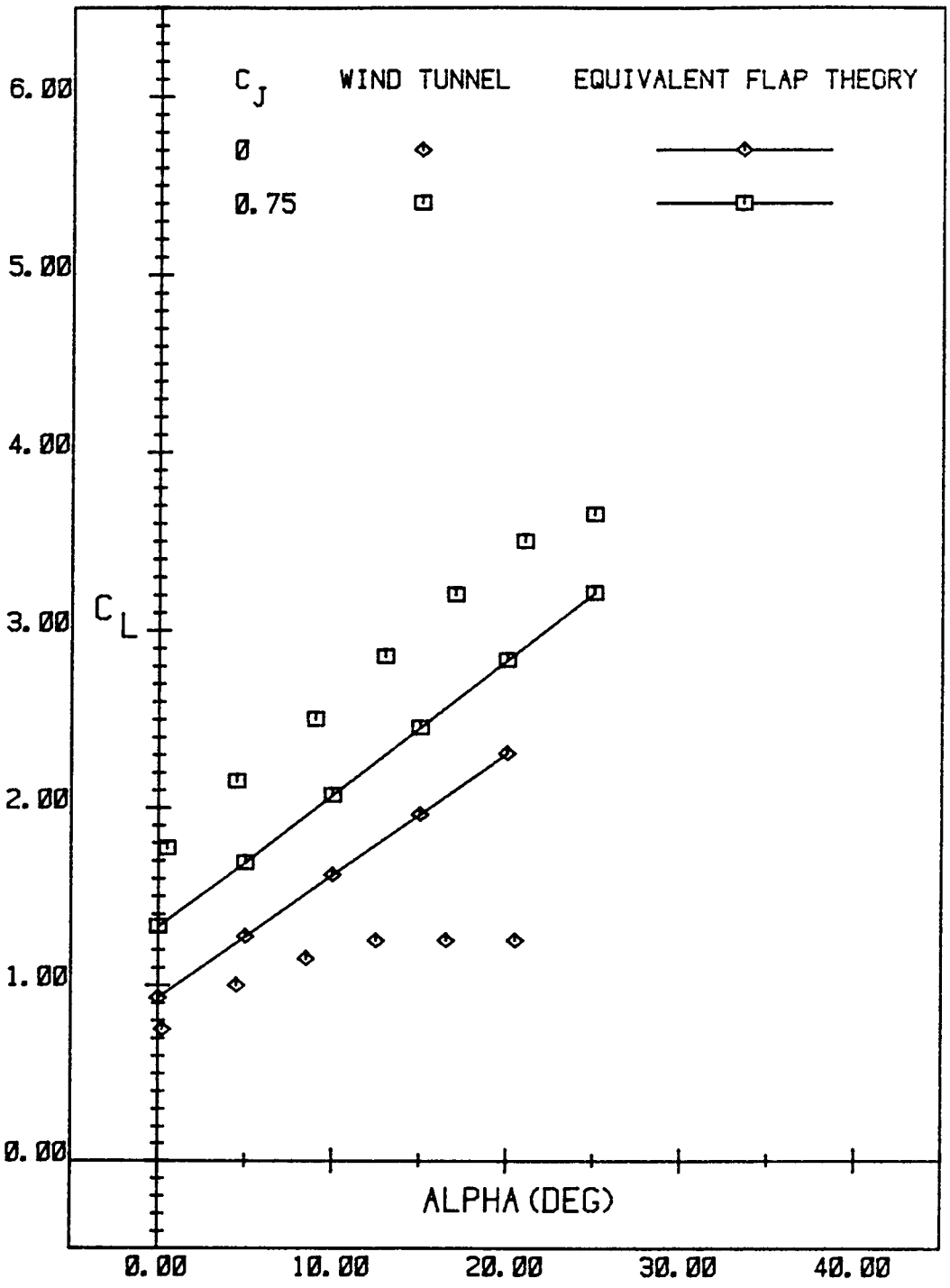


Figure 3.5 Comparison of Equivalent Flap Theory with full scale data for $\delta_F = 30^0$ (upper wing removed)

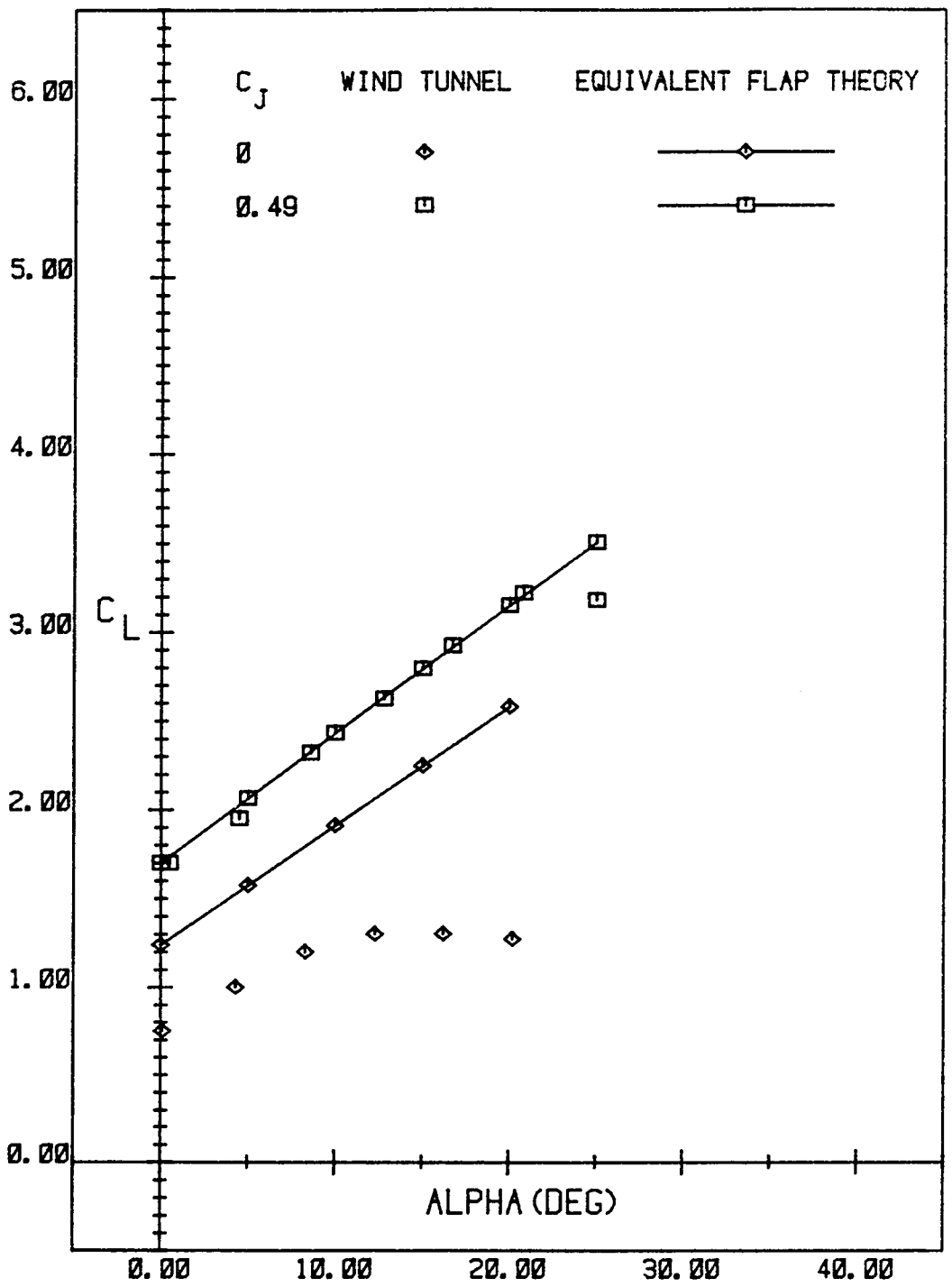


Figure 3.6 Comparison of Equivalent Flap Theory with full scale data for $\delta_F = 45^\circ$ (upper wing removed)

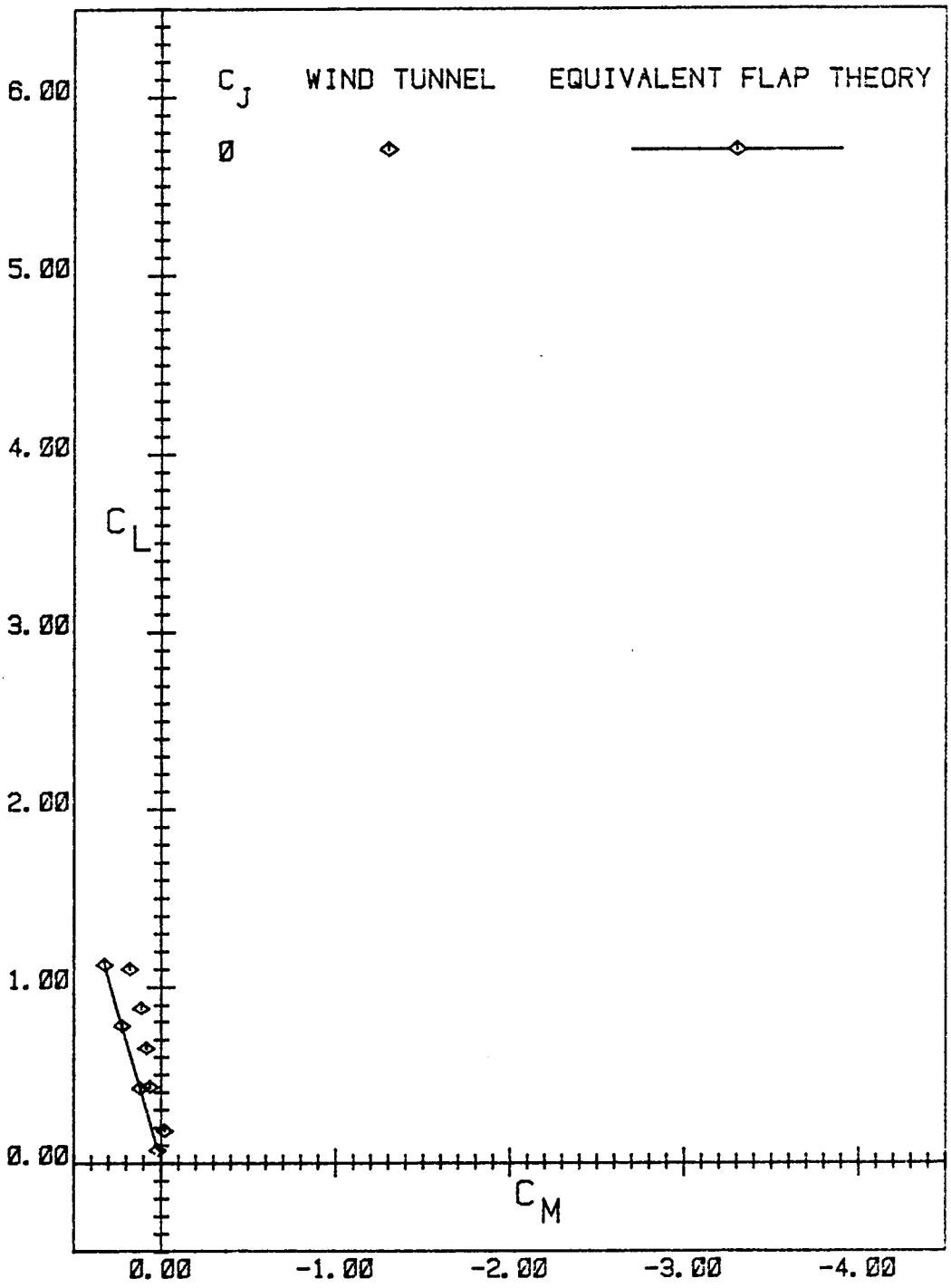


Figure 3.7 Comparison of Equivalent Flap Theory with full scale data for $\delta_F = 0^\circ$ (upper wing and horizontal tail removed)

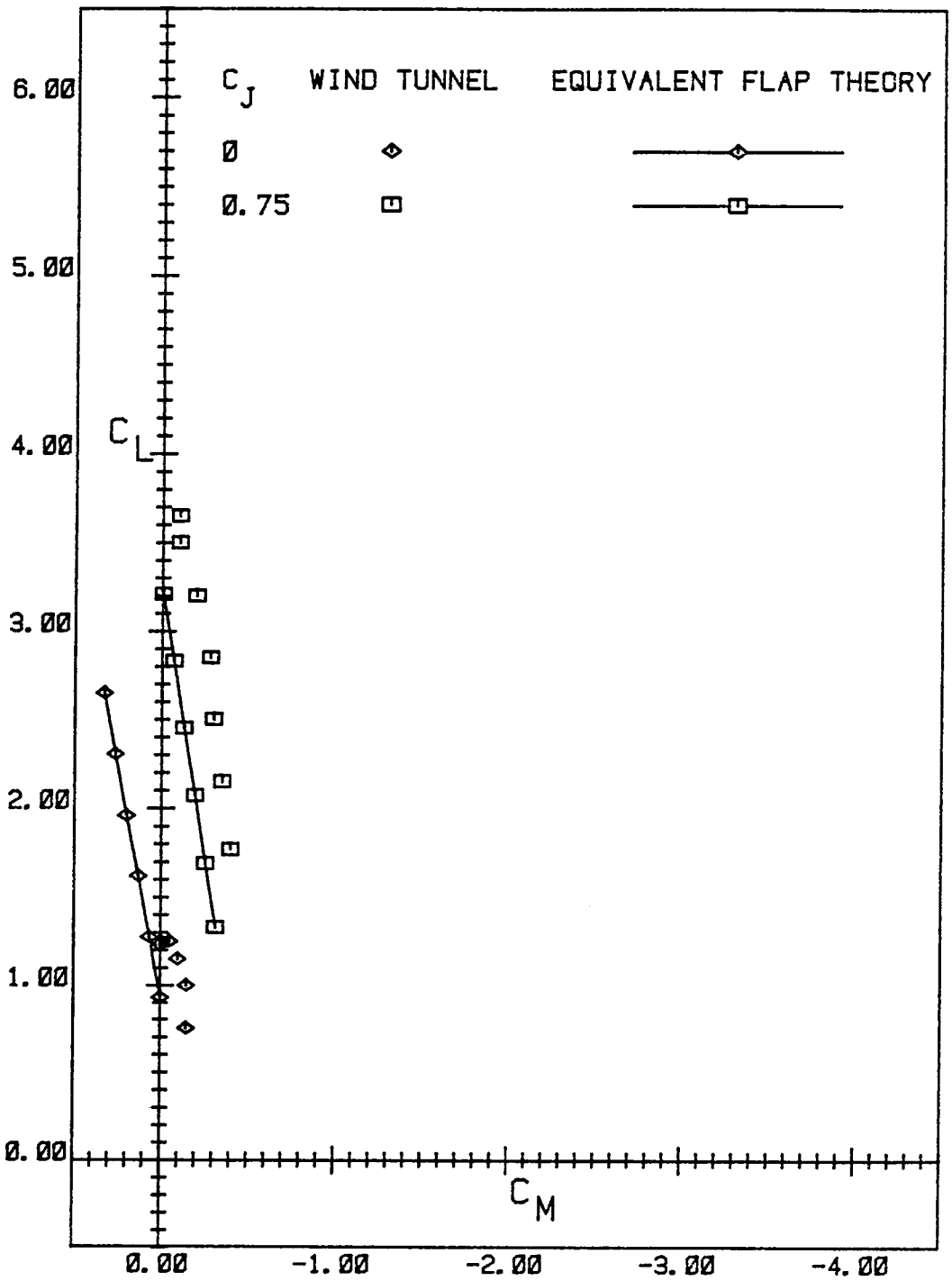


Figure 3.8 Comparison of Equivalent Flap Theory with full scale data for $\delta_F = 30^\circ$ (upper wing and horizontal tail removed)

full scale wind tunnel experiments for the JETWING aircraft with the upper wing removed. Figure (3.9) through Figure (3.13) show the predicted spanwise distribution of local C_ℓ and local C_m.

It is quite obvious that for $C_J = 0$ cases, C_L is being overpredicted for all but when $\delta_F = 0$. A possible cause for this is the nozzle on the wing upper surface, causing the flow to separate, substantially reducing the lift generated. For $\delta_F = 0$, the flow may reattach itself on the upper surface somewhere downstream of a "separation bubble". In this case there would be practically no loss of lift. Again, for $C_J > 0$ cases, C_L is consistently being underpredicted for all δ_F. Also, this shortfall in C_L increases with increasing α and increasing C_J. This can be explained by the fact that Jacob's Equivalent Flap Theory assumes that the jet is being issued at the trailing edge of the mechanical flap, whereas in reality the nozzle exit in the JETWING aircraft is situated somewhere around 33% of the chord aft of the wing leading edge.

This leads to two opposing effects: First, the actual lift is lower than the theoretical lift due to scrubbing losses of the jet sheet on the upper surface. Hence, equivalent flap length and resulting theoretical lift should have been smaller if the jet velocity at the trailing edge was used instead of actual nozzle exit velocity. Second, the actual lift is higher than the theoretical value. This is due to the increase in velocity on the upper surface of the wing, induced by the jet, which also causes circulation to increase. This additional circulation is directly proportional to the velocity difference between the upper and lower wing surface, and should more than offset the loss due

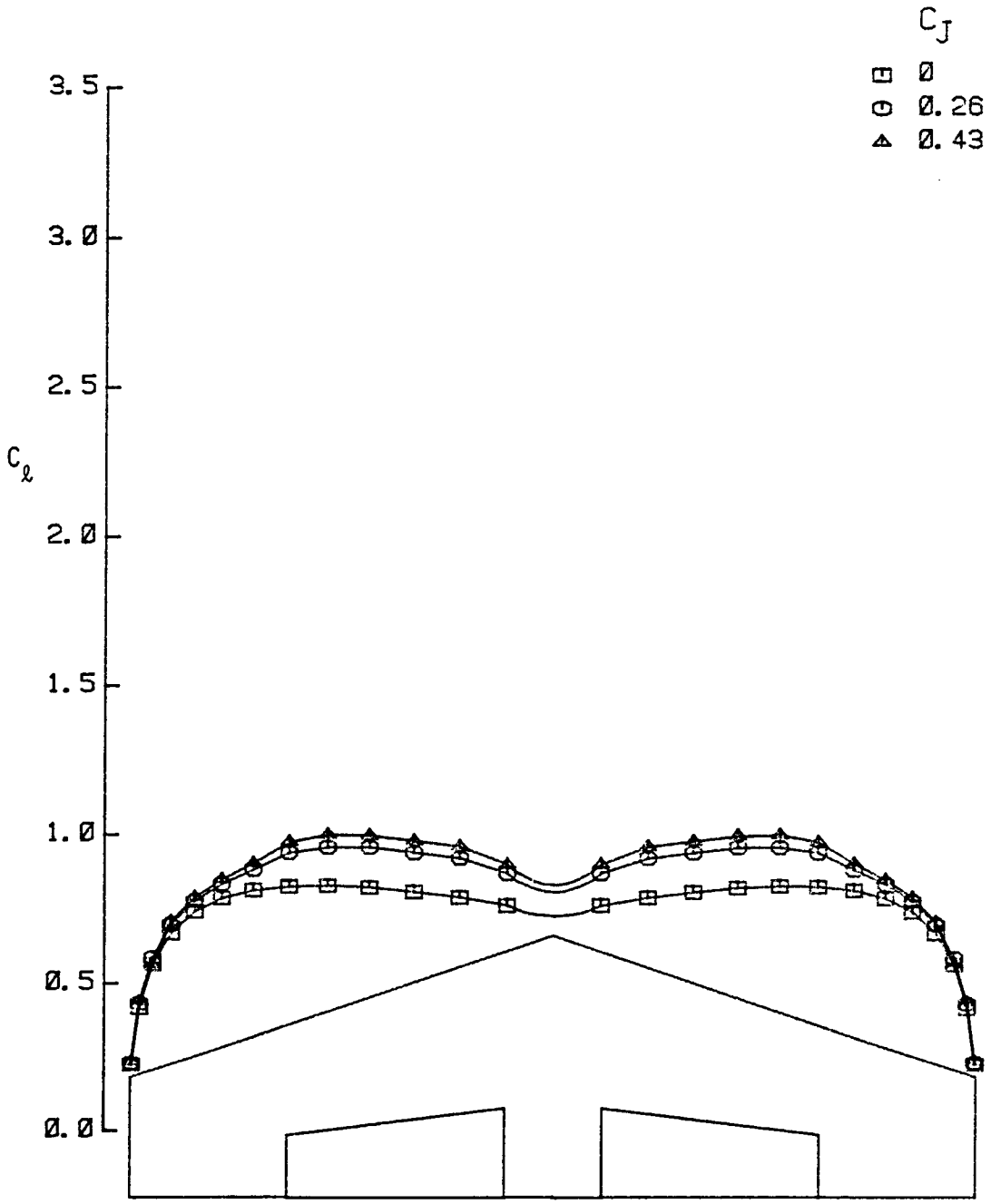


Figure 3.9 Spanwise distribution of C_ℓ for $\alpha = 10^\circ$ and $\delta_F = 0^\circ$

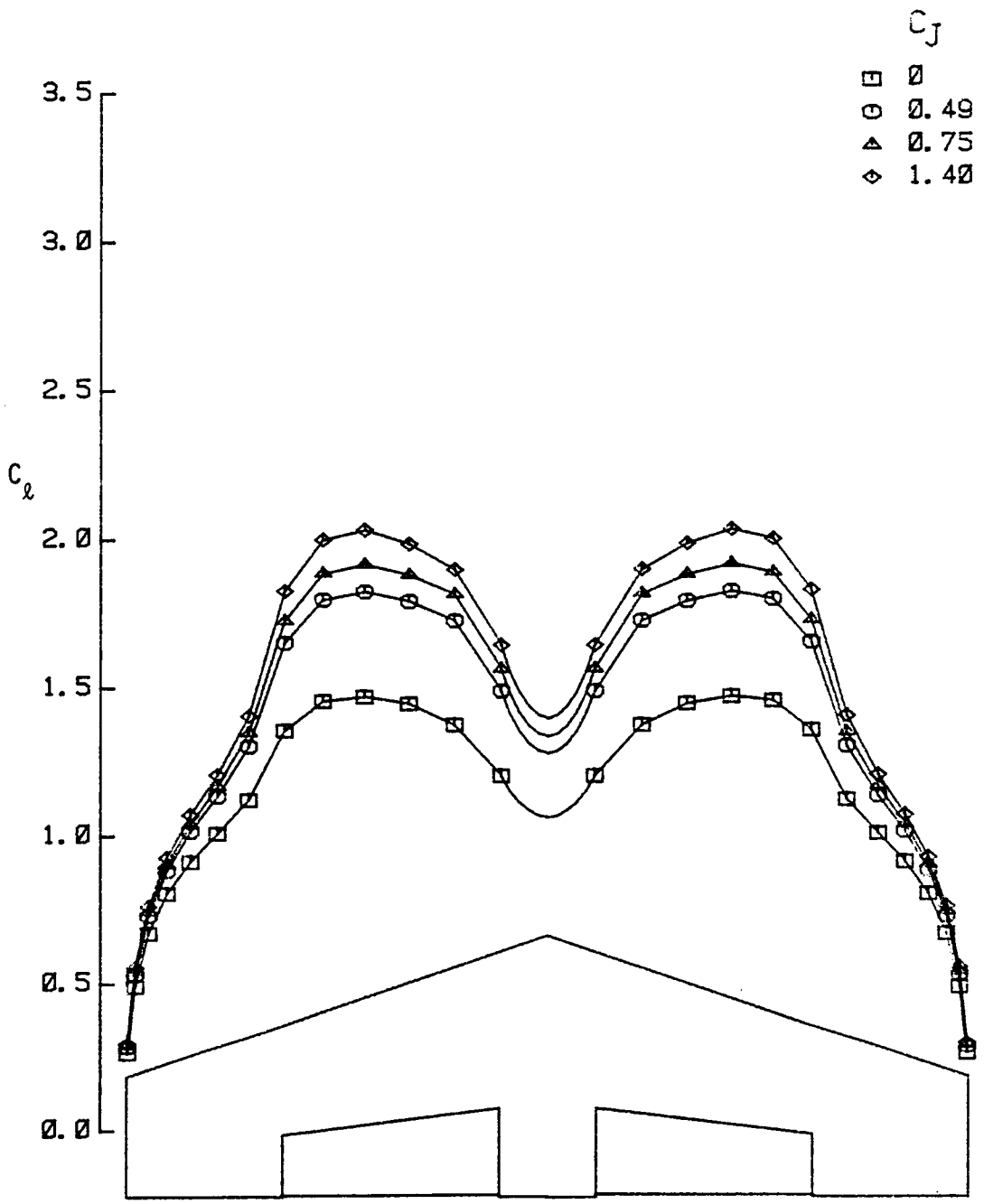


Figure 3.10 Spanwise distribution of C_ℓ for $\alpha = 10^\circ$ and $\delta_F = 15^\circ$

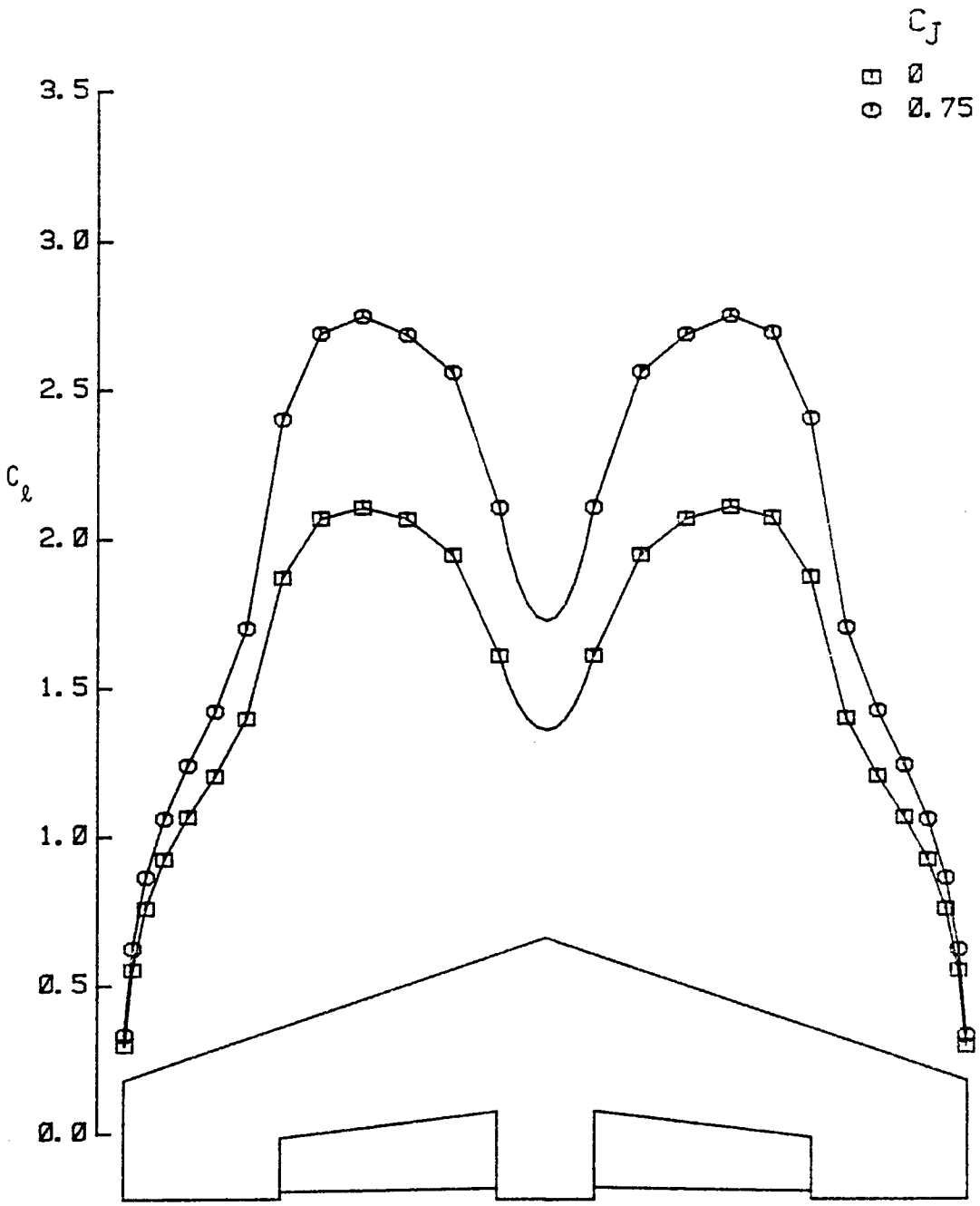


Figure 3.11 Spanwise distribution of C_ℓ for $\alpha = 10^\circ$ and $\delta_F = 30^\circ$

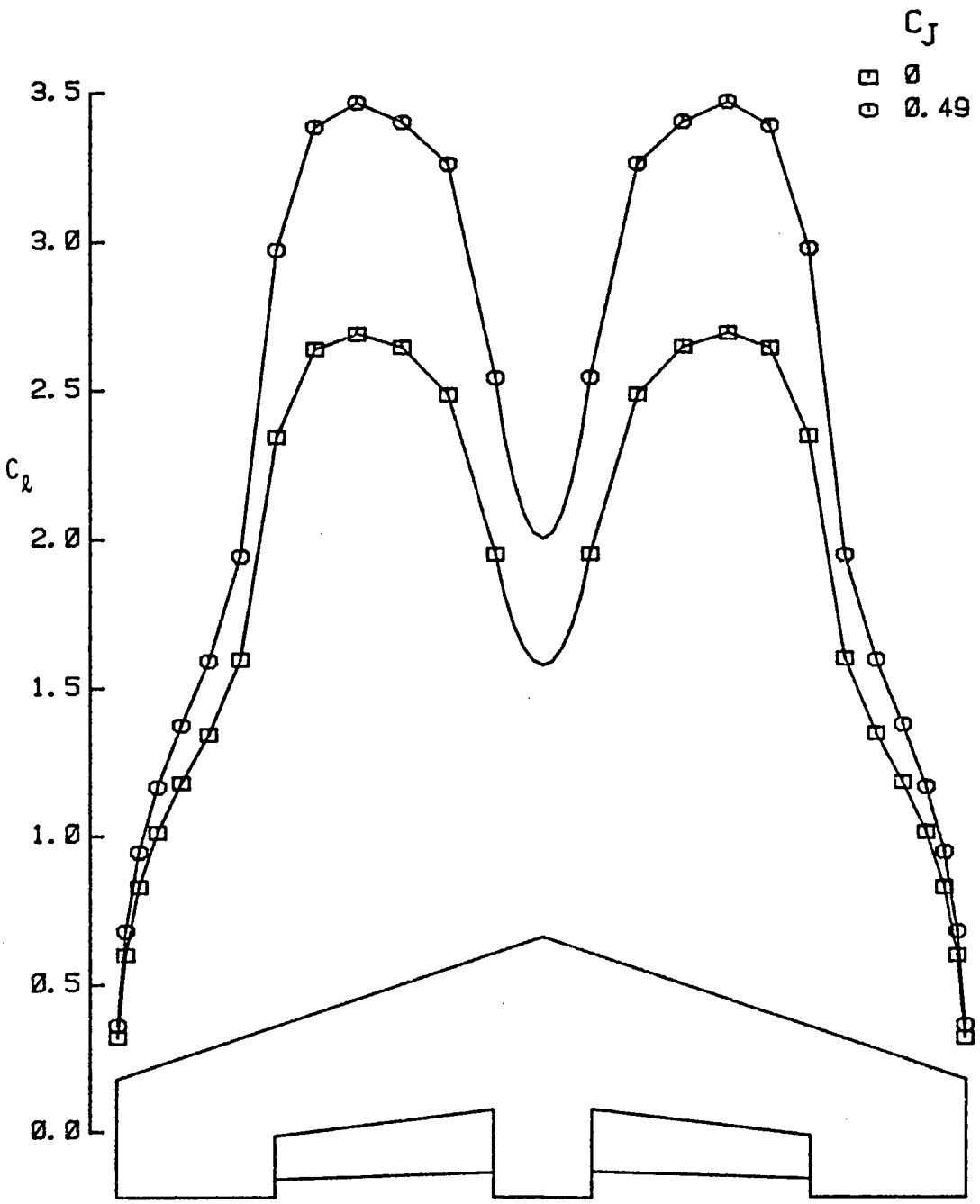


Figure 3.12 Spanwise distribution of C_ℓ for $\alpha = 10^\circ$ and $\delta_F = 45^\circ$

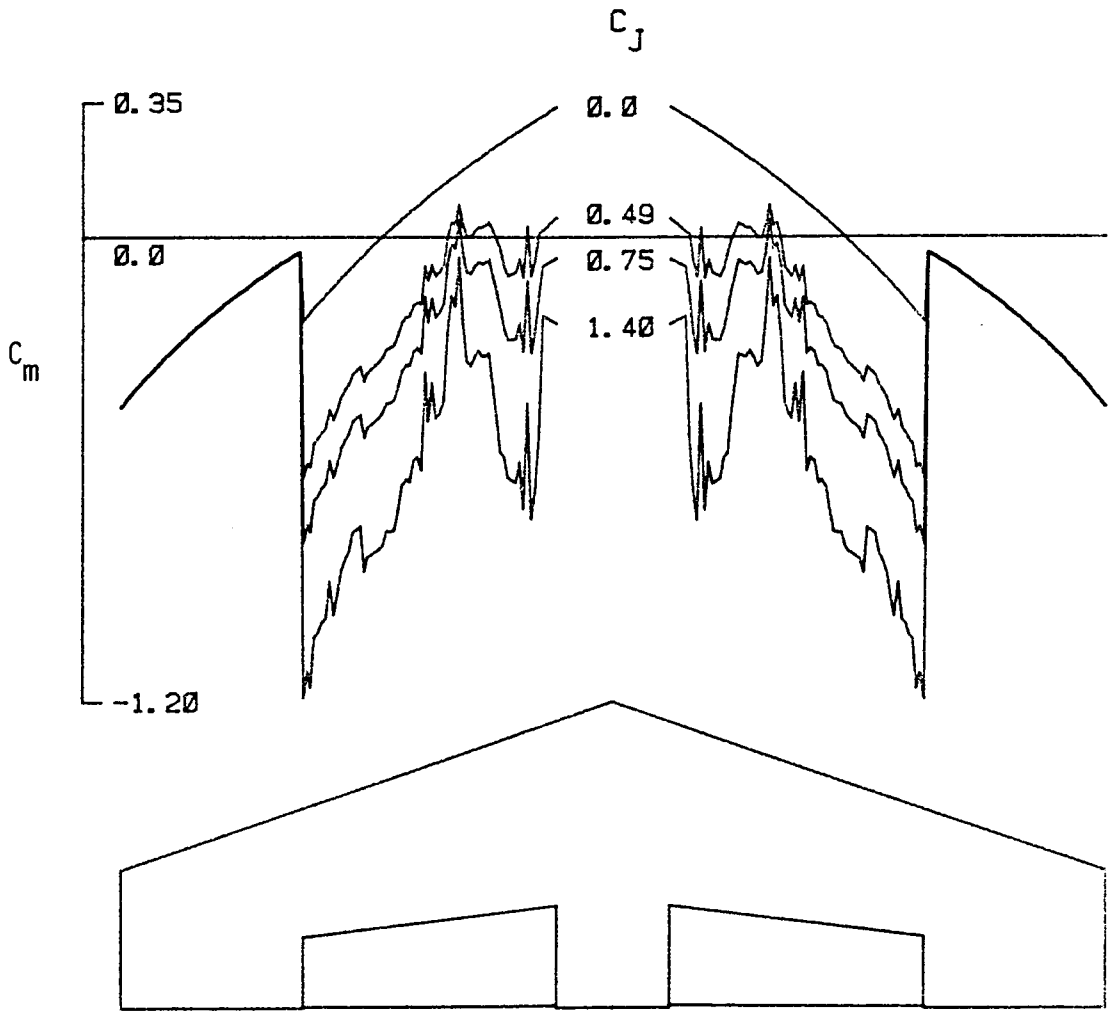


Figure 3.13 Spanwise distribution of C_m for α = 10° and δ_F = 15°

to scrubbing. Again, it is easy to see that with increasing C_J this additional lift will also increase. This additional supercirculation lift is concentrated in the rear portion of the wing which generates an additional negative pitching moment. Hence, if this lift is accounted for, the predicted C_L should be more positive and C_M more negative than the present values. This change would bring the theoretical C_L vs. C_M plots closer to the experimental plots.

It is felt that without getting into the theory of a turbulent wall jet, this missing supercirculation lift cannot be estimated. Hence, in the next couple of chapters a theory of a turbulent wall jet in an adverse pressure gradient is developed and is used to obtain the additional lift from the momentum consideration.

One problem for the Equivalent Flap Theory is that for high C_J, particularly if coupled with high δ_F, computer convergence on the induced angle of attack may be unreasonably time consuming. However, this time has been found to be satisfactory up to approximately $C_J = 1$ and $\delta_F = 30°$. For lower δ_F, higher values of C_J can be used in order to achieve a comparable run time.

Multhopp's Lifting Line Theory is used here because of its simplicity. Another method can be used in its place if better accuracy is desired.

CHAPTER IV

THEORY OF TURBULENT JETS

Turbulent Wall Jets

The term "wall jet" was probably first introduced by Glauert [43] to describe the flow of a jet along a straight wall when the pressure everywhere equals that of the surrounding fluid which is at rest. A tangential wall jet is the flow of high velocity fluid emanating from a narrow slot and blowing tangentially over a rigid wall. The flow of a wall jet mixing with an external moving stream has drawn considerable basic and applied interest in the past because it incorporates the characteristics of both a boundary layer and a free jet. Tangential wall jets are generally used in practice: (a) to control turbulent boundary layer separation on high lift airfoils and thereby achieve a large increase in lift, (b) to prevent separation and improve the pressure recovery in wide angle diffusers, (c) to cool a surface exposed to a stream of hot gas as in the case of combustion chambers and exhaust nozzles of rocket motors, (d) to heat a surface exposed to cold temperatures.

A typical wall jet velocity profile is shown in Figure 4.1. This type of blown boundary layer is referred to as a "simple" wall jet to distinguish it from the even more complicated flow which can exist downstream of the blowing slot when the upstream boundary layer has a relatively large momentum deficit and the pressure gradient is strongly adverse (Figure 4.2). In the latter case, the profile would have a

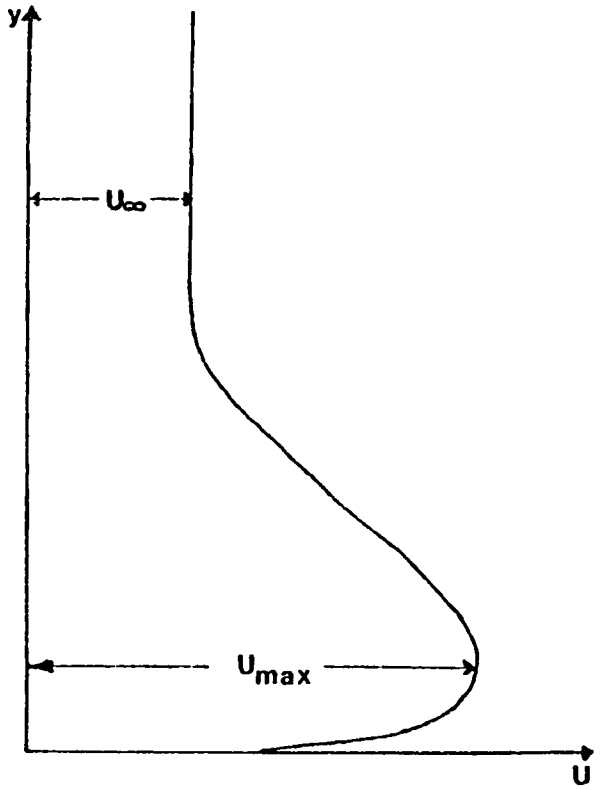


Figure 4.1 Velocity profile for a "Simple" wall jet

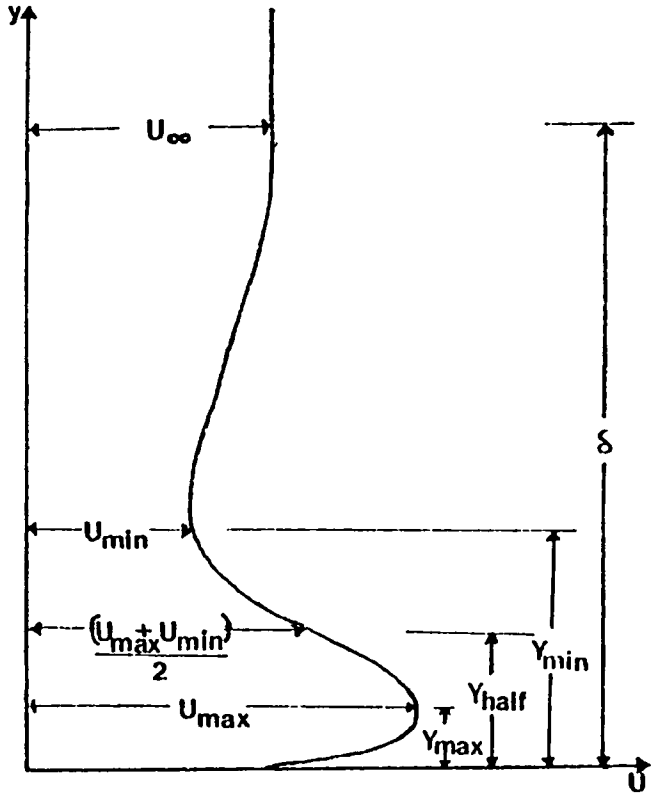


Figure 4.2 Velocity profile for a blown boundary layer

velocity minimum. Although, the word "simple" is used to describe the profile shown in Figure 4.1, it is nevertheless more complicated than many two-dimensional shear flows, incorporating some features of a boundary layer and some features of a free jet.

Previous Work on Wall Jets

Wall jets have been investigated quite extensively in the past. However, most work is concerned with the case where the ratio of jet velocity to free stream velocity is large (in the range of 2 to infinity), and with a negligible upstream boundary layer at the slot. The reason for the concentration of effort on the higher velocity ratio is mainly because of the fact that the velocity profiles contain only a velocity maximum. In such cases the flow can be analyzed approximately by methods of velocity profile similarity. Glauert [43] obtained similarity solutions for both laminar and turbulent, radial and plane, wall jets in which the form of velocity distribution across the jet does not vary along its length. Even in the cases where the study of wall jets at low velocity ratios was attempted, the momentum deficit of the upstream boundary layer at the slot was small. In practical applications, however, the jet usually mixes with a thick upstream boundary layer, giving rise to a velocity profile shown in Figure 4.2, rather than that of a "simple" wall jet as shown in Figure 4.1.

Recently Launder and Rodi [44] have given a comprehensive review of experimental measurements and modeling of turbulent wall jets. Bradshaw and Gee [45] presented mean flow measurements in a blown boundary layer

along with measurements in simple wall jets on curved and plane surfaces. They identified two essentially different modes of "separation", one involving reversed flow at the wall, and the other having reversed flow in the wake at the velocity minimum. Newman [46] described the mechanism of two-dimensional, incompressible, turbulent jets around a circular cylinder, and the reattachment of a jet to an inclined wall. This mechanism was obtained from the entrainment properties of the jet. Gartshore and Newman [47] described an integral calculation method for wall jets in arbitrary pressure gradients. This method is primarily for the use with small upstream boundary layers. However, they did attempt to account for a large upstream boundary layer by changing the starting conditions. They also presented measurements of mean quantities for wall jets under zero, and adverse, pressure gradients with small upstream boundary layers. Kind [48] extended Gartshore and Newman's calculation method to deal with strongly curved wall jets in the presence of moderately thick upstream boundary layers. The upstream boundary layer was accounted for by using a revised method of starting, and by assuming that the stagnation pressure remains constant along streamlines outside the wall jet. He also presented mean flow measurements of wall jets on the cylindrical trailing edge of a circulation control airfoil.

The methods mentioned above were applicable for high jet velocity ratios (greater than 2.0) and small upstream boundary layers. Goradia and Colwell [49] measured mean velocity profiles of several wall jets under adverse pressure gradients in a two-dimensional diffuser with low jet velocity ratios (in the neighborhood of 1 to 2). The velocity data

were used to formulate empirical relationships between parameters such as the form factor, H, and energy form factor, and to derive empirical expressions for the velocity profiles. The measurements were also utilized for the calculation of wall shear, and shear distribution, by numerical methods. Saripalli and Simpson [50] conducted measurements, and made theoretical prediction, of flow properties of a two-dimensional, incompressible, asymmetric wall jet with a velocity ratio of less than 2. These measurements and predictions were made with the wall jet submerged under a thick upstream boundary layer with zero and adverse pressure gradients. Mabuchi and Kumada [51] considered the heat transfer characteristics of turbulent wall jets with adjacent boundaries.

Formulation of the Problem

If a nozzle is located on the upper surface of an airfoil, the flow of engine exhaust behind that nozzle constitutes a turbulent wall jet in the presence of a coflowing external stream in an adverse pressure gradient. This flow is shown in Figure 4.3. Abramovich [52] has given a fairly comprehensive theory for this type of flow. This theory has been modified to account for the flow over an airfoil at an angle of attack.

For the sake of simplicity, we shall assume the composition of the jet is the same as that of the surrounding medium which is incompressible. In addition, we shall assume that in the first section at the free boundary, a velocity change occurs from u_{o1} to u_{o2} and the thickness of the boundary layer at the wall is equal to zero, i.e., the

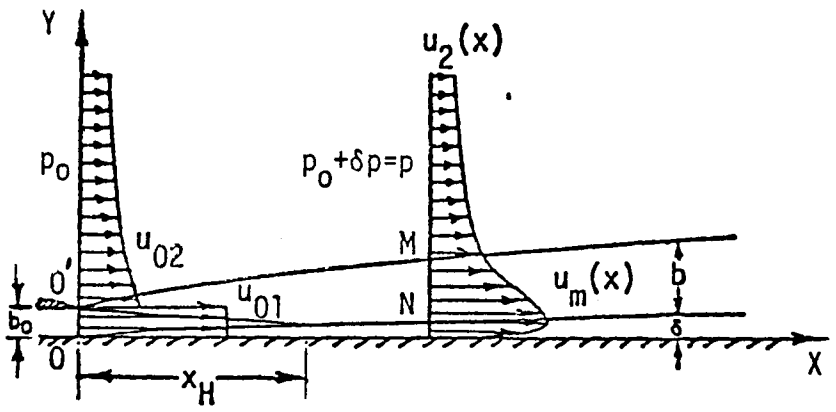


Figure 4.3 Idealized flow produced by a turbulent wall jet in a coflowing external stream in adverse pressure gradient

boundary layer at both edges of the jet begins to develop at the initial section 00'. Initially, there exists a potential core which gradually decreases in width as both the mixing layer and the wall boundary layer expand. When those two layers join, the potential core completely disappears, and the velocity profile takes the form given in Figure 4.1. The region where the potential core exists is called the initial region of the flow and the subsequent flow is called the main region of the flow. Some workers have considered a transition region in between them. For convenience, we shall assume that the length of the transition region is zero, i.e., the transition region reduces to a transition section. In the next few sections, we shall consider, analytically, the development of the flow parameters in both the initial and the main regions.

Mixing Zone of a Two-Dimensional Jet of Finite Thickness in a Coflowing External Stream in an Adverse Pressure Gradient

We shall consider the influence of varying pressure in the mixing zone on the fundamental flow properties (see Figure 4.4). If the thickness of the mixing zone is small in comparison with the length ($b \ll x$), which is an inherent property of the boundary layer, then one can neglect the pressure change across the thickness of the mixing zone.

Suppose, we are given the pressure change along the length of the mixing zone, $p = f(x)$, and the initial values of the main components of velocities u_{01} and u_{02}. Because both flows beyond the limits of the mixing zone are potential, the total pressures on the boundary of this zone are constants, but are not identical, i.e.,

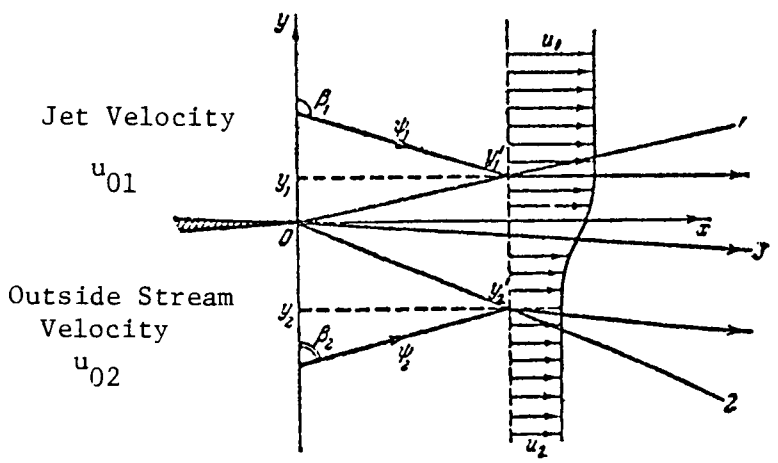


Figure 4.4 Boundary layer of a jet in a coflowing stream ($u_2 > 0$)

$$p_2^* = p_{o2}^* = \text{Constant}, \quad p_1^* = p_{o1}^* = \text{Constant} \tag{4.1}$$

where * refers to total parameters.

Also, the static pressures are same when x is identical, i.e.,

$$p = p_1 = p_2 = f(x) \tag{4.2}$$

The relation between local velocity and pressure in the potential part of the flow can be derived from compressible Bernoulli's equation using isentropic relation, and takes the form:

$$\frac{p}{p_{o1}^*} = \left(1 - \frac{u_1^2}{u_{1max}^2}\right)^{\frac{k}{k-1}}$$

$$\frac{p}{p_{o2}^*} = \left(1 - \frac{u_2^2}{u_{2max}^2}\right)^{\frac{k}{k-1}} \tag{4.3}$$

Where u_1 and u_2 are the velocities of the flow at the boundaries of the mixing zone, and u_{1max} and u_{2max} are the maximum possible values of the gas velocities, corresponding to its state, at these boundaries. All through this analysis, while using Bernoulli's equation, the transverse velocities are neglected, assuming them to be very small compared to the longitudinal velocities. At low subsonic gas velocities, instead of equation (4.3), we may assume

$$p_{o1}^* - p = \rho_1 \frac{u_1^2}{2} \quad \text{or} \quad p_o - p = \frac{1}{2}\rho_1(u_1^2 - u_{o1}^2)$$

$$p_{o2}^* - p = \rho_2 \frac{u_2^2}{2} \quad \text{or} \quad p_o - p = \frac{1}{2}\rho_2(u_2^2 - u_{o2}^2) \tag{4.4}$$

where p_o = static pressure at the nozzle exit.

For the case of mixing of jets of an identical incompressible fluid ($\rho_1 = \rho_2 = \rho$ = constant), we obtain from equation (4.4),

$$u_2^2 - u_{o2}^2 = u_1^2 - u_{o1}^2 \tag{4.5}$$

We define,

$$\frac{u_1^2}{u_{o1}^2} = a_1 = \frac{1 - m_o^2}{1 - m^2} \tag{4.6}$$

where,

$$m = \frac{u_2}{u_1}\ ,\ m_o = \frac{u_{o2}}{u_{o1}}\ ,\ a_1 = 1 + \frac{p_o - p}{\rho \frac{u_{o1}^2}{2}} \tag{4.7}$$

It follows from equation (4.4) that a longitudinal pressure gradient is possible only in the presence of fluid motion at both boundaries of the mixing zone, i.e., $u_1 \neq 0$, $u_2 \neq 0$.

The magnitude of the negative pressure gradient is in no way limited. The positive pressure gradient, however, must not exceed a certain value, because this might bring to a complete halt the stream which has the smaller initial velocity.

Actually, we see from equation (4.6) that for ρ = constant, the value $m = 0$, (i.e., $u_2 = 0$) is obtained when

$$a_1 = 1 - m_o^2,\ \text{or}\ \bar{p} = \frac{p - p_o}{\rho \frac{u_{o1}^2}{2}} = m_o^2 \tag{4.8}$$

Thus, the possible increase of pressure in the mixing zone is restricted by the condition:

$$\bar{p} \leq m_o^2 \tag{4.9}$$

For instance, when $m_0 = 0.5$, the pressure increase in the mixing zone cannot be greater than one-fourth of the total head of the jet which has a larger velocity.

It is known that the velocity profile in the boundary layer of a fluid moving near a solid wall depends on the longitudinal pressure gradient, for a negative gradient the velocity profile is fuller, and for a positive gradient it is less full. In the mixing region of the jet, the velocity profile should not depend on the longitudinal pressure gradient. Because, on the edges of the jet boundary layer (of finite thickness) the transverse velocity gradients in all cases would be zero. Thus, in solving the problem of a jet boundary layer in the presence of a pressure gradient the velocity profile can be determined from an empirical expression based on experimental observation,

$$\frac{u_1 - u}{u_1 - u_2} = f(\eta) = (1 - \eta^{3/2})^2 \quad , \eta = \frac{y - y_2}{b} \tag{4.10}$$

which was first encountered in the works of Schlichting. The equation of continuity for the contour depicted in Figure 4.4 by a dashed curve can be written in the form:

$$\left(u_{o1}y_1 - \int_0^x v_1 dx\right) + \left(-u_{o2}y_2 + \int_0^x v_2 dx\right) = \int_{y_2}^{y_1} u dy \tag{4.11}$$

where, v_1 and v_2 are the transverse velocities on the edges of the mixing zone, i.e., o1 and o2 respectively.

The momentum equation for the same contour gives:

$$(p_o - p)(y_1 - y_2) + \rho u_{o1}\left\{u_{o1}y_1 - \int_0^x v_1 dx\right\}$$

$$+ \rho u_{o2}\left\{- u_{o2}y_2 + \int_0^x v_2 dx\right\} = \rho \int_{y_2}^{y_1} u^2 dy \tag{4.12}$$

In equations (4.11) and (4.12), the transverse component of velocities (v_1, v_2) on the boundaries of the mixing zone are variables.

Multiplying both sides of equation (4.11) by ρu_{02} and subtracting the resulting expression from equation (4.12), we obtain,

$$(p_o - p)(y_1 - y_2) + \rho(u_{o1} - u_{02}) \left\{ u_{o1} y_1 - \int_0^x v_1 \, dx \right\}$$

$$= \rho \int_{y_2}^{y_1} u(u - u_{02}) \, dy \tag{4.13}$$

From the differential equation of continuity,

$$\frac{\partial u_1}{\partial x} + \frac{\partial v_1}{\partial y} = 0 \tag{4.14}$$

we obtain, $v_1 = -\int \frac{\partial u_1}{\partial x} \, dy + \text{constant}$.

Since, we are considering the case in which the pressure changes only along the x-axis, i.e., the magnitude of $\frac{\partial u_1}{\partial x}$ is independent of y, then,

$$v_1 = - y_1 \frac{\partial u_1}{\partial x} + \text{constant} \tag{4.15}$$

where the integration constant is determined from the boundary condition. In our case, the mixing layer boundary will be exactly the same as in the case of an expansion of a jet of finite thickness ($2 b_o$) with velocity u_{o1}, into an infinite stream of the same fluid having velocity u_{02} at the initial cross section of the jet. Then, it follows from the symmetry condition that on the axis of this jet $y_1 = b_o$ and $v_1 = 0$.

Then, $b_o \frac{\partial u_1}{\partial x} = \text{constant}, \; v_1 = (b_o - y_1) \frac{\partial u_1}{\partial x}$ (4.16)

Integrating equation (4.16), we obtain,

$$\int_0^x v_1 dx = (b_o - y_1) \int_0^x \frac{\partial u_1}{\partial x} dx = (b_o - y_1)(u_1 - u_{o1}) \tag{4.17}$$

If we substitute, equation (4.17) into equation (4.13), we have,

$$(p_o - p)(y_1 - y_2) + \rho(u_{o1} - u_{o2})[u_{o1}y_1 + (b_o - y_1)(u_{o1} - u_1)]$$
$$= \rho \int_{y_2}^{y_1} u(u - u_{o2}) \, dy \tag{4.18}$$

or after dividing by $b\rho u_{o1}^2$, and introducing the notation defined in equation (4.7),

$$2(a_1 - 1) + (1 - m_o)\left[\frac{b_o}{b} - \left(\frac{b_o}{b} - \frac{y_1}{b}\right)\frac{u_1}{u_{o1}}\right]$$
$$= \left(\frac{u_1}{u_{o1}}\right)^2 \int_0^1 \left(\frac{u}{u_1}\right)^2 d\eta - m_o \frac{u_1}{u_{o1}} \int_0^1 \frac{u}{u_1} d\eta \tag{4.19}$$

Here, $b = y_1 - y_2$ is the thickness of the mixing region,

$$\eta = \frac{y - y_2}{b}, \quad d\eta = d\left(\frac{y}{b}\right)$$

The integrals in equation (4.19) has been obtained in Appendix IV by using the velocity profile of equation (4.10).

$$\int_0^1 \left(\frac{u}{u_1}\right)^2 d\eta = 0.416 + 0.268 \, m + 0.316 \, m^2$$

$$\int_0^1 \frac{u}{u_1} d\eta = 0.55 + 0.45 \, m$$

When we use these equalities, and also equations (4.6) and (4.19), we obtain the following system of two equations in three unknowns $\left(m, \frac{y_1}{b} \text{ and } \frac{b_o}{b}\right)$:

$$2(a_1 - 1) + (1 - m_o)(1 - \sqrt{a_1}) \frac{b_o}{b} + (1 - m_o) \frac{y_1}{b} \sqrt{a_1} =$$

$$a_1(0.416 + 0.268\, m + 0.316\, m^2) - m_o\sqrt{a_1}(0.55 + 0.45\, m) \qquad (4.20)$$

$$m = \sqrt{\frac{a_1 - 1 + m_o^2}{a_1}} \qquad (4.21)$$

The rate of thickening of the mixing region given by an empirical relation based upon the experimental observation,

$$b = 0.27 \frac{1 - m}{1 + m} x \qquad (4.22)$$

completes the system of equations required to obtain the flow parameters.

Initial Region of a Wall Jet

In order to obtain the length of the initial region, x_H, in which the equations derived in the previous section are valid, one has to resort to an iterative technique. The initial region extends from the nozzle to the section where the wall boundary layer and mixing layer joins together. Hence,

$$b_o = \delta_H + y_1' \qquad (4.23)$$

where,

b_o = nozzle width

δ_H = wall boundary layer thickness at x_H

y_1' = transverse coordinate of the lower edge of the mixing zone at x_H measured from the longitudinal plane passing through the upper edge of the nozzle.

According to the boundary layer theory, the relative thickness of the turbulent boundary layer at the wall, without a pressure gradient is,

$$\frac{\delta_H}{x_H} = \frac{0.37}{Re_{x_H}^{0.2}} \tag{4.24}$$

where, $Re_{x_H} = \frac{\rho u_1 x_H}{\mu}$

Therefore, from equation (4.23), it can be written,

$$\frac{x_H}{b_o} = \frac{1}{\frac{y_1'}{x_H} + \frac{\delta_H}{x_H}} \tag{4.25}$$

Since, x_H appears on both sides of the equation (4.25), a Newton-Rapson approach was adopted for solving it. The velocity profile in the wall boundary layer is assumed to comply with the (1/7)th power law, i.e.,

$$\frac{u}{u_1} = \left(\frac{y}{\delta}\right)^{(1/7)} \tag{4.26}$$

and in the mixing region it is assumed as,

$$\frac{u}{u_1} = 1 - (1 - m)\left[1 - \left\{\frac{y - y_2}{b}\right\}^{1.5}\right]^2 \tag{4.27}$$

which is the same as equation (4.10).

Main Region of a Wall Jet

This region consists of a wall boundary layer and a jet mixing layer. Here again, we assume the velocity profile in the wall boundary layer obeys the (1/7)th power law, i.e.,

$$\frac{u}{u_m} = \left(\frac{y}{\delta}\right)^{(1/7)} = (\bar{y})^{(1/7)} \tag{4.28}$$

where, u_m = velocity at the edge of the wall boundary layer.

The equation for the velocity profile in the mixing layer of the jet takes the form:

$$\frac{u}{u_m} = m + (1 - m)(1 - \xi^{1.5})^2 \tag{4.29}$$

where, $\xi = \frac{y - \delta}{b}$ and $m = \frac{u_2}{u_m}$

To determine the characteristics of the flow, we write the momentum equation applicable to the contour OO'MN (see Figure 4.3):

$$\frac{1}{\rho} p_o b_o - \frac{1}{\rho} (p_o + \delta p)\, b$$

$$= - u_{o1}^2 b_o - \int_0^x u_2 \frac{\partial}{\partial x} \left(\int_0^{\delta} u dy + \int_{\delta}^{b+\delta} u dy \right) dx$$

$$+ \int_0^x u_m(x) \frac{\partial}{\partial x} \left(\int_0^{\delta} u dy \right) dx + \int_{\delta}^{b+\delta} u^2 dy \tag{4.30}$$

Differentiating equation (4.30) with respect to x, we obtain,

$$- \frac{b}{\rho}\frac{dp}{dx} - \frac{1}{\rho}(p_o + \delta p)\frac{db}{dx} = - u_2 \frac{\partial}{\partial x}\left[\int_0^{\delta} u\,dy + \int_{\delta}^{b+\delta} u\,dy\right]$$

$$+ u_m \frac{\partial}{\partial x}\left[\int_0^{\delta} u\,dy\right] + \int_{\delta}^{b+\delta} \frac{\partial(u^2)}{\partial x}\,dy$$

$$\text{or } - \left(\frac{b+1}{\rho}\right)\frac{dp}{dx} - \frac{1}{\rho}(p_o + \delta p)\frac{db}{dx} = (u_m - u_2)\int_0^{\delta} \frac{\partial u}{\partial x}\,dy$$

$$+ \int_{\delta}^{b+\delta} \frac{\partial(u^2)}{\partial x}\,dy - u_2 \int_{\delta}^{b+\delta} \frac{\partial u}{\partial x}\,dy \qquad (4.31)$$

After it is divided by u_2^2, equation (4.31) is transformed to,

$$\left(\frac{u_2 - u_m}{u_2}\right)\delta\int_0^1 \frac{\partial \bar{u}}{\partial x}\frac{dy}{\delta} + b\int_0^1 \frac{\partial \bar{u}}{\partial x}\frac{dy}{b} - b\int_0^1 \frac{\partial(\bar{u})^2}{\partial x}\frac{dy}{b}$$

$$= \frac{1}{u_2^2}\left[\frac{b}{\rho}\frac{dp}{dx} + \frac{p}{\rho}\frac{db}{dx}\right] \qquad (4.32)$$

where, $\bar{u} = \dfrac{u}{u_2}$

We define, $\chi = \dfrac{1}{m} = \dfrac{u_m}{u_2}$.

Hence, $(1 - \chi)\,\delta\displaystyle\int_0^1 \frac{\partial \bar{u}}{\partial x}\frac{dy}{\delta} + b\int_0^1 \frac{\partial \bar{u}}{\partial x}\frac{dy}{b} - b\int_0^1 \frac{\partial(\bar{u})^2}{\partial x}\frac{dy}{b} = \dfrac{(pb)'}{\rho u_2^2}$ (4.33)

From equation (4.28) and (4.29), it follows that within limits of the wall boundary layer, the velocity distribution law may be written in the form:

$$\bar{u} = \chi\, \bar{y}^{\,1/7} \tag{4.34}$$

and in the mixing layer of the jet in the form:

$$\bar{u} = 1 + (\chi - 1)(1 - \xi^{1.5})^2 \tag{4.35}$$

Differentiating equation (4.34) with respect to x, we obtain,

$$\frac{\partial \bar{u}}{\partial x} = \bar{y}^{1/7}\left(\chi' - \frac{\chi}{7}\frac{\delta'}{\delta}\right) \tag{4.36}$$

Hence, $$\int_0^1 \frac{\partial \bar{u}}{\partial x}\, d\bar{y} = \frac{7}{8}\left(\chi' - \frac{\chi}{7}\frac{\delta'}{\delta}\right) \tag{4.37}$$

From equation (4.35), it follows that

$$\frac{\partial \bar{u}}{\partial x} = \chi'\left(1 - \xi^{3/2}\right)^2 + \frac{3(\chi - 1)}{b}\,\delta'\xi^{1/2}\left(1 - \xi^{3/2}\right) + \frac{3(\chi - 1)}{b}\,b'\xi^{3/2}(1 - \xi^{3/2}) \tag{4.38}$$

$$\bar{u}\frac{\partial \bar{u}}{\partial x} = \chi'\left(1 - \xi^{3/2}\right)^2 + \frac{3(\chi - 1)}{b}\,\delta'\xi^{1/2}\left(1 - \xi^{3/2}\right) + \frac{3(\chi - 1)}{b}\,b'\xi^{3/2}\left(1 - \xi^{3/2}\right) + \chi'(\chi' - 1)\left(1 - \xi^{3/2}\right)^4 + \frac{3(\chi - 1)^2}{b}\,\delta'\xi^{1/2}(1 - \xi^{3/2})^3 + \frac{3(\chi - 1)^2}{b}\,b'\xi^{3/2}(1 - \xi^{3/2})^3 \tag{4.39}$$

Hence,

$$b\int_0^1 \frac{\partial \bar{u}}{\partial x}\, d\xi = 0.45\, b\chi' + (\chi - 1)\delta' + 0.45\, b'(\chi - 1) \tag{4.40}$$

$$b\int_0^1 \frac{\partial(\bar{u}^2)}{\partial x} d\xi = 2b\int_0^1 \bar{u}\frac{\partial \bar{u}}{\partial x}\, d\xi = 2\,[0.45\, b\chi' + (\chi - 1)\delta'$$

$$+ 0.45\, b'(\chi - 1) + 0.316\, b\chi'(\chi - 1) + 0.5(\chi - 1)^2\delta' +$$

$$+ 0.156(\chi - 1)^2 b'] \tag{4.41}$$

Substituting equations (4.37), (4.40) and (4.41) in equation (4.33), we have,

$$b\chi'(0.632\chi - 0.182) + b'(\chi - 1)(0.312\chi + 0.138)$$

$$+ \frac{7}{8}(\chi - 1)(\delta'\chi + \delta\chi') = \frac{bp' + pb'}{\rho u_2^2} \tag{4.42}$$

$$b'\left[(\chi - 1)(0.312\chi + 0.138) + \frac{0.7}{8}\chi^2 - \frac{p}{\rho u_2^2}\right] =$$

$$- b\left[\chi'(0.632\chi - 0.182) + \frac{0.7}{8}\frac{\chi'(\chi^2 - 2\chi)}{(\chi - 1)} - \frac{p'}{\rho u_2^2}\right]$$

$$\text{Hence, } \frac{b'}{b} = -\left(\frac{\chi'(0.632\chi - 0.182) + 0.0875\,\dfrac{\chi'(\chi^2 - 2\chi)}{(\chi - 1)} - \dfrac{p'}{\rho u_2^2}}{(\chi - 1)(0.312\chi + 0.138) + 0.0875\chi^2 - \dfrac{p}{\rho u_2^2}}\right) \tag{4.43}$$

Since it is not possible to obtain an analytic expression for p' for the problem in question, equation (4.43) has to be solved numerically. A forward marching technique along the chord was adopted.

In order to obtain the dependency of δ on x, one more equation is needed. From the treatment of the experimental data, Abramovich [52] concludes that in the absence of an accompanying flow, at any distance from the nozzle and in a wide range of variation of Reynold's numbers, an accurate relationship is:

$$\frac{\delta}{b} = 0.1 \tag{4.44}$$

With an accompanying flow, the relationship between the thickness of the wall boundary layer δ and the thickness of the jet b may be ascertained by the following method. It is known that the value of the fluctuation velocity at any point of the flow is proportional to the transverse gradient of the axial component of the velocity, i.e., $u' \sim \frac{\partial u}{\partial y}$. Differentiating equation (4.28) and (4.29) with respect to y, we obtain expressions for the fluctuation velocity in the jet:

$$u_1' = \frac{3(u_m - u_2)}{b} (1 - \xi_o^{3/2}) \xi_o^{1/2} = C_1 \frac{u_m - u_2}{b} \tag{4.45}$$

and in the wall boundary layer:

$$u_2' = \frac{u_m}{\delta} \frac{1}{7} (\bar{y}_o)^{-6/7} = C_2 \frac{u_m}{\delta} \tag{4.46}$$

Here ξ_o and $\bar{y}_o$ are the dimensionless coordinates of the points at which the fluctuation velocities u_1' and u_2' are determined. Assuming that in any cross section of the flow the order of magnitude of the fluctuations in the jet and in the wall boundary layer (by virtue of their interaction) is the same,

$$\text{i.e., } u_1' = u_2' \tag{4.47}$$

we obtain the equation relating the thickness of the jet and the thickness of the wall boundary layer:

$$\frac{\delta}{b} = \frac{C_2}{C_1} \frac{u_m}{u_m - u_2} \tag{4.48}$$

If $u_2 = 0$, $\frac{\delta}{b} = \frac{C_2}{C_1}$

Proceeding from the empirical condition, i.e., equation (4.44), if we assume $\frac{C_2}{C_1} = 0.1$, then equation (4.48) can be rewritten as:

$$\frac{\delta}{b} = 0.1 \frac{u_m}{u_m - u_2} = 0.1 \frac{x}{x - 1} \tag{4.49}$$

Equation (4.49) was used to calculate the wall boundary layer thickness, δ, knowing the jet thickness, b, as a function of x.

CHAPTER V

DETERMINATION OF ADDITIONAL SUPERCIRCULATION LIFT

An Analytical Method of Obtaining the Jet Velocity

In order to obtain the additional supercirculation lift due to the presence of a high energy jet on the upper surface of the wing, it was felt necessary to analytically predict the jet velocity at the nozzle exit.

From momentum considerations, we can write,

Gross Thrust = Net Thrust + Ram Drag

If we neglect fuel mass, then,

$$(\rho_{j1}A_{j1}V_{j1}^2 + \rho_{j2}A_{j2}V_{j2}^2) + A_{j1}(p_{j1} - p_a) + A_{j2}(p_{j2} - p_a)$$

$$= F_{net} + (\rho_{j1}A_{j1}V_{j1} + \rho_{j2}A_{j2}V_{j2}).V \qquad (5.1)$$

where,

A_j = Area of the jet

F_{net} = Net thrust

p_a = Ambient static pressure

p_j = static pressure of the jet

V = Aircraft speed

V_j = Velocity of the jet

ρ_j = Density of the jet

1 : Hot core air

2 : Cold by-pass air

Neglecting the pressure terms and dividing both sides by the product of the freestream dynamic pressure and the wing reference area, we get,

$$\frac{\rho_{j1}A_{j1}V_{j1}^2 + \rho_{j2}A_{j2}V_{j2}^2}{\frac{1}{2}\rho V^2 S} = \frac{F_{net}}{\frac{1}{2}\rho V^2 S} + \frac{(\rho_{j1}A_{j1}V_{j1} + \rho_{j2}A_{j2}V_{j2})\cdot V}{\frac{1}{2}\rho V^2 S}$$

Hence, $$\frac{\rho_{j1}A_{j1}}{\frac{1}{2}\rho S}\left(\frac{V_{j1}}{V}\right)^2 \left\{1 + \frac{\rho_{j2}A_{j2}V_{j2}^2}{\rho_{j1}A_{j1}V_{j1}^2}\right\}$$

$$= C_{T_N} + \frac{\rho_{j1}A_{j1}}{\frac{1}{2}\rho S}\left(\frac{V_{j1}}{V}\right)\left\{1 + \frac{\rho_{j2}A_{j2}V_{j2}}{\rho_{j1}A_{j1}V_{j1}}\right\} \qquad (5.2)$$

where C_{T_N} is the net thrust coefficient.

Now, $\frac{\rho_{j2}A_{j2}V_{j2}^2}{\rho_{j1}A_{j1}V_{j1}^2}$ = Ratio of cold to hot gross thrust

and $\frac{\rho_{j2}A_{j2}V_{j2}}{\rho_{j1}A_{j1}V_{j1}}$ = Ratio of cold to hot mass flow = By-pass ratio

These ratios are a stronger function of engine R.P.M. than velocity or altitude. Hence, for a particular engine R.P.M., they can be assumed constant. According to the engine analysis code developed by Pratt & Whitney specifically for JT15D-1, which powers the JETWING, the cold to hot gross thrust ratio at 55% N_1 (fan R.P.M.) and sealevel, static condition is about 3.25. Also, from the laser velocimeter thrust measurement experimental data, the cold to hot jet exhaust velocity ratio is found to be approximately 0.88 for 55% N_1.

Hence, by-pass ratio = $\frac{3.25}{0.88}$ = 3.69

Substituting,

$$1 + \frac{\rho_{j2}A_{j2}V_{j2}^2}{\rho_{j1}A_{j1}V_{j1}^2} = X \quad \text{and} \quad 1 + \frac{\rho_{j2}A_{j2}V_{j2}}{\rho_{j1}A_{j1}V_{j1}} = Y$$

and dividing both sides of equation (5.2) by $\frac{\rho_{j1}A_{j1}}{(1/2)\rho S}$, we obtain,

$$X\left(\frac{V_{j1}}{V}\right)^2 = \frac{C_{T_N}\frac{1}{2}\rho S}{\rho_{j1}A_{j1}} + Y\left(\frac{V_{j1}}{V}\right) \tag{5.3}$$

Dividing both sides of equation (5.3) by X, we get,

$$\left(\frac{V_{j1}}{V}\right)^2 - \left(\frac{Y}{X}\right)\left(\frac{V_{j1}}{V}\right) - C_{T_N}\frac{1}{2}\frac{\rho S}{X\,\rho_{j1}A_{j1}} = 0 \tag{5.4}$$

$$\text{Hence, } \frac{V_{j1}}{V} = \frac{1}{2}\left[\frac{Y}{X} + \sqrt{\left(\frac{Y}{X}\right)^2 + \frac{2\rho S}{X\,\rho_{j1}A_{j1}}\,C_{T_N}}\right] \tag{5.5}$$

Again, the net thrust coefficient, C_{T_N}, can be further expanded as:

$$C_{T_N} = C_J - \frac{A_0\rho(V\cos\alpha)^2}{\frac{1}{2}\rho SV^2} \tag{5.6}$$

where,

C_J = Gross thrust coefficient or blowing coefficient

α = aircraft's angle of attack

A_0 = inlet area = 4 sq.ft.

S = Wing reference area = 105.6 sq.ft.

Substituting equation (5.6) in equation (5.5), we finally obtain the expression for core air exhaust velocity as:

$$V_{j1} = \frac{V}{2}\left[\frac{Y}{X} + \sqrt{\left(\frac{Y}{X}\right)^2 + \frac{2}{X}\left(\frac{\rho}{\rho_{j1}}\right)\left(\frac{S}{A_{j1}}\right)\left(C_J - 2\frac{A_0}{S}\cos^2\alpha\right)}\right] \tag{5.7}$$

We obtain V_{j1} for the JETWING aircraft at 55% N_1 by substituting,

$X = 1 + 3.25 = 4.25$

$Y = 1 + 3.69 = 4.69$

$A_{j1} = 0.6688$ sq.ft.

As the density of the hot core gas is also needed, the temperature at the exhaust is obtained from the engine code as 425°C at 55% N_1. Hence,

$$\rho_{j1} = \frac{p_{j1}}{RT_{j1}} = \frac{2116.2}{(53.33)(1257)} = 0.03157 \text{ lbm/ft}^3$$

Then from equation (5.7) we obtain,

$$V_{j1} = \frac{V}{2}\left[1.1043 + \sqrt{1.2194 + 180.1(C_J - 0.0758\cos^2\alpha)}\right] \tag{5.8}$$

and $V_{j2} = 0.88V_{j1}$ (5.9)

Jet Induced Momentum--A Measure of Jet Induced Circulation

The additional circulation created by the presence of the jet over the upper surface of the wing is estimated as the integrated effect of the increase in momentum because of the jet, over the momentum created by the equivalent wing, nondimensionalized with respect to the momentum of the freestream.

The additional C_L can be written as,

$$\Delta C_L = \frac{\rho V^2 \int_{\text{span}} \int_{0.33c}^{c} \gamma_\Delta \, dxdz}{\frac{1}{2}\rho V^2 S} = \frac{2}{S}\int_{\text{span}}\int_{0.33c}^{c} \gamma_\Delta dxdz \tag{5.10}$$

where,

$$\gamma_\Delta = \frac{\int_0^y \rho_j u_j^2 dy}{\rho V^2 y} - \frac{\int_0^y (V + \frac{\gamma'}{2} V)^2 dy}{V^2 y}$$

u_j = jet velocity as obtained in the previous chapter

V = freestream velocity, i.e., aircraft speed

y = transverse distance

γ' = circulation due to equivalent wing

ρ = ambient air density

ρ_j = density of the jet

Velocity decay outside the mixing layer, in the transverse direction, is given by Oswatitsch [53] as,

$$U = \frac{U_0}{\left(1 + \frac{yU_0\left\{1 - \frac{U_0}{6}\right\}}{h}\right)^2} \tag{5.11}$$

where,

$$U = \frac{u - V}{c - V}$$

$$U_0 = \frac{u_S - V}{c - V}$$

c = Speed of sound

u_S = Velocity at the point from where y is measured

h = Reduced airfoil half thickness

$$= \frac{h'}{\beta\left(\frac{c}{V} - 1\right)}$$

h' = Upper surface coordinate

$$\beta = \sqrt{1 - M_\infty^2}$$

M_∞ = Freestream Mach No.

h' is obtained from Abbott and Doenhoff [54] for NACA 23018 section.

Results and Discussion

Figure (5.1) through Figure (5.3) show the comparison between the theoretical values of C_L vs. α predicted by the Modified Equivalent Flap Theory (which accounts for the jet induced supercirculation lift) with that of full scale wind tunnel and flight test data on the JETWING aircraft. These values are given for different flap deflections and blowing coefficients. The comparison can be considered very good as the theoretical values lie in between the wind tunnel and the flight test data.

Figure (5.4) shows the comparison of theoretical values of C_L vs. C_M with that of full scale wind tunnel test data on JETWING aircraft without the horizontal tail. The comparison is not satisfactory. The reason for the discrepancy may be from either of two causes: a) overestimation of additional supercirculation lift because of failure to account for change in density in the hot exhaust gas which is much less than ambient air density, or b) underestimation of lift in the forward part of the wing due to increased suction caused by blowing. However, the slope of the theoretical plot checks reasonably well with that of experimental data. As dC_M/dC_L is the most important stability parameter from the preliminary design standpoint, the theory developed here can be considered as a useful tool in designing upper surface blown aircraft.

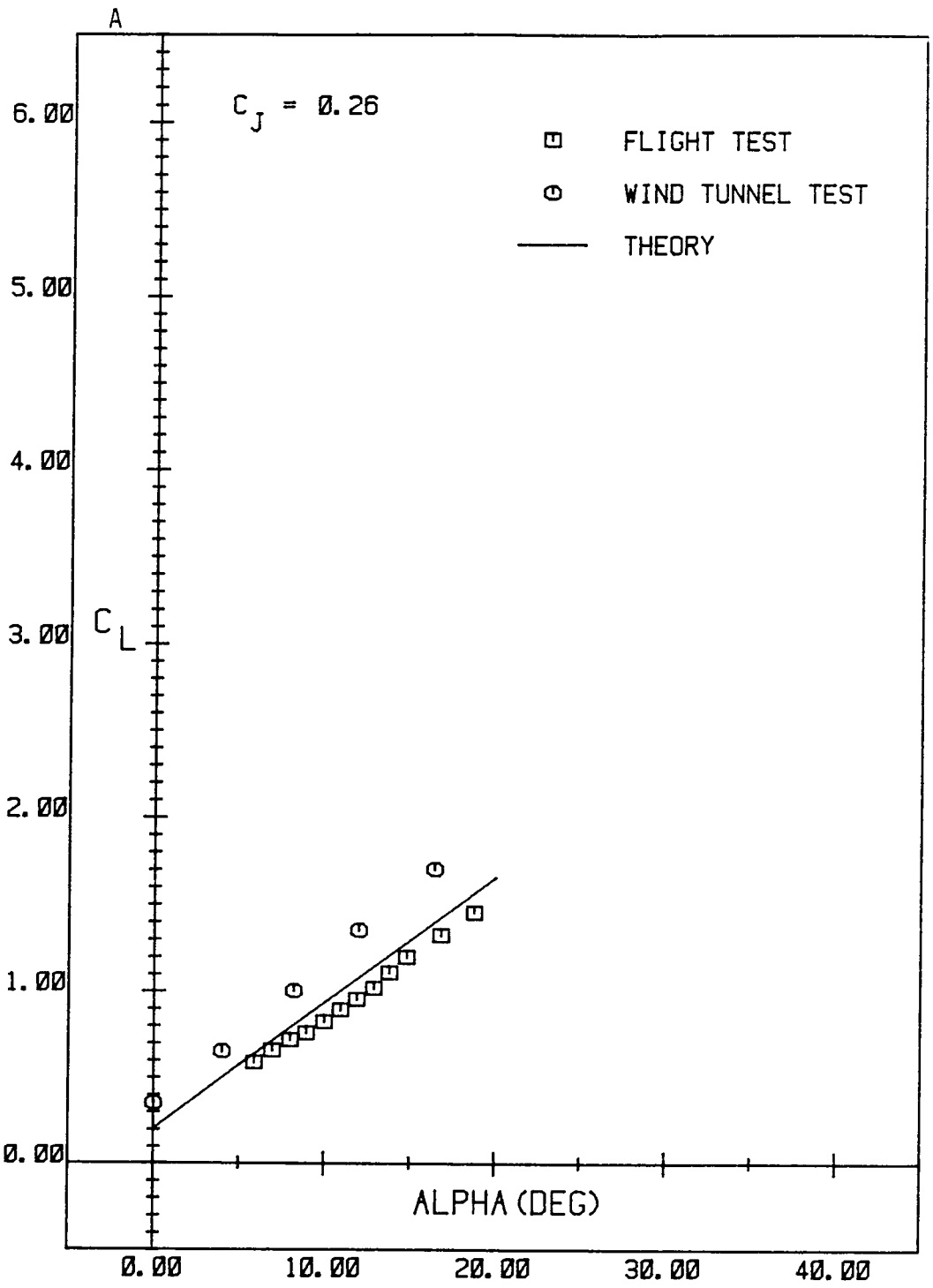


Figure 5.1 Comparison of Modified Equivalent Flap Theory with flight and full scale wind tunnel data for $\delta_F = 0^\circ$ (upper wing removed)

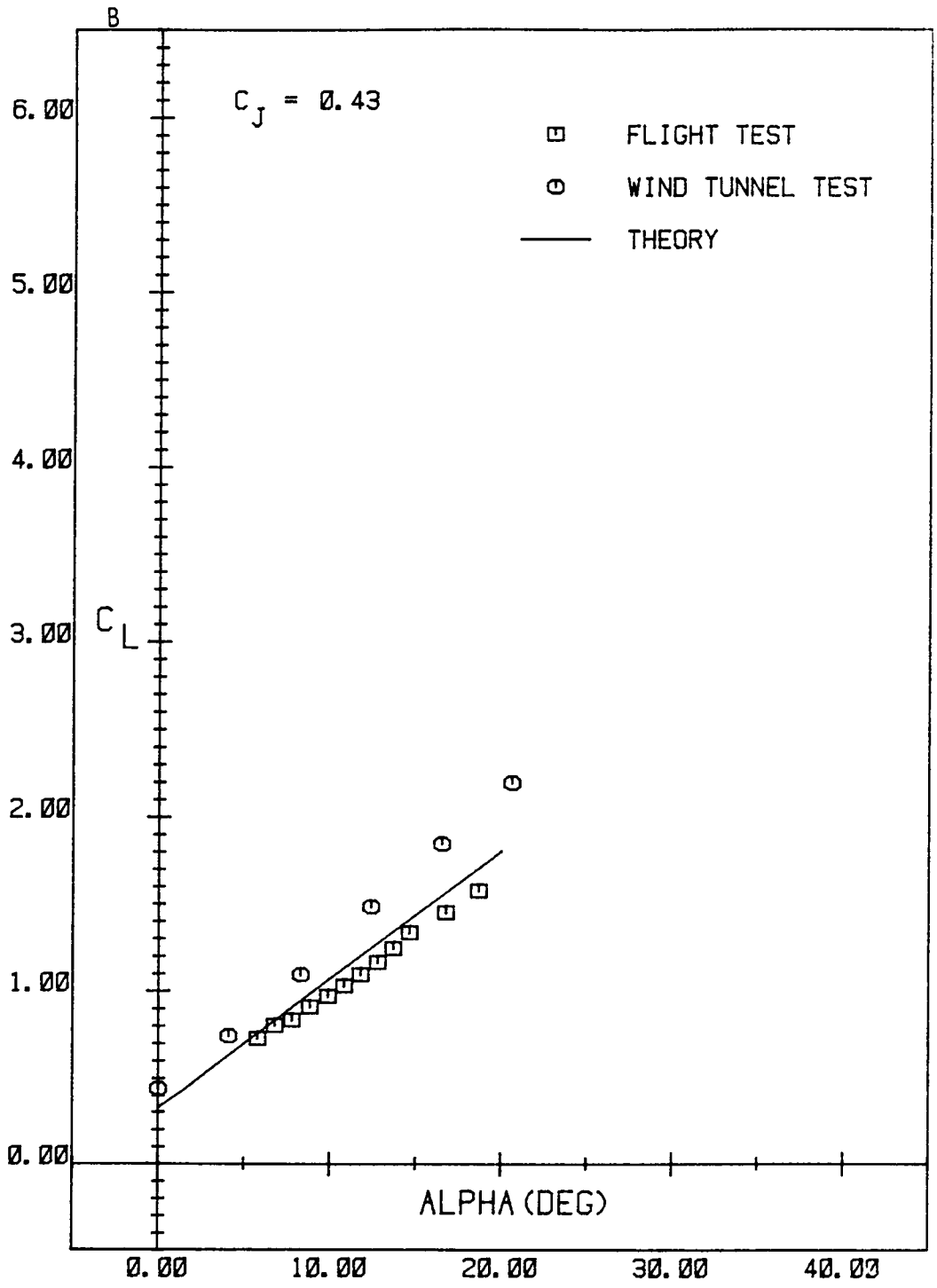


Figure 5.1 (continued)

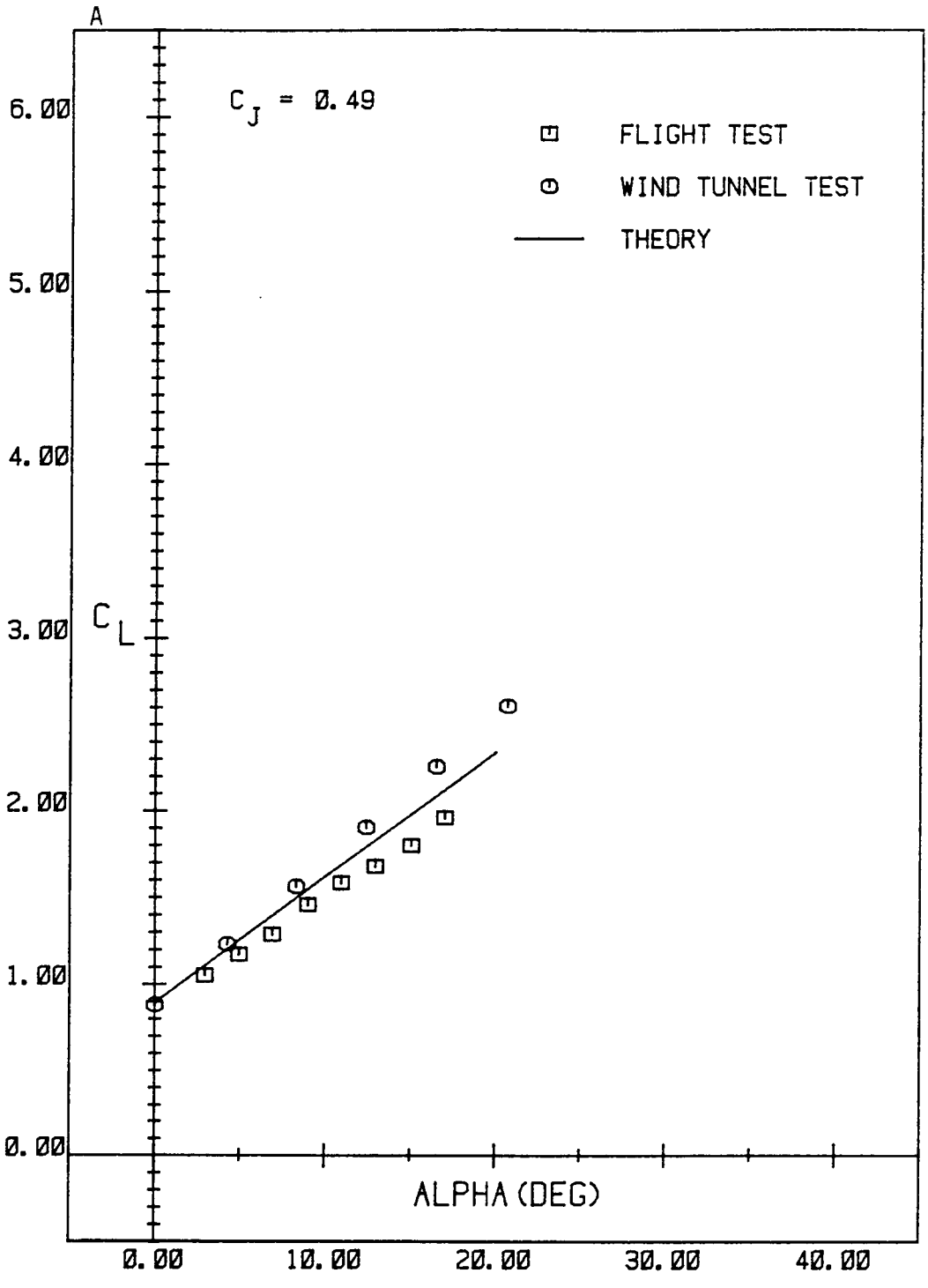


Figure 5.2 Comparison of Modified Equivalent Flap Theory with flight and full scale wind tunnel data for $\delta_F = 15^\circ$ (upper wing removed)

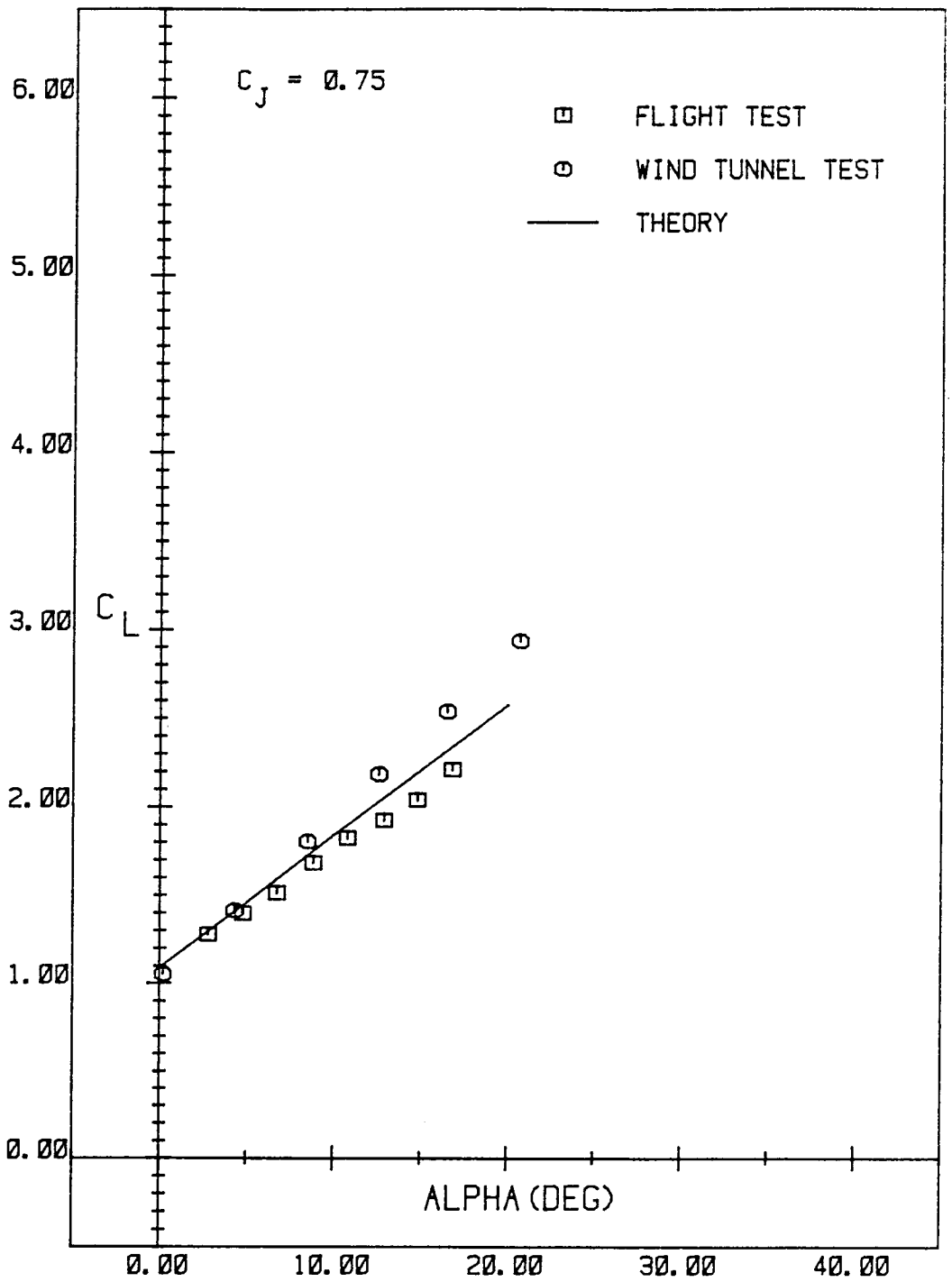


Figure 5.2 (continued)

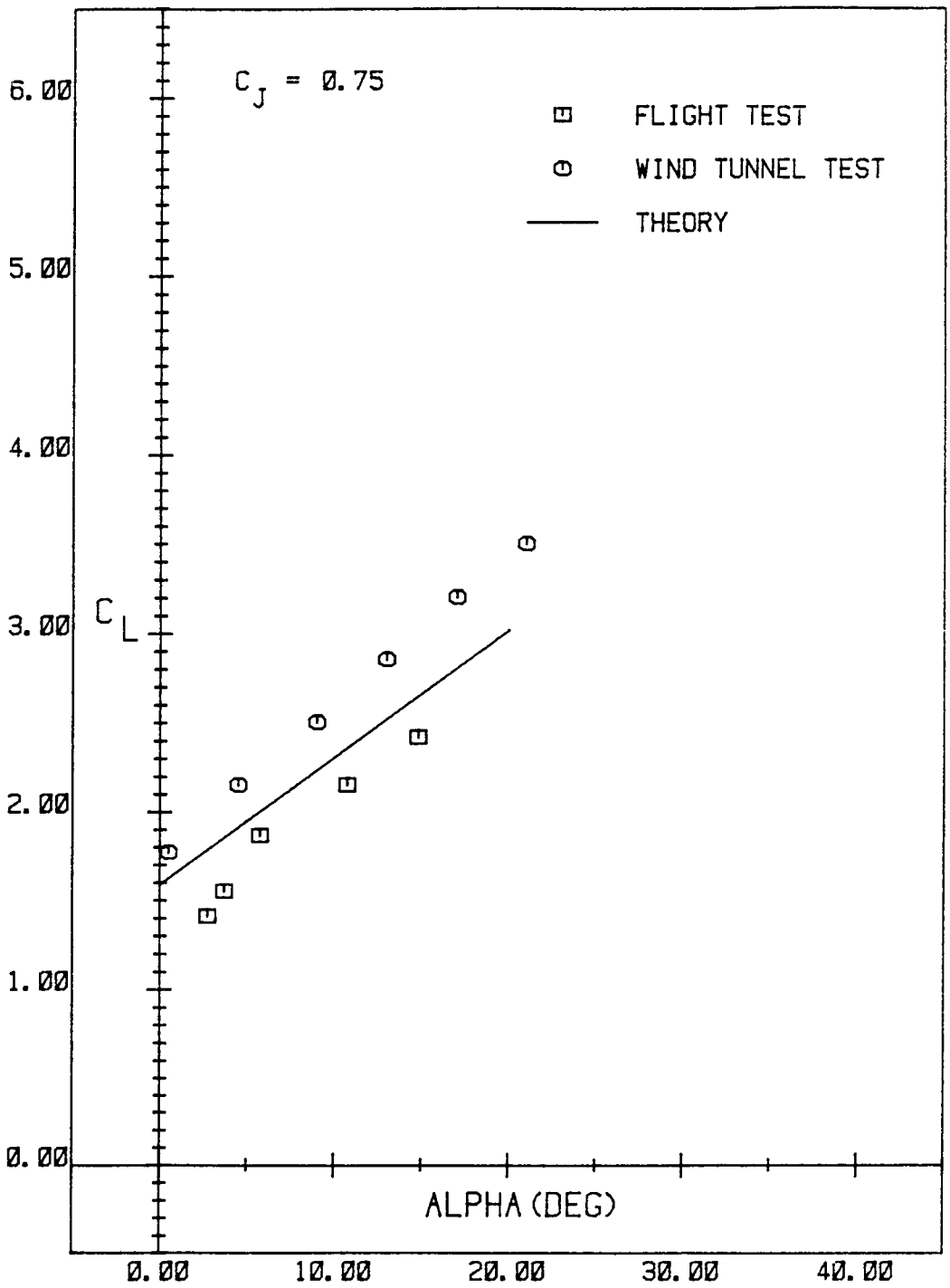


Figure 5.3 Comparison of Modified Equivalent Flap Theory with flight and full scale wind tunnel data for $\delta_F = 30^\circ$ (upper wing removed)

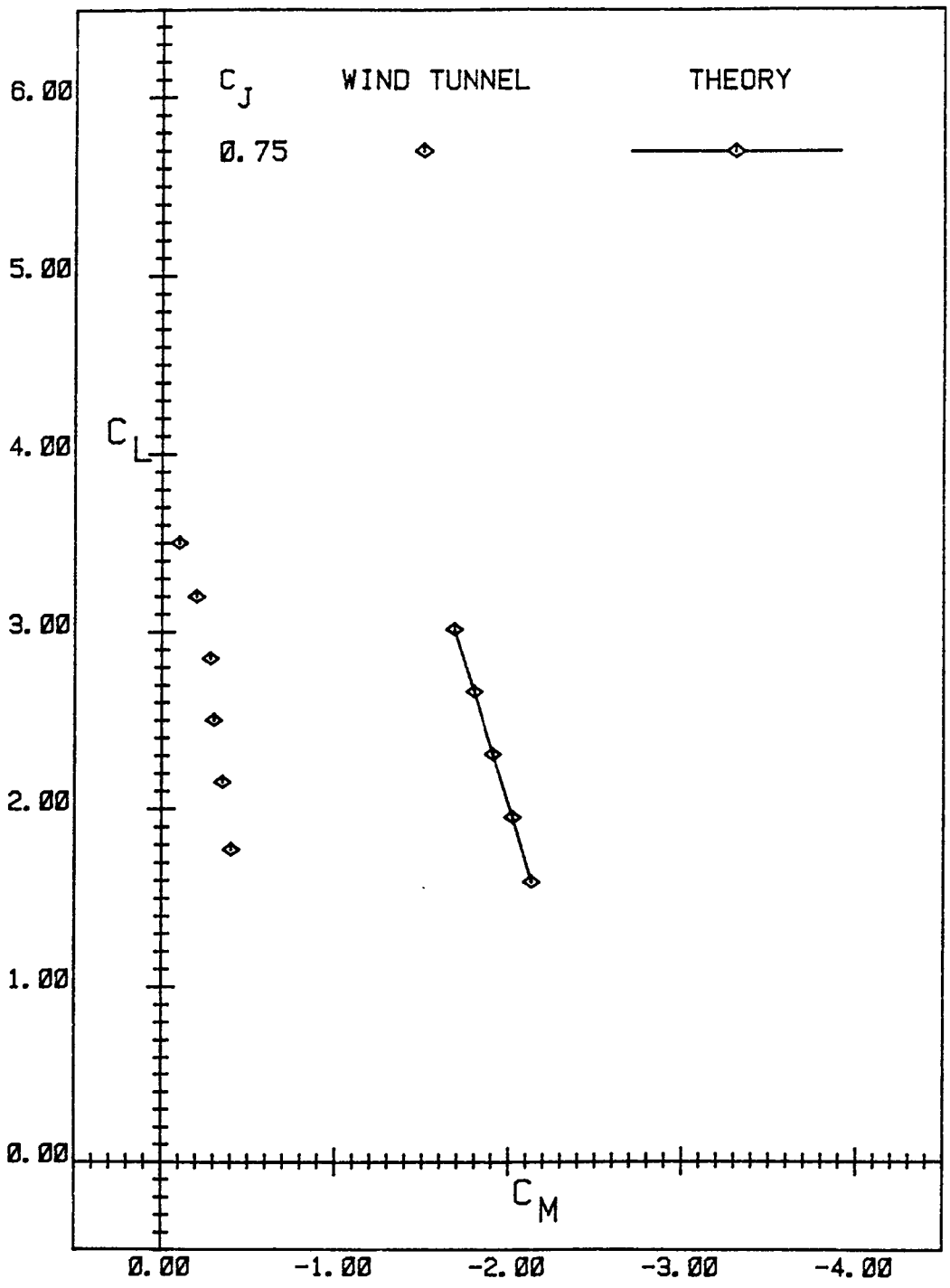


Figure 5.4 Comparison of Modified Equivalent Flap Theory with full scale wind tunnel data for $\delta_F = 30^\circ$ (upper wing and horizontal tail removed)

CHAPTER VI

CONCLUSIONS AND RECOMMENDATIONS

The empirical method of replacing the jet momentum by an equivalent flap, appears to be one of the simplest ways to predict the lift and pitching moment as long as blowing is effected at the trailing edge. For blowing upstream of the trailing edge, the empirical solution for the additional supercirculation lift from momentum considerations is a good first approximation for preliminary design of an upper surface blown jetwing aircraft with a rectangular nozzle. For an aircraft with circular or elliptical nozzle, spanwise spreading of the jet has to be accounted for.

Also, the pressure field induced on the wing upper surface changes with change in the jet velocity, i.e., blowing coefficient, even if the other parameters, such as angle of attack and flap deflection, remain unchanged. The modification of the pressure field, from the one originally induced by the unblown wing, changes the flow development aft of the nozzle and hence would change the theoretical value of the additional supercirculation lift. Again, the change in the pressure field ahead of the nozzle, because of the increase in blowing coefficient, would create additional suction on the front part of the wing which would contribute to the lift and nose up pitching moment. This would bring the theoretical pitching moment characteristic closer to the one obtained experimentally. Another reason for the discrepancy between theoretical and experimental values of the pitching moment coefficient,

is the unaccounting of the moment created by the turning of the free-stream air as it enters the engine inlet. This can only be determined if the upwash at the inlet can be modeled. Also, the incompressible theory used here neglects the variation of density with temperature change.

Any further extension of the work has to consider the temperature, hence, the density variation in the expanding jet, particularly, the hot core exhaust. It should also consider a more correct modeling of the induced pressure field due to blowing.

BIBLIOGRAPHY

BIBLIOGRAPHY

1. Kohlman, D. L., "Introduction to V/STOL Airplanes," The Iowa State University Press, Ames, Iowa 1981.

2. Seibold, W., "Development Tendencies for Short and Medium Haul Air Traffic," Lecture presented at the short course on "STOL and Short-Haul Aircraft Technology and the Community," The University of Tennessee Space Institute, Tullahoma, Tennessee, April 22-26, 1974.

3. "V/STOL: A Practical Weapon System," A report by the AIAA V/STOL Aircraft Systems Technical Committee, Astronautics & Aeronautics, January 1983.

4. Lundry, J. L., "High Lift System Development for Transport Aircraft," Lecture presented at the short course on "High Lift Technology," The University of Tennessee Space Institute, Tullahoma, Tennessee, March 6-10, 1978.

5. Goodmanson, L. T., and Gratzer, L. B., "Recent Advances in Aerodynamics for Transport Aircraft," Astronautics & Aeronautics, December 1973 and January 1974.

6. Williams, J., Butler, S. F. J., and Wood, M. N., "The Aerodynamics of Jet Flaps," Aeronautical Research Council Reports and Memoranda No. 3304, January 1961.

7. Schubauer, G. B., "Jet Propulsion with Special Reference to Thrust Augmentations," National Advisory Committee for Aeronautics Technical Note 442, January 1933.

8. Hagedorn, H., and Ruden, P., "Windkanaluntersuchungen an einem Junkers-Doppelflugel mit Ausblaseschlitz am Heck des Hauptflugels," Report by the Institute fur Aeromechanik und Flugtechnik der Technischen Hochschule Hannover, Lilienthal Gesellschaft, Bericht A64, 1938.

9. Aiken, T. N., and Cook, A. M., "Results of Full-Scale Wind Tunnel Tests on the H.126 Jet Flap Aircraft," National Aeronautics and Space Administration Technical Note D-7252, April 1973.

10. Englar, R. J., "Circulation Control for High Lift and Drag Generation on STOL Aircraft," Journal of Aircraft, Vol. 12, No. 5, May 1975.

11. Englar, R. J., et al., "Design of the Circulation Control Wing STOL Demonstrator Aircraft," American Institute of Aeronautics and Astronautics Paper No. 79-1842, presented at the AIAA Aircraft Systems and Technology Meeting, New York, New York, August 20-22, 1979.

12. Pugliese, A. J., and Englar, R. J., "Flight Testing the Circulation Control Wing," American Institute of Aeronautics and Astronautics Paper No. 79-1791, presented at the AIAA Aircraft Systems and Technology Meeting, New York, New York, August 20-22, 1979.

13. Eppel, J. C., et al., "Static Investigation of the Circulation-Control-Wing/Upper-Surface-Blowing Concept Applied to the Quiet Short-Haul Research Aircraft," National Aeronautics and Space Administration Technical Memorandum 84232, July 1982.

14. Davenport, F. J., and Hunt, D. N., "Deflection of a Thick Jet by a Convex Surface: A Practical Problem for Powered Lift," American Institute of Aeronautics and Astronautics Paper No. 75-167, presented at the AIAA 13th Aerospace Sciences Meeting, Pasadena, California, January 20-22, 1975.

15. May, F. W., and Bean, G. E., "Aerodynamic Design of the Boeing YC-14 Advanced Medium STOL Transport (AMST)," American Institute of Aeronautics and Astronautics Paper No. 75-1015, presented at the AIAA 1975 Aircraft Systems and Technology Meeting, Los Angeles, California, August 4-7, 1975.

16. Cochrane, J. A., Riddle, D. W., and Stevens, V. C., "Quiet Short-Haul Research Aircraft - The First Three Years of Flight Research," American Institute of Aeronautics and Astronautics Paper No. 81-2625, presented at the AIAA/NASA Ames V/STOL Conference, Palo Alto, California, December 7-9, 1981.

17. "Jetwing from Colorado," Air International, Vol. 14, No. 2, pp. 69-71, February 1978.

18. "Jetwing, A Very Quiet Machine," Professional Pilot, pp. 16-19 April 1978.

19. Fink, D. E., "Propulsive Lift Concepts Flight Tested," Aviation Week & Space Technology, September 19, 1977.

20. Kimberlin, R. D., "A Flight Test Evaluation of the Ball-Bartoe Jetwing Propulsive Lift Concept," UTSI Report 81-1, The University of Tennessee Space Institute, Tullahoma, Tennessee, July 1, 1981.

21. Kimberlin, R. D., Solies, U. P., and Sinha, A. K., "A Flight Test Evaluation and Analytical Study of the Ball-Bartoe Jetwing Propulsive Lift Concept without Ejector," UTSI Report 82/17, The University of Tennessee Space Institute, Tullahoma, Tennessee, October 1, 1982.

22. Maskell, E. C., and Gates, S. B., "Preliminary Analysis for a Jet-Flap System in Two-Dimensional Inviscid Flow," Aeronautical Research Council Current Paper No. 359, June 1955.

23. Spence, D. A., "The Lift-Coefficient of a Thin, Jet-Flapped Wing," Proceedings of the Royal Society of London, Series A, Vol. 238, No. 1212, pp. 46-68, December 1956.

24. Spence, D. A., "The Lift on a Thin Aerofoil with a Jet-Augmented Flap," The Aeronautical Quarterly, Vol. IX, Pt. 3, pp. 287-299, August 1958.

25. Maskell, E. C., and Spence, D. A., "A Theory of the Jet Flap in Three Dimensions," Proceedings of the Royal Society of London, Series A, Vol. 251, pp. 407-425, 1959.

26. Hartunian, R. A., "The Finite Aspect Ratio Jet Flap," Cornell Aeronautical Laboratory Report AI-1190-A-3, October 1959.

27. Kerney, K. P., "A Theory of the High-Aspect-Ratio Jet Flap," AIAA Journal, Vol. 9, No. 3, pp. 431-435, March 1971.

28. Tokuda, N., "An Asymptotic Theory of the Jet Flap in Three Dimensions," Journal of Fluid Mechanics, Vol. 46, Part 4, pp. 705-726, April 27, 1971.

29. Ross, A. J., "The Theoretical Evaluation of the Downwash Behind Jet-Flapped Wings," Aeronautical Research Council Reports and Memoranda No. 3119, January 1958.

30. Thomas, H. H. B. M., and Ross, A. J., "The Calculation of the Rotary Lateral Stability Derivatives of a Jet-Flapped Wing," Aeronautical Research Council Reports and Memoranda No. 3277, January 1958.

31. Taylor, A. S., "A Theoretical Investigation of the Longitudinal Stability, Control and Response Characteristics of Jet-Flap Aircraft. Part I," Aeronautical Research Council Reports and Memoranda No. 3272, February 1960.

32. Das, A., "Tragfluchentheorie fur Traflugel mit Strahklappen," Jahrbuch der Wissenschaftlichen Gesellschaft fur Luftfahrt, 1960, pp. 112-133. Translated to: "Lifting Surface Theory for Wings with Jet Flaps," National Research Council of Canada Report NRC-77-1122, 1964.

33. Shen, C. C., Lopez, M. L., and Wasson, N. F., "Jet-Wing Lifting-Surface Theory Using Elementary Vortex Distributions," Journal of Aircraft, Vol. 12, No. 5, pp. 448-456, May 1975.

34. Woolard, H. W., "A Review of Some Air Force STOL Aircraft Aerodynamic Prediction Methods," American Institute of Aeronautics and Astronautics Paper No. 74-992, presented at the AIAA 6th Aircraft Design, Flight Test and Operations Meeting, Los Angeles, California, August 12-14, 1974.

35. Chen, Z. L., and Wu, J. M., "Jet Wing Vortex Lattice Theory with Nonlinear Wake and Tip Flows," American Institute of Aeronautics and Astronautics Paper No. 83-0263, presented at the AIAA 21st Aerospace Sciences Meeting, Reno, Nevada, January 10-13, 1983.

36. Mendenhall, M. R., and Spangler, S. B., "Calculation of the Longitudinal Aerodynamic Characteristics of Upper-Surface-Blown Wing-Flap Configurations," American Institute of Aeronautics and Astronautics Paper No. 79-0120, presented at the AIAA 17th Aerospace Sciences Meeting, New Orleans, Louisiana, January 15-17, 1979.

37. Stratford, B. S., "Early Thoughts on the Jet Flap," The Aeronautical Quarterly, Vol. 7, pp. 45-59, February 1956.

38. Jacobs, W. F., "Theory of the Jet-Augmented Flap in Two Dimensions," Report No. LG72ER0083, Lockheed-Georgia Company, November 1, 1972.

39. Jacobs, W. F., "Theory of the Jet-Augmented Flap in Three Dimensions," Report No. LG73ER0023, Lockheed-Georgia Company, December 1, 1972.

40. Multhopp, H., "Methods for Calculating the Lift Distribution of Wings (Subsonic Lifting-Surface Theory)," Aeronautical Research Council Reports and Memoranda No. 2884, January 1950.

41. Sheela, B. V., and Ramamoorthy, P., "SWIFT-A New Constrained Optimization Technique," Computer Methods in Applied Mechanics and Engineering 6 (1975), pp. 309-318, North-Holland Publishing Company.

42. Munk, M. M., "The Aerodynamic Forces on Airship Hulls," National Advisory Committee for Aeronautics Report No. 184, 1923.

43. Glauert, M. B., "The Wall Jet," Journal of Fluid Mechanics, Vol. 1, pp. 625-643, 1956.

44. Launder, B. E., and Rodi, W., "The Turbulent Wall Jet - Measurements and Modeling," Annual Review of Fluid Mechanics, Vol. 15, pp. 429-459, 1983.

45. Bradshaw, P., and Gee, M. T., "Turbulent Wall Jets with and without an External Stream," Aeronautical Research Council Reports and Memoranda No. 3252, June 1960.

46. Newman, B. G., "Deflection of a Plane Jet by Adjacent Boundaries - Coanda Effect," Boundary Layer and Flow Control, Vol. 1, Edited by G. V. Lachmann, Pergamon Press, 1961.

47. Gartshore, I. S., and Newman, B. G., "The Turbulent Wall Jet in an Arbitrary Pressure Gradient," The Aeronautical Quarterly, Vol. 20, pp. 25-56, February 1969.

48. Kind, R. J., "A Calculation Method for Boundary Layer Control by Tangential Blowing," C.A.S.I. Transactions, Vol. 4, pp. 88-98, September 1971.

49. Goradia, S. H., and Colwell, G. T., "Parametric Study of a Two Dimensional Turbulent Wall Jet in a Moving Stream with Arbitrary Pressure Gradient," AIAA Journal, Vol. 9, pp. 2156-2165, November 1971.

50. Saripalli, K. R., and Simpson, R. L., "Investigation of Blown Boundary Layers with an Improved Wall Jet System," National Aeronautics and Space Administration Contractor Report 3340, November 1980.

51. Mabuchi, I., and Kumada, M., "Studies on Heat Transfer to Turbulent Jets with Adjacent Boundaries," Bulletin of Japan Society of Mechanical Engineers, Vol. 15, No. 88, pp. 1236-1245, October 1972.

52. Abramovich, G. N., "The Theory of Turbulent Jets," The M.I.T. Press, Cambridge, Massachusetts, 1963.

53. Oswatitsch, K., "Contributions to the Development of Gasdynamics," Friedr. Vieweg & Sohn, Braunschweig/Wiesbaden, 1980.

54. Abbott, I. H., and Von Doenhoff, A. E., "Theory of Wing Sections," Dover Publications, Inc., New York, 1959.

APPENDIXES

APPENDIX I

EVALUATION OF THE INTEGRAL IN EQUATION (3.4)

$$\frac{2}{\pi}\int_0^{\psi_1}\left[\delta_F\left\{\psi_o\tan\frac{\psi}{2}+\ln\left|\frac{\sin\frac{\psi+\psi_o}{2}}{\sin\frac{\psi-\psi_o}{2}}\right|\right\}\right.$$

$$\left.+\alpha\left\{\pi\tan\frac{\psi}{2}+\ln\left|\frac{\sin\frac{\psi+\pi}{2}}{\sin\frac{\psi-\pi}{2}}\right|\right\}\right]\sin\psi\,d\psi$$

$$=\frac{2}{\pi}\left[\underbrace{\int_0^{\psi_1}(\delta_F\,\psi_o+\alpha\pi)\tan\frac{\psi}{2}\sin\psi\,d\psi}_{I_1}\right.$$

$$+\underbrace{\delta_F\int_0^{\psi_1}\ln\left\{\left|\sin\frac{\psi+\psi_o}{2}\right|\right\}\sin\psi\,d\psi}_{I_2}$$

$$-\underbrace{\delta_F\int_0^{\psi_1}\ln\left\{\left|\sin\frac{\psi-\psi_o}{2}\right|\right\}\sin\psi\,d\psi}_{I_3}$$

$$+\underbrace{\alpha\int_0^{\psi_1}\ln\left\{\left|\sin\frac{\psi+\pi}{2}\right|\right\}\sin\psi\,d\psi}_{I_4}$$

$$\left.-\underbrace{\alpha\int_0^{\psi_1}\ln\left\{\left|\sin\frac{\psi-\pi}{2}\right|\right\}\sin\psi\,d\psi}_{I_5}\right]$$

$$=\frac{2}{\pi}\left[I_1+I_2-I_3+I_4-I_5\right]$$

$$I_1 = \int_0^{\psi_1} (\delta_F \psi_0 + \alpha\pi) \tan\frac{\psi}{2} \sin\psi \, d\psi$$

$$= (\delta_F \psi_0 + \alpha\pi) \int_0^{\psi_1} \frac{\sin\frac{\psi}{2}}{\cos\frac{\psi}{2}} \cdot 2 \sin\frac{\psi}{2} \cdot \cos\frac{\psi}{2} \, d\psi$$

$$= (\delta_F \psi_0 + \alpha\pi) \int_0^{\psi_1} 2 \sin^2\frac{\psi}{2} \, d\psi = (\delta_F \psi_0 + \alpha\pi) \int_0^{\psi_1} (1 - \cos\psi) \, d\psi$$

$$= (\delta_F \psi_0 + \alpha\pi) (\psi - \sin\psi) \Big|_0^{\psi_1} = (\delta_F \psi_0 + \alpha\pi) (\psi_1 - \sin\psi_1)$$

$$I_2 = \delta_F \int_0^{\psi_1} \ln \left\{ \left| \sin\frac{\psi + \psi_0}{2} \right| \right\} \sin\psi \, d\psi$$

$$= \delta_F \int_0^{\psi_1} \ln \left(\sin\frac{\psi + \psi_0}{2}\right) \sin\psi \, d\psi$$

Substituting $\frac{\psi}{2} = x$ and $\frac{\psi_0}{2} = a$, i.e., $\psi = 2x$, $d\psi = 2dx$, we have,

$$I_2 = 2\delta_F \int_0^{\frac{\psi_1}{2}} \ln \{\sin(x + a)\} \sin 2x \, dx$$

Substituting $x + a = \xi$, i.e., $x = (\xi - a)$, $dx = d\xi$, we have,

$$I_2 = 2\delta_F \int_{\frac{\psi_0}{2}}^{\frac{\psi_0 + \psi_1}{2}} \ln (\sin\xi) \sin 2(\xi - a) \, d\xi$$

Therefore,

$$I_2 = 2\delta_F \left[-\ln(\sin \xi) \frac{\cos 2(\xi - a)}{2} \Big|_{\frac{\psi_0}{2}}^{\frac{\psi_0 + \psi_1}{2}} + \int_{\frac{\psi_0}{2}}^{\frac{\psi_0 + \psi_1}{2}} \frac{\cos \xi}{\sin \xi} \cdot \frac{\cos 2(\xi - a)}{2} d\xi \right]$$

$$= \delta_F \left[\ln \left(\sin \frac{\psi_0}{2}\right) \cdot 1 - \ln \left\{ \sin \left(\frac{\psi_0 + \psi_1}{2} \right) \right\} \cdot \cos \psi_1 \right]$$

$$+ \delta_F \int_{\frac{\psi_0}{2}}^{\frac{\psi_0}{2} + \frac{\psi_1}{2}} (\cos 2a \cos 2\xi + \sin 2a \sin 2\xi) \frac{\cos \xi}{\sin \xi} d\xi$$

$$= \delta_F \left[\ln \left(\sin \frac{\psi_0}{2}\right) - \ln \left\{ \sin \left(\frac{\psi_0 + \psi_1}{2} \right) \right\} \cos \psi_1 \right]$$

$$+ \delta_F \cos 2a \int_{\frac{\psi_0}{2}}^{\frac{\psi_0 + \psi_1}{2}} (1 - 2 \sin^2 \xi) \frac{\cos \xi}{\sin \xi} d\xi$$

$$+ \delta_F \sin 2a \int_{\frac{\psi_0}{2}}^{\frac{\psi_0 + \psi_1}{2}} 2 \sin \xi \cos \xi \frac{\cos \xi}{\sin \xi} d\xi$$

Therefore,

$$I_2 = \delta_F \left[\ln \left(\sin \frac{\psi_0}{2}\right) - \ln \left\{\sin \left(\frac{\psi_0 + \psi_1}{2}\right)\right\} \cos \psi_1 \right]$$

$$+ \delta_F \cos 2a \ln \left| \sin \xi \right| \Bigg|_{\frac{\psi_0}{2}}^{\frac{\psi_0 + \psi_1}{2}} + \delta_F \cos 2a \frac{\cos 2\xi}{2} \Bigg|_{\frac{\psi_0}{2}}^{\frac{\psi_0 + \psi_1}{2}}$$

$$+ \delta_F \sin 2a \int_{\frac{\psi_0}{2}}^{\frac{\psi_0 + \psi_1}{2}} (1 + \cos 2\xi)\, d\xi$$

$$= \delta_F \left[\ln \left(\sin \frac{\psi_0}{2}\right) - \ln \left\{\sin \left(\frac{\psi_0 + \psi_1}{2}\right)\right\} \cos \psi_1 \right]$$

$$+ \delta_F \cos \psi_0 \left[\ln \sin \left(\frac{\psi_0 + \psi_1}{2}\right) - \ln \left(\sin \frac{\psi_0}{2}\right) \right.$$

$$\left. + \frac{\cos (\psi_0 + \psi_1) - \cos \psi_0}{2} \right] + \delta_F \sin 2a \left(\xi + \frac{\sin 2\xi}{2}\right) \Bigg|_{\frac{\psi_0}{2}}^{\frac{\psi_0 + \psi_1}{2}}$$

$$= \delta_F \left[\ln \left(\sin \frac{\psi_0}{2}\right) - \ln \left\{\sin \left(\frac{\psi_0 + \psi_1}{2}\right)\right\} \cos \psi_1 \right]$$

$$+ \delta_F \cos \psi_0 \left[\ln \frac{\sin \frac{\psi_0 + \psi_1}{2}}{\sin \frac{\psi_0}{2}} + \frac{\cos(\psi_0 + \psi_1) - \cos \psi_0}{2} \right]$$

$$+ \delta_F \sin \psi_0 \left[\frac{\psi_1}{2} + \frac{\sin (\psi_0 + \psi_1) - \sin \psi_0}{2} \right]$$

$$I_3 = \delta_F \int_0^{\psi_1} \ln \left\{ \left| \sin \frac{\psi - \psi_0}{2} \right| \right\} \sin \psi \, d\psi$$

Substituting $\frac{\psi}{2} = x$ and $\frac{\psi_0}{2} = a$, i.e., $\psi = 2x$, $d\psi = 2dx$, we have,

$$I_3 = 2\delta_F \int_0^{\frac{\psi_1}{2}} \ln \left\{ \left| \sin (x - a) \right| \right\} \sin 2x \, dx$$

As maximum value of x, i.e., $\frac{\psi_1}{2} < \frac{\psi_0}{2}$,

therefore, $$I_3 = 2\delta_F \int_0^{\frac{\psi_1}{2}} \ln \{\sin (a - x)\} \sin 2x \, dx$$

Substituting $a - x = \xi$, i.e., $x = a - \xi$, $dx = - d\xi$, we have,

$$I_3 = - 2\delta_F \int_{\frac{\psi_0}{2}}^{\frac{\psi_0 - \psi_1}{2}} \ln (\sin \xi) \sin 2(a - \xi) \, d\xi$$

$$= 2\delta_F \int_{\frac{\psi_0 - \psi_1}{2}}^{\frac{\psi_0}{2}} \ln (\sin \xi) \sin 2(a - \xi) \, d\xi$$

$$= 2\delta_F \left[\ln (\sin \xi) \frac{\cos 2(a - \xi)}{2} \Bigg|_{\frac{\psi_0 - \psi_1}{2}}^{\frac{\psi_0}{2}} - \int_{\frac{\psi_0 - \psi_1}{2}}^{\frac{\psi_0}{2}} \frac{\cos \xi}{\sin \xi} \cdot \frac{\cos 2(a - \xi)}{2} \, d\xi \right]$$

Therefore,

$$I_3 = \delta_F \left[\ln \left(\sin \frac{\psi_o}{2}\right) - \ln \left(\sin \frac{\psi_o - \psi_1}{2}\right) \cdot \cos \psi_1 \right]$$

$$- \delta_F \int_{\frac{\psi_o - \psi_1}{2}}^{\frac{\psi_o}{2}} \frac{\cos \xi}{\sin \xi} [\cos 2a \cos 2\xi + \sin 2a \sin 2\xi] \, d\xi$$

$$= \delta_F \left[\ln \left(\sin \frac{\psi_o}{2}\right) - \ln \left(\sin \frac{\psi_o - \psi_1}{2}\right) \cos \psi_1 \right]$$

$$- \delta_F \cos 2a \int_{\frac{\psi_o - \psi_1}{2}}^{\frac{\psi_o}{2}} \frac{\cos \xi}{\sin \xi} (1 - 2 \sin^2 \xi) \, d\xi$$

$$- \delta_F \sin 2a \int_{\frac{\psi_o - \psi_1}{2}}^{\frac{\psi_o}{2}} \frac{\cos \xi}{\sin \xi} \cdot 2 \sin \xi \cos \xi \, d\xi$$

$$= \delta_F \left[\ln \left(\sin \frac{\psi_o}{2}\right) - \ln \left(\sin \frac{\psi_o - \psi_1}{2}\right) \cos \psi_1 \right]$$

$$- \delta_F \cos \psi_o \left[\ln |\sin \xi| + \frac{\cos 2\xi}{2} \right] \Bigg|_{\frac{\psi_o - \psi_1}{2}}^{\frac{\psi_o}{2}}$$

$$- \delta_F \sin \psi_o \int_{\frac{\psi_o - \psi_1}{2}}^{\frac{\psi_o}{2}} (1 + \cos 2\xi) \, d\xi$$

Therefore,

$$I_3 = \delta_F \left[\ln \left(\sin \frac{\psi_0}{2}\right) - \ln \left(\sin \frac{\psi_0 - \psi_1}{2}\right) \cdot \cos \psi_1 \right]$$

$$- \delta_F \cos \psi_0 \left[\ln \left(\sin \frac{\psi_0}{2}\right) + \frac{\cos \psi_0}{2} - \ln \left(\sin \frac{\psi_0 - \psi_1}{2}\right) \right.$$

$$\left. - \frac{\cos(\psi_0 - \psi_1)}{2} \right] - \delta_F \sin \psi_0 \left[\xi + \frac{\sin 2\xi}{2} \right] \Bigg|_{\frac{\psi_0 - \psi_1}{2}}^{\frac{\psi_0}{2}}$$

$$= \delta_F \left[\ln \left(\sin \frac{\psi_0}{2}\right) - \ln \left(\sin \frac{\psi_0 - \psi_1}{2}\right) \cdot \cos \psi_1 \right]$$

$$- \delta_F \cos \psi_0 \left[\ln \frac{\sin \frac{\psi_0}{2}}{\sin \frac{\psi_0 - \psi_1}{2}} + \frac{\cos \psi_0 - \cos (\psi_0 - \psi_1)}{2} \right]$$

$$- \delta_F \sin \psi_0 \left[\frac{\psi_1}{2} + \frac{\sin \psi_0 - \sin (\psi_0 - \psi_1)}{2} \right]$$

Hence, $I_2 - I_3 = \delta_F \left[\psi_1 \sin \psi_0 + \cos \psi_0 \ln \frac{\sin \frac{\psi_0 + \psi_1}{2}}{\sin \frac{\psi_0 - \psi_1}{2}} \right.$

$$\left. + \cos \psi_1 \ln \frac{\sin \frac{\psi_0 - \psi_1}{2}}{\sin \frac{\psi_0 + \psi_1}{2}} \right]$$

$$I_4 = \alpha \int_0^{\psi_1} \ln \left\{ \left| \sin \frac{\psi + \pi}{2} \right| \right\} \sin \psi \, d\psi$$

Substituting $\frac{\psi}{2} = x$ and $\frac{\pi}{2} = a$, i.e., $\psi = 2x$, $d\psi = 2dx$, we have,

$$I_4 = 2\alpha \int_0^{\frac{\psi_1}{2}} \ln \left\{ \left| \sin (x + a) \right| \right\} \sin 2x \, dx$$

Substituting $x + a = \xi$, i.e., $x = \xi - a$, $dx = d\xi$, we have,

$$I_4 = 2\alpha \int_{\frac{\pi}{2}}^{\frac{\pi + \psi_1}{2}} \ln(\sin \xi) \sin 2(\xi - a)\, d\xi$$

$$= 2\alpha \left[- \ln(\sin \xi) \cdot \frac{\cos 2(\xi - a)}{2} \Bigg|_{\frac{\pi}{2}}^{\frac{\pi + \psi_1}{2}} + \int_{\frac{\pi}{2}}^{\frac{\pi + \psi_1}{2}} \frac{\cos \xi}{\sin \xi} \cdot \frac{\cos 2(\xi - a)}{2}\, d\xi \right]$$

$$= \alpha \left[- \ln(\sin \frac{\pi + \psi_1}{2}) \cdot \cos \psi_1 \right] + \alpha \int_{\frac{\pi}{2}}^{\frac{\pi + \psi_1}{2}} \frac{\cos \xi}{\sin \xi} \cdot (\cos 2\xi \cos 2a + \sin 2\xi \sin 2a)\, d\xi$$

$$= - \alpha \ln(\sin \frac{\pi + \psi_1}{2}) \cdot \cos \psi_1 + \alpha \cos 2a \int_{\frac{\pi}{2}}^{\frac{\pi + \psi_1}{2}} \frac{\cos \xi}{\sin \xi} \cdot (1 - 2 \sin^2 \xi)\, d\xi$$

$$+ \alpha \sin 2a \int_{\frac{\pi}{2}}^{\frac{\pi + \psi_1}{2}} \frac{\cos \xi}{\sin \xi} \cdot 2 \sin \xi \cos \xi\, d\xi$$

Therefore,

$$I_4 = -\alpha \ln\left(\sin\frac{\pi+\psi_1}{2}\right)\cos\psi_1 - \alpha\int_{\frac{\pi}{2}}^{\frac{\pi+\psi_1}{2}} \frac{\cos\xi}{\sin\xi}\,d\xi$$

$$+ \alpha\int_{\frac{\pi}{2}}^{\frac{\pi+\psi_1}{2}} \sin 2\xi\,d\xi + 0$$

$$= -\alpha \ln\left(\sin\frac{\pi+\psi_1}{2}\right)\cos\psi_1 - \alpha \ln\left|\sin\xi\right|\Bigg|_{\frac{\pi}{2}}^{\frac{\pi+\psi_1}{2}}$$

$$- \alpha\frac{\cos 2\xi}{2}\Bigg|_{\frac{\pi}{2}}^{\frac{\pi+\psi_1}{2}}$$

$$= -\alpha \ln\left(\sin\frac{\pi+\psi_1}{2}\right)\cos\psi_1$$

$$- \alpha \ln\left(\sin\frac{\pi+\psi_1}{2}\right) - \frac{\alpha}{2}\left[\cos(\pi+\psi_1) + 1\right]$$

$$I_5 = \alpha\int_0^{\psi_1} \ln\left\{\left|\sin\frac{\psi-\pi}{2}\right|\right\}\sin\psi\,d\psi$$

Substituting $\frac{\psi}{2} = x$, $\frac{\pi}{2} = a$, i.e., $\psi = 2x$, $d\psi = 2dx$, we have,

$$I_5 = 2\alpha\int_0^{\frac{\psi_1}{2}} \ln\left\{\left|\sin(x-a)\right|\right\}\sin 2x\,dx$$

As maximum value of x, i.e., $\frac{\psi_1}{2} < \frac{\pi}{2}$,

therefore, $I_5 = 2\alpha\int_0^{\frac{\psi_1}{2}} \ln\{\sin(a-x)\}\sin 2x\,dx$

Substituting $a - x = \xi$, i.e., $x = a - \xi$, $dx = - d\xi$, we have,

$$I_5 = - 2\alpha \int_{\frac{\pi}{2}}^{\frac{\pi - \psi_1}{2}} \ln (\sin \xi) \sin 2(a - \xi)\, d\xi$$

$$= - 2\alpha \left[\ln (\sin\xi) \frac{\cos 2(a - \xi)}{2} \Bigg|_{\frac{\pi}{2}}^{\frac{\pi - \psi_1}{2}} \right.$$

$$\left. - \int_{\frac{\pi}{2}}^{\frac{\pi - \psi_1}{2}} \frac{\cos \xi}{\sin \xi} \cdot \frac{\cos 2(a - \xi)}{2}\, d\xi \right]$$

$$= - \alpha \ln \left(\sin \frac{\pi - \psi_1}{2}\right) \cdot \cos \psi_1$$

$$+ \alpha \int_{\frac{\pi}{2}}^{\frac{\pi - \psi_1}{2}} \frac{\cos \xi}{\sin \xi} (\cos 2a \cos 2\xi + \sin 2a \sin 2\xi)\, d\xi$$

$$= - \alpha \ln \left(\sin \frac{\pi - \psi_1}{2}\right) \cos \psi_1$$

$$+ \alpha \cos 2a \int_{\frac{\pi}{2}}^{\frac{\pi - \psi_1}{2}} \frac{\cos \xi}{\sin \xi} (1 - 2 \sin^2 \xi)\, d\xi$$

$$+ \alpha \sin 2a \int_{\frac{\pi}{2}}^{\frac{\pi - \psi_1}{2}} \frac{\cos \xi}{\sin \xi} \sin 2\xi\, d\xi$$

Therefore,

$$I_5 = -\alpha \ln\left(\sin\frac{\pi-\psi_1}{2}\right)\cos\psi_1 - \alpha \ln\left|\sin\xi\right|\Bigg|_{\frac{\pi}{2}}^{\frac{\pi-\psi_1}{2}}$$

$$-\alpha\,\frac{\cos 2\xi}{2}\Bigg|_{\frac{\pi}{2}}^{\frac{\pi-\psi_1}{2}} + 0$$

$$= -\alpha \ln\left(\sin\frac{\pi-\psi_1}{2}\right)\cos\psi_1 - \alpha \ln\left(\sin\frac{\pi-\psi_1}{2}\right)$$

$$-\frac{\alpha}{2}\left[\cos(\pi-\psi_1)+1\right]$$

Hence, $I_4 - I_5 = \alpha\left\{\ln\dfrac{\sin\frac{\pi-\psi_1}{2}}{\sin\frac{\pi+\psi_1}{2}}\ (\cos\psi_1+1)\right\}$

Therefore, the given integral $= \dfrac{2}{\pi}\left[I_1 + I_2 - I_3 + I_4 - I_5\right]$

$$= \frac{2}{\pi}\Bigg[(\delta_F\,\psi_0 + \alpha\pi)(\psi_1 - \sin\psi_1)$$

$$+\delta_F\left\{\psi_1\sin\psi_0 + (\cos\psi_1 - \cos\psi_0)\ln\frac{\sin\frac{\psi_0-\psi_1}{2}}{\sin\frac{\psi_0+\psi_1}{2}}\right\}$$

$$+\alpha\left\{\ln\frac{\sin\frac{\pi-\psi_1}{2}}{\sin\frac{\pi+\psi_1}{2}}\ (\cos\psi_1+1)\right\}\Bigg]$$

As $\sin\left(\frac{\pi}{2}-\frac{\psi_1}{2}\right) = \sin\left(\frac{\pi}{2}+\frac{\psi_1}{2}\right)$, hence $\ln\dfrac{\sin\frac{\pi-\psi_1}{2}}{\sin\frac{\pi+\psi_1}{2}} = \ln 1 = 0$

Therefore the given integral reduces to

$$\frac{2}{\pi}\left[(\delta_F\,\psi_0 + \alpha\pi)\cdot(\psi_1 - \sin\psi_1) + \delta_F\left\{\psi_1 \sin\psi_0 + (\cos\psi_1 - \cos\psi_0)\cdot \ln\frac{\sin\frac{\psi_0 - \psi_1}{2}}{\sin\frac{\psi_0 + \psi_1}{2}}\right\}\right]$$

APPENDIX II

EVALUATION OF SECTIONAL BLOWING COEFFICIENT (C_j)

In the Equivalent Flap Theory, the following procedure has been adopted for the evaluation of the spanwise variation of two-dimensional "sectional" blowing coefficient C_j. The input data for this evaluation is jet velocity and nozzle area distribution.

From the definition of a three-dimensional blowing coefficient

$$C_J = \frac{F_G}{qS}, \quad (F_G = \text{gross thrust}), \tag{II-1}$$

true airspeed can be written as:

$$V = \sqrt{\frac{F_G}{\frac{1}{2}\rho C_J S}} \tag{II-2}$$

For the required value of C_J; V and F_G were determined by an iterative procedure between equation (II-2) and the data obtained from the thrust calibration plot (Figure 40 [20]), corresponding to 55% N_1 (fan R.P.M.).

Sectional blowing coefficient for any spanwise section C_j is obtained as:

$$C_j = \frac{\int_0^{b+\delta} a_j \rho_j u_j^2}{\frac{1}{2}\rho V^2 c} \tag{II-3}$$

where,

a_j = local area of the nozzle

ρ_j = density of the jet exhaust gas

u_j = jet exhaust velocity

ρ = ambient air density

c = local airfoil chord

δ = wall boundary layer thickness

b = jet thickness

APPENDIX III

EVALUATION OF THE INTEGRALS IN EQUATION (3.11)

The required integral is,

$$\int \gamma(\psi)(1 + 2p + \cos\psi) \sin\psi \, d\psi = (1 + 2p) \int \gamma(\psi) \sin\psi \, d\psi + \int \gamma(\psi) \cos\psi \sin\psi \, d\psi$$

where $$\gamma(\psi) = \frac{2V}{\pi} \left[\delta_F \left\{ \psi_0 \tan\frac{\psi}{2} + \ln \left| \frac{\sin\frac{\psi + \psi_0}{2}}{\sin\frac{\psi - \psi_0}{2}} \right| \right\} \right.$$

$$\left. + \alpha \left\{ \pi \tan\frac{\psi}{2} + \ln \left| \frac{\sin\frac{\psi + \pi}{2}}{\sin\frac{\psi - \pi}{2}} \right| \right\} \right]$$

This integral can be written as:

$$I = (1 + 2p) \frac{2V}{\pi} \int \left[\delta_F \left\{ \psi_0 \tan\frac{\psi}{2} + \ln \left| \frac{\sin\frac{\psi + \psi_0}{2}}{\sin\frac{\psi - \psi_0}{2}} \right| \right\} \right.$$

$$\left. + \alpha \left\{ \pi \tan\frac{\psi}{2} + \ln \left| \frac{\sin\frac{\psi + \pi}{2}}{\sin\frac{\psi - \pi}{2}} \right| \right\} \right] \sin\psi \, d\psi$$

$$+ \frac{2V}{\pi} \int \left[\delta_F \left\{ \psi_0 \tan\frac{\psi}{2} + \ln \left| \frac{\sin\frac{\psi + \psi_0}{2}}{\sin\frac{\psi - \psi_0}{2}} \right| \right\} \right.$$

$$\left. + \alpha \left\{ \pi \tan\frac{\psi}{2} + \ln \left| \frac{\sin\frac{\psi + \pi}{2}}{\sin\frac{\psi - \pi}{2}} \right| \right\} \right] \sin\psi \cos\psi \, d\psi$$

Therefore,

$$I = (1 + 2p)\underbrace{\frac{2V}{\pi}\int (\delta_F\psi_0 + \alpha\pi)\tan\frac{\psi}{2}\sin\psi\,d\psi}_{I_1}$$

$$+\underbrace{\frac{2V}{\pi}\int (\delta_F\psi_0 + \alpha\pi)\tan\frac{\psi}{2}\cos\psi\sin\psi\,d\psi}_{I_2}$$

$$+(1 + 2p)\underbrace{\frac{2V}{\pi}\int \delta_F \ln\left|\sin\frac{\psi + \psi_0}{2}\right|\sin\psi\,d\psi}_{I_3}$$

$$+\underbrace{\frac{2V}{\pi}\int \delta_F \ln\left|\sin\frac{\psi + \psi_0}{2}\right|\sin\psi\cos\psi\,d\psi}_{I_4}$$

$$-(1 + 2p)\underbrace{\frac{2V}{\pi}\int \delta_F \ln\left|\sin\frac{\psi - \psi_0}{2}\right|\sin\psi\,d\psi}_{I_5}$$

$$-\underbrace{\frac{2V}{\pi}\int \delta_F \ln\left|\sin\frac{\psi - \psi_0}{2}\right|\sin\psi\cos\psi\,d\psi}_{I_6}$$

$$+(1 + 2p)\underbrace{\frac{2V}{\pi}\int \alpha \ln\left|\sin\frac{\psi + \pi}{2}\right|\sin\psi\,d\psi}_{I_7}$$

$$+\underbrace{\frac{2V}{\pi}\int \alpha \ln\left|\sin\frac{\psi + \pi}{2}\right|\sin\psi\cos\psi\,d\psi}_{I_8}$$

$$-(1 + 2p)\underbrace{\frac{2V}{\pi}\int \alpha \ln\left|\sin\frac{\psi - \pi}{2}\right|\sin\psi\,d\psi}_{I_9}$$

$$-\underbrace{\frac{2V}{\pi}\int \alpha \ln\left|\sin\frac{\psi - \pi}{2}\right|\sin\psi\cos\psi\,d\psi}_{I_{10}}$$

$$I_1 = \frac{2V}{\pi}(\delta_F\psi_o + \alpha\pi)\int \tan\frac{\psi}{2}\sin\psi\, d\psi$$

$$= \frac{2V}{\pi}(\delta_F\psi_o + \alpha\pi)\int \frac{\sin\frac{\psi}{2}}{\cos\frac{\psi}{2}}\cdot 2\sin\frac{\psi}{2}\cos\frac{\psi}{2}\, d\psi$$

$$= \frac{2V}{\pi}(\delta_F\psi_o + \alpha\pi)\int 2\sin^2\frac{\psi}{2}\, d\psi$$

$$= \frac{2V}{\pi}(\delta_F\psi_o + \alpha\pi)\int (1 - \cos\psi)\, d\psi = \frac{2V}{\pi}(\delta_F\psi_o + \alpha\pi)(\psi - \sin\psi)$$

$$I_2 = \frac{2V}{\pi}(\delta_F\psi_o + \alpha\pi)\int \tan\frac{\psi}{2}\cos\psi\sin\psi\, d\psi$$

$$= \frac{2V}{\pi}(\delta_F\psi_o + \alpha\pi)\int (1 - \cos\psi)\cos\psi\, d\psi$$

$$= \frac{2V}{\pi}(\delta_F\psi_o + \alpha\pi)\int (\cos\psi - \frac{1}{2} - \frac{1}{2}\cos 2\psi)\, d\psi$$

$$= \frac{2V}{\pi}(\delta_F\psi_o + \alpha\pi)(\sin\psi - \frac{\psi}{2} - \frac{1}{4}\sin 2\psi)$$

$$I_3 = \frac{2V}{\pi}\int \delta_F \ln\left|\sin\frac{\psi + \psi_o}{2}\right|\sin\psi\, d\psi$$

$$= \frac{2V\delta_F}{\pi}\int \ln\left(\sin\frac{\psi + \psi_o}{2}\right)\sin\psi\, d\psi$$

Substituting $\frac{\psi}{2} = x$ and $\frac{\psi_o}{2} = a$, i.e., $\psi = 2x$ and $d\psi = 2dx$, we have,

$$I_3 = \frac{4V\delta_F}{\pi}\int \ln\{\sin(x + a)\}\cdot\sin 2x\, dx$$

Substituting $x + a = \xi$, i.e., $x = \xi - a$ and $dx = d\xi$, we have,

$$I_3 = \frac{4V\delta_F}{\pi}\int \ln(\sin\xi)\cdot\sin 2(\xi - a)\, d\xi$$

$$= \frac{4V\delta_F}{\pi}\left[-\ln(\sin\xi)\cdot\frac{\cos 2(\xi - a)}{2} + \int\frac{\cos\xi}{\sin\xi}\,\frac{\cos 2(\xi - a)}{2}\, d\xi\right]$$

Therefore, $I_3 = \frac{4V\delta_F}{\pi}\left[- \ln(\sin \xi) \cdot \frac{\cos 2(\xi - a)}{2}\right.$

$$\left. + \int(\cos 2\xi \cos 2a + \sin 2\xi \sin 2a) \frac{\cos \xi}{2 \sin \xi}\, d\xi\right]$$

$$= \frac{2V\delta_F}{\pi}\left[- \ln(\sin \xi) \cdot \cos 2(\xi - a)\right.$$

$$+ \cos 2a \int (1 - 2\sin^2 \xi) \frac{\cos \xi}{\sin \xi}\, d\xi$$

$$\left. + \sin 2a \int \frac{2 \sin \xi \cdot \cos \xi \cdot \cos \xi}{\sin \xi}\, d\xi\right]$$

$$= \frac{2V\delta_F}{\pi}\left[- \ln(\sin \xi) \cdot \cos 2(\xi - a) + \cos 2a \int \cot \xi\, d\xi\right.$$

$$\left. - \cos 2a \int \sin 2\xi\, d\xi + \sin 2a \int (1 + \cos 2\xi)\, d\xi\right]$$

$$= \frac{2V\delta_F}{\pi}\left[- \ln(\sin \xi) \cdot \cos 2(\xi - a) + \cos 2a \ln|\sin \xi|\right.$$

$$\left. + \cos 2a \frac{\cos 2\xi}{2} + \sin 2a \cdot \xi + \sin 2a \frac{\sin 2\xi}{2}\right]$$

$$= \frac{2V\delta_F}{\pi}\left[- \ln\{\sin (x + a)\} \cdot \cos 2x + \cos \psi_0 \left\{\ln|\sin (x + a)|\right.\right.$$

$$\left.\left. + \frac{\cos 2 (x + a)}{2}\right\} + \sin \psi_0 \left\{x + a + \frac{\sin 2(x + a)}{2}\right\}\right]$$

$$= \frac{2V\delta_F}{\pi}\left[- \ln(\sin \frac{\psi + \psi_0}{2}) \cdot \cos \psi + \cos \psi_0 \left\{\ln\left|\sin \frac{\psi + \psi_0}{2}\right|\right.\right.$$

$$\left.\left. + \frac{\cos (\psi + \psi_0)}{2}\right\} + \sin \psi_0 \left\{\frac{\psi + \psi_0}{2} + \frac{\sin (\psi + \psi_0)}{2}\right\}\right]$$

$$I_4 = \frac{2V}{\pi} \int \delta_F \ln\left|\sin \frac{\psi + \psi_0}{2}\right| \cdot \sin \psi \cos \psi\, d\psi$$

$$= \frac{V\delta_F}{\pi} \int \ln (\sin \frac{\psi + \psi_0}{2}) \cdot \sin 2\psi\, d\psi$$

Substituting $\frac{\psi}{2} = x$ and $\frac{\psi_o}{2} = a$, i.e., $\psi = 2x$ and $d\psi = 2dx$, we have,

$$I_4 = \frac{2V\delta_F}{\pi} \int \ln \{\sin (x + a)\} \cdot \sin 4x \, dx$$

Substituting $x + a = \xi$, i.e., $x = \xi - a$ and $dx = d\xi$, we have,

$$I_4 = \frac{2V\delta_F}{\pi} \int \ln (\sin \xi) \cdot \sin 4(\xi - a) \, d\xi$$

$$= \frac{2V\delta_F}{\pi} \left[- \ln(\sin \xi) \frac{\cos 4(\xi - a)}{4} + \int \frac{\cos \xi}{\sin \xi} \frac{\cos 4(\xi - a)}{4} d\xi \right]$$

$$= \frac{2V\delta_F}{\pi} \left[- \ln(\sin \xi) \frac{\cos 4(\xi - a)}{4} \right.$$

$$\left. + \int (\cos 4\xi \cos 4a + \sin 4\xi \sin 4a) \frac{\cos \xi}{4 \sin \xi} d\xi \right]$$

$$= \frac{2V\delta_F}{\pi} \left[-\ln(\sin \xi) \frac{\cos 4(\xi - a)}{4} \right.$$

$$+ \cos 4a \int (1 - 2 \sin^2 2\xi) \frac{\cos \xi}{4 \sin \xi} d\xi$$

$$\left. + 2 \sin 4a \int \sin 2\xi \cos 2\xi \frac{\cos \xi}{4 \sin \xi} d\xi \right]$$

$$= \frac{2V\delta_F}{\pi} \left[-\ln(\sin \xi) \frac{\cos 4(\xi - a)}{4} + \frac{\cos 4a}{4} \int \frac{\cos \xi}{\sin \xi} d\xi \right.$$

$$- \frac{\cos 4a}{2} \int \sin 2\xi \frac{2 \sin \xi \cos^2 \xi}{\sin \xi} d\xi$$

$$\left. + 2 \sin 4a \int \sin 2\xi (1 - 2 \sin^2 \xi) \frac{\cos \xi}{4 \sin \xi} d\xi \right]$$

Therefore,

$$I_4 = \frac{2V\delta_F}{\pi}\left[- \ln(\sin \xi) \frac{\cos 4 (\xi - a)}{4} + \frac{\cos 4a}{4} \int \cot \xi \, d\xi \right.$$

$$- \cos 4a \int \sin 2\xi \left(\frac{1 + \cos 2\xi}{2}\right) d\xi$$

$$+ 2 \sin 4a \int \frac{2 \sin \xi \cos^2 \xi}{4 \sin \xi} d\xi$$

$$\left. - 2 \sin 4a \int \sin 2\xi \frac{2 \sin^2 \xi \cos \xi}{4 \sin \xi} d\xi \right]$$

$$= \frac{2V\delta_F}{\pi}\left[-\ln(\sin \xi) \frac{\cos 4(\xi - a)}{4} + \frac{\cos 4a}{4} \ln | \sin \xi | \right.$$

$$+ \cos 4a \frac{\cos 2\xi}{4} - \cos 4a \int \frac{\sin 4\xi}{4} d\xi$$

$$\left. + \frac{2 \sin 4a}{4} \int (1 + \cos 2\xi) \, d\xi - \frac{\sin 4a}{4} \int (1 - \cos 4\xi) \, d\xi \right]$$

$$= \frac{2V\delta_F}{\pi}\left[-\ln(\sin \xi) \frac{\cos 4(\xi - a)}{4} + \frac{\cos 4a}{4} \ln | \sin \xi | \right.$$

$$+ \cos 4a \frac{\cos 2\xi}{4} + \cos 4a \frac{\cos 4\xi}{16}$$

$$\left. + \frac{\sin 4a}{2} \left(\xi + \frac{\sin 2\xi}{2}\right) - \frac{\sin 4a}{4} \left(\xi - \frac{\cos 4\xi}{4}\right) \right]$$

$$= \frac{2V\delta_F}{\pi}\left[-\ln \{\sin (x + a)\} \frac{\cos 4x}{4} + \frac{\cos 2\psi_o}{4} \ln | \sin (x + a) | \right.$$

$$+ \cos 2\psi_o \frac{\cos 2(x + a)}{4} + \cos 2\psi_o \frac{\cos 4(x + a)}{16}$$

$$+ \frac{\sin 2\psi_o}{2} \left\{x + a + \frac{\sin 2(x + a)}{2}\right\}$$

$$\left. - \frac{\sin 2\psi_o}{4} \left\{x + a - \frac{\cos 4(x + a)}{4}\right\} \right]$$

Therefore,

$$I_4 = \frac{2V\delta_F}{\pi}\left[-\ln\left(\sin\frac{\psi+\psi_0}{2}\right)\cdot\frac{\cos 2\psi}{4}\right.$$

$$+\frac{\cos 2\psi_0}{4}\ln\left|\sin\frac{\psi+\psi_0}{2}\right| + \cos 2\psi_0\,\frac{\cos(\psi+\psi_0)}{4}$$

$$+\cos 2\psi_0\,\frac{\cos 2(\psi+\psi_0)}{16} + \frac{\sin 2\psi_0}{2}\left\{\frac{\psi+\psi_0}{2} + \frac{\sin(\psi+\psi_0)}{2}\right\}$$

$$\left.-\frac{\sin 2\psi_0}{4}\left\{\frac{\psi+\psi_0}{2} - \frac{\cos 2(\psi+\psi_0)}{4}\right\}\right]$$

$$= \frac{V\delta_F}{2\pi}\left[(\cos 2\psi_0 - \cos 2\psi)\cdot\ln\left|\sin\frac{\psi+\psi_0}{2}\right|\right.$$

$$+\cos 2\psi_0\left\{\cos(\psi+\psi_0) + \frac{\cos 2(\psi+\psi_0)}{4}\right\}$$

$$\left.+\sin 2\psi_0\left\{\frac{\psi+\psi_0}{2} + \sin(\psi+\psi_0) + \frac{\cos 2(\psi+\psi_0)}{4}\right\}\right]$$

$$I_5 = \frac{2V}{\pi}\int\delta_F \ln\left|\sin\frac{\psi-\psi_0}{2}\right|\sin\psi\,d\psi$$

Substituting $\frac{\psi}{2} = x$ and $\frac{\psi_0}{2} = a$, i.e., $\psi = 2x$ and $d\psi = 2dx$, we have,

$$I_5 = \frac{4V\delta_F}{\pi}\int\ln\left|\sin(x-a)\right|\sin 2x\,dx$$

As maximum value of $x < a$,

hence, $I_5 = \frac{4V\delta_F}{\pi}\int\ln\{\sin(a-x)\}\sin 2x\,dx$

Substituting $a - x = \xi$, i.e., $x = a - \xi$ and $dx = -d\xi$, we have,

$$I_5 = -\frac{4V\delta_F}{\pi}\int\ln(\sin\xi)\sin 2(a-\xi)\,d\xi$$

Therefore,

$$I_5 = -\frac{4V\delta_F}{\pi}\left[\ln(\sin\xi)\cdot\frac{\cos 2(a-\xi)}{2} - \int\frac{\cos\xi}{\sin\xi}\cdot\frac{\cos 2(a-\xi)}{2}\,d\xi\right]$$

$$= \frac{2V\delta_F}{\pi}\left[\int\frac{\cos\xi}{\sin\xi}(\cos 2a\cos 2\xi + \sin 2a\sin 2\xi)\,d\xi\right.$$

$$\left. - \ln|\sin\xi|\cdot\cos 2(a-\xi)\right]$$

$$= \frac{2V\delta_F}{\pi}\left[\cos 2a\int\frac{\cos\xi}{\sin\xi}(1-2\sin^2\xi)\,d\xi\right.$$

$$\left. + \sin 2a\int\frac{\cos\xi}{\sin\xi}2\sin\xi\cos\xi\,d\xi - \ln|\sin\xi|\cos 2(a-\xi)\right]$$

$$= \frac{2V\delta_F}{\pi}\left[\cos 2a\{\int\cot\xi\,d\xi - \int\sin 2\xi\,d\xi\}\right.$$

$$\left. + \sin 2a\int(1+\cos 2\xi)\,d\xi - \ln|\sin\xi|\cdot\cos 2(a-\xi)\right]$$

$$= \frac{2V\delta_F}{\pi}\left[\cos 2a\left\{\ln|\sin\xi| + \frac{\cos 2\xi}{2}\right\} + \sin 2a\left\{\xi + \frac{\sin 2\xi}{2}\right\}\right.$$

$$\left. - \ln|\sin\xi|\cdot\cos 2(a-\xi)\right]$$

$$= \frac{2V\delta_F}{\pi}\left[\cos\psi_o\left\{\ln\left|\sin\frac{\psi_o-\psi}{2}\right| + \frac{1}{2}\cos(\psi_o-\psi)\right\}\right.$$

$$\left. + \frac{\sin\psi_o}{2}\{\psi_o - \psi + \sin(\psi_o-\psi)\} - \ln\left|\sin\frac{\psi_o-\psi}{2}\right|\cdot\cos\psi\right]$$

$$I_6 = \frac{2V}{\pi}\int\delta_F\ln\left|\sin\frac{\psi-\psi_o}{2}\right|\sin\psi\cos\psi\,d\psi$$

Substituting $\frac{\psi}{2} = x$ and $\frac{\psi_o}{2} = a$, i.e., $\psi = 2x$ and $dx = 2dx$, we have,

$$I_6 = \frac{4V\delta_F}{\pi}\int\ln|\sin(x-a)|\sin 2x\cos 2x\,dx$$

As maximum value of $x < a$,

hence, $I_6 = \frac{4V\delta_F}{\pi}\int\ln\{\sin(a-x)\}\sin 2x\cos 2x\,dx$

Substituting $a - x = \xi$, i.e., $x = a - \xi$ and $dx = - d\xi$, we have,

$$I_6 = - \frac{4V\delta_F}{\pi} \int \ln (\sin \xi) \cdot \sin 2(a - \xi) \cos 2(a - \xi)\, d\xi$$

$$= - \frac{2V\delta_F}{\pi} \int \ln (\sin \xi) \cdot \sin 4(a - \xi)\, d\xi$$

$$= - \frac{2V\delta_F}{\pi} \left[\ln(\sin \xi) \frac{\cos 4(a - \xi)}{4} - \int \frac{\cos \xi}{\sin \xi} \cdot \frac{\cos 4(a - \xi)}{4}\, d\xi \right]$$

$$= \frac{V\delta_F}{2\pi} \left[\int \frac{\cos \xi}{\sin \xi} (\cos 4a \cos 4\xi + \sin 4a \sin 4\xi)\, d\xi \right.$$

$$\left. - \ln (\sin \xi) \cos 4(a - \xi) \right]$$

$$= \frac{V\delta_F}{2\pi} \left[\cos 4a \int \frac{\cos \xi}{\sin \xi} (1 - 2 \sin^2 2\xi) d\xi \right.$$

$$\left. + \sin 4a \int \frac{\cos \xi}{\sin \xi} 2 \sin 2\xi \cos 2\xi\, d\xi - \ln (\sin \xi) \cos 4(a - \xi) \right]$$

$$= \frac{V\delta_F}{2\pi} \left[\cos 4a \int \frac{\cos \xi}{\sin \xi} d\xi \right.$$

$$- 2 \cos 4a \int \frac{\cos \xi}{\sin \xi} \sin 2\xi \cdot 2 \sin \xi \cos \xi\, d\xi$$

$$+ 2 \sin 4a \int \frac{\cos \xi}{\sin \xi} \sin 2\xi (1 - 2 \sin^2 \xi) d\xi$$

$$\left. - \ln (\sin \xi) \cos 4(a - \xi) \right]$$

$$= \frac{V\delta_F}{2\pi} \left[\cos 4a \ln |\sin \xi| - 2 \cos 4a \int \sin 2\xi (1 + \cos 2\xi)\, d\xi \right.$$

$$+ 2 \sin 4a \int \frac{\cos \xi}{\sin \xi} \cdot 2 \sin \xi \cos \xi\, d\xi$$

$$- 2 \sin 4a \int \frac{\sin 2\xi \cdot 2 \sin^2 \xi \cos \xi}{\sin \xi} d\xi$$

$$\left. - \ln (\sin \xi) \cdot \cos 4(a - \xi) \right]$$

Therefore,

$$I_6 = \frac{V\delta_F}{2\pi}\left[\cos 4a \ln|\sin\xi| + 2\cos 4a \frac{\cos 2\xi}{2}\right.$$

$$- \cos 4a \int \sin 4\xi \, d\xi + 2 \sin 4a \int (1 + \cos 2\xi) \, d\xi$$

$$\left. - 2 \sin 4a \int \sin^2 2\xi \, d\xi - \ln(\sin\xi) \cos 4(a - \xi)\right]$$

$$= \frac{V\delta_F}{2\pi}\left[\cos 4a \ln|\sin\xi| + \cos 4a \cos 2\xi + \cos 4a \frac{\cos 4\xi}{4}\right.$$

$$+ 2 \sin 4a \left\{\xi + \frac{\sin 2\xi}{2}\right\}$$

$$\left. + \sin 4a \int (\cos 4\xi - 1) \, d\xi - \ln(\sin\xi) \cdot \cos 4(a - \xi)\right]$$

$$= \frac{V\delta_F}{2\pi}\left[\cos 4a \ln|\sin\xi| + \cos 4a \cos 2\xi + \cos 4a \frac{\cos 4\xi}{4}\right.$$

$$+ 2 \sin 4a\left(\xi + \frac{\sin 2\xi}{2}\right) + \sin 4a \left(\frac{\sin 4\xi}{4} - \xi\right)$$

$$\left. - \ln(\sin\xi) \cdot \cos 4(a - \xi)\right]$$

$$= \frac{V\delta_F}{2\pi}\left[\cos 2\psi_o \left\{\ln\left|\sin\frac{\psi_o - \psi}{2}\right| + \cos(\psi_o - \psi) + \frac{\cos 2(\psi_o - \psi)}{4}\right\}\right.$$

$$+ \sin 2\psi_o \left\{\frac{\psi_o - \psi}{2} + \sin(\psi_o - \psi) + \frac{\sin 2(\psi_o - \psi)}{4}\right\}$$

$$\left. - \ln\left|\sin\frac{\psi_o - \psi}{2}\right| \cdot \cos 2\psi\right]$$

$$I_7 = \frac{2V}{\pi} \int \alpha \ln\left|\sin\frac{\psi + \pi}{2}\right| \sin\psi \, d\psi$$

Comparing with I_3, we can write,

$$I_7 = \frac{2V\alpha}{\pi}\left[(\cos\pi - \cos\psi) \cdot \ln\left|\sin\frac{\psi + \pi}{2}\right| + \cos\pi \cdot \frac{\cos(\psi + \pi)}{2}\right.$$

$$\left. + \sin\pi \left\{\frac{\psi + \pi}{2} + \frac{\sin(\psi + \pi)}{2}\right\}\right]$$

Therefore,

$$I_7 = -\frac{2V\alpha}{\pi}\left[(1 + \cos\psi) \cdot \ln\left|\sin\frac{\psi+\pi}{2}\right| + \frac{1}{2}\cos(\psi+\pi)\right]$$

$$I_8 = \frac{2V}{\pi}\int\alpha \ln\left|\sin\frac{\psi+\pi}{2}\right| \sin\psi\cos\psi\, d\psi$$

Comparing with I_4, we can write,

$$I_8 = \frac{V\alpha}{2\pi}\left[(\cos 2\pi - \cos 2\psi)\ln\left|\sin\frac{\pi+\psi}{2}\right|\right.$$

$$\left. + \cos 2\pi\left\{\cos(\psi+\pi) + \frac{\cos 2(\psi+\pi)}{4}\right\}\right]$$

$$= \frac{V\alpha}{2\pi}\left[(1 - \cos 2\psi)\ln\left|\sin\frac{\pi+\psi}{2}\right| + \cos(\pi+\psi) + \frac{\cos 2(\pi+\psi)}{4}\right]$$

$$I_9 = \frac{2V}{\pi}\int\alpha \ln\left|\sin\frac{\psi-\pi}{2}\right| \sin\psi\, d\psi$$

Comparing with I_5, we can write,

$$I_9 = \frac{2V\alpha}{\pi}\left[(\cos\pi - \cos\psi)\cdot\ln\left|\sin\frac{\pi-\psi}{2}\right| + \frac{\cos\pi}{2}\cos(\pi-\psi)\right.$$

$$\left. + \frac{\sin\pi}{2}\{\pi - \psi + \sin(\pi-\psi)\}\right]$$

$$= -\frac{2V\alpha}{\pi}\left[(1 + \cos\psi)\cdot\ln\left|\sin\frac{\pi-\psi}{2}\right| + \frac{1}{2}\cos(\pi-\psi)\right]$$

$$I_{10} = \frac{2V}{\pi}\int\alpha \ln\left|\sin\frac{\psi-\pi}{2}\right| \sin\psi\cos\psi\, d\psi$$

Comparing with I_6, we can write,

$$I_{10} = \frac{V\alpha}{2\pi}\left[(\cos 2\pi - \cos 2\psi)\ln\left|\sin\frac{\pi-\psi}{2}\right|\right.$$

$$+ \cos 2\pi\left\{\cos(\pi-\psi) + \frac{\cos 2(\pi-\psi)}{4}\right\}$$

$$\left. + \sin 2\pi\left\{\frac{\pi-\psi}{2} + \sin(\pi-\psi) + \frac{\sin 2(\pi-\psi)}{4}\right\}\right]$$

Therefore,

$$I_{10} = \frac{V\alpha}{2\pi}\left[(1 - \cos 2\psi)\cdot \ln\left|\sin\frac{\pi - \psi}{2}\right| + \cos(\pi - \psi) + \frac{\cos 2(\pi - \psi)}{4}\right]$$

Substituting and rearranging the terms, the given integral can be written as,

$$I = \frac{V}{\pi}(\delta_F\psi_0 + \alpha\pi)\left[(1 + 4p)\,\psi - \sin\psi\,(\cos\psi + 4p)\right]$$

$$+ \frac{V\delta_F}{\pi}\left[\{2\,(1 + 2p)(\cos\psi_0 - \cos\psi)\right.$$

$$\left. + \frac{1}{2}(\cos 2\psi_0 - \cos 2\psi)\right\}\cdot \ln\left|\frac{\sin\frac{\psi + \psi_0}{2}}{\sin\frac{\psi_0 - \psi}{2}}\right|$$

$$+ (1 + 2p)\sin\psi_0\,\{2\psi + \sin(\psi + \psi_0) - \sin(\psi_0 - \psi)\}$$

$$+ (1 + 2p)\cos\psi_0\,\{\cos(\psi + \psi_0) - \cos(\psi_0 - \psi)\}$$

$$+ \frac{\cos 2\psi_0}{2}\{\cos(\psi + \psi_0) - \cos(\psi_0 - \psi)$$

$$+ \frac{\cos 2(\psi + \psi_0) - \cos 2(\psi_0 - \psi)}{4}\}$$

$$+ \frac{\sin 2\psi_0}{2}\{\psi + \sin(\psi + \psi_0) - \sin(\psi_0 - \psi)$$

$$+ \frac{\cos 2(\psi + \psi_0) - \sin 2(\psi_0 - \psi)}{4}\}\Big]$$

Therefore,

$$\int_0^{\pi} \gamma(\psi)\,(1 + \cos\psi + 2p)\sin\psi\,d\psi$$

$$= V\,(\delta_F\psi_0 + \alpha\pi)(1 + 4p) + 2(1 + 2p)\cdot V\delta_F\cdot\sin\psi_0 + \frac{V\delta_F}{2}\sin 2\psi_0$$

$$= V\left[(\delta_F\psi_0 + \alpha\pi)(1 + 4p) + \delta_F\sin\psi_0\,2(1 + 2p) + \delta_F\sin\psi_0\cos\psi_0\right]$$

$$= V\left[(1 + 4p)(\delta_F\,\psi_0 + \alpha\pi) + \delta_F\sin\psi_0\,\{2(1 + 2p) + \cos\psi_0\}\right]$$

$$\int_0^{\psi_1} \gamma(\psi)(1 + \cos\psi + 2p)\sin\psi\, d\psi$$

$$= \frac{V}{\pi}(\delta_F\psi_0 + \alpha\pi)\left[(1 + 4p)\psi_1 - \sin\psi_1(\cos\psi_1 + 4p)\right]$$

$$+ \frac{V\delta_F}{\pi}\left[\{2(1 + 2p)(\cos\psi_0 - \cos\psi_1)\right.$$

$$\left. + \frac{1}{2}(\cos 2\psi_0 - \cos 2\psi_1)\right\} \cdot \ln\left|\frac{\sin\frac{\psi_0 + \psi_1}{2}}{\sin\frac{\psi_0 - \psi_1}{2}}\right|$$

$$+ (1 + 2p)\sin\psi_0\{2\psi_1 + \sin(\psi_0 + \psi_1) - \sin(\psi_0 - \psi_1)\}$$

$$+ (1 + 2p)\cos\psi_0\{\cos(\psi_0 + \psi_1) - \cos(\psi_0 - \psi_1)\}$$

$$+ \frac{\cos 2\psi_0}{2}\left\{\cos(\psi_0 + \psi_1) - \cos(\psi_0 - \psi_1)\right.$$

$$\left. + \frac{\cos 2(\psi_0 + \psi_1) - \cos 2(\psi_0 - \psi_1)}{4}\right\}$$

$$+ \frac{\sin 2\psi_0}{2}\left\{\psi_1 + \sin(\psi_0 + \psi_1) - \sin(\psi_0 - \psi_1)\right.$$

$$\left. + \frac{\cos 2(\psi_0 + \psi_1) - \sin 2(\psi_0 - \psi_1) - \cos 2\psi_0 + \sin 2\psi_0}{4}\right\}\Big]$$

$$= \frac{V}{\pi}(\delta_F\psi_0 + \alpha\pi)\left\{(\psi_1 - \sin\psi_1\cos\psi_1) + 4p(\psi_1 - \sin\psi_1)\right\}$$

$$+ \frac{V\delta_F}{\pi} \cdot \ln\left|\frac{\sin\frac{\psi_0 + \psi_1}{2}}{\sin\frac{\psi_0 - \psi_1}{2}}\right| \cdot \left\{2(1 + 2p)(\cos\psi_0 - \cos\psi_1)\right.$$

$$\left. + \frac{1}{2}(\cos 2\psi_0 - \cos 2\psi_1)\right\} + 2(1 + 2p)\frac{V\delta_F}{\pi}\psi_1\sin\psi_0$$

$$- \frac{V\delta_F}{2\pi}\left[\cos 2\psi_0(2\sin\psi_0\sin\psi_1 + \frac{1}{2}\sin 2\psi_1\sin 2\psi_0)\right.$$

$$- \sin 2\psi_0 \{\psi_1 + 2 \sin \psi_1 \cos \psi_0$$

$$+ \frac{1}{4} \cdot (\cos 2\psi_0 - \sin 2\psi_0)(\cos 2\psi_1 + \sin 2\psi_1 - 1)\}]$$

Substituting the above results in equation (3.11), we get,

$$M = - pV \frac{c'^2}{4} \cdot V [(1 + 4p)(\delta_F \psi_0 + \alpha\pi)$$

$$+ \delta_F \sin \psi_0 \{2(1 + 2p) + \cos \psi_0\}]$$

$$+ \rho V \frac{c'^2}{4} \cdot \frac{V}{\pi} [(\delta_F \psi_0 + \alpha\pi) \{(\psi_1 - \sin \psi_1 \cos \psi_1)$$

$$+ 4p (\psi_1 - \sin \psi_1)\}$$

$$+ \delta_F \cdot \ln \frac{\left| \sin \frac{\psi_1 + \psi_0}{2} \right|}{\left| \sin \frac{\psi_0 - \psi_1}{2} \right|} \cdot \{2(1 + 2p)(\cos \psi_0 - \cos \psi_1)$$

$$+ \frac{1}{2} (\cos 2\psi_0 - \cos 2\psi_1)\} + 2(1 + 2p) \delta_F \psi_1 \sin \psi_0$$

$$- \frac{\delta_F}{2} \{\cos 2\psi_0 (2 \sin \psi_0 \sin \psi_1 + \frac{1}{2} \sin 2\psi_1 \sin 2\psi_0)$$

$$- \sin 2\psi_0 (\psi_1 + 2 \sin \psi_1 \cos \psi_0$$

$$+ \frac{1}{4} \cdot \overline{\cos 2\psi_0 - \sin 2\psi_0} \cdot \overline{\cos 2\psi_1 + \sin 2\psi_1 - 1}) \}]$$

$$- \dot{M}_j V_j \sin (\delta_F + \delta_j) \frac{c'}{2} (1 + \cos \psi_1 + 2p)$$

APPENDIX IV

EVALUATION OF THE INTEGRALS IN EQUATION (4.19)

The velocity profile given by equation (4.10) is:

$$\frac{u_1 - u}{u_1 - u_2} = f(\eta) = (1 - \eta^{3/2})^2, \quad \eta = \frac{y - y_2}{b}$$

Considering the boundary conditions

$$f(\eta_1) = 0 \text{ for } \eta_1 = 1$$

$$f(\eta_2) = 1 \text{ for } \eta_2 = 0$$

we obtain,

$$\int_0^1 f \, d\eta = 0.45 \qquad \int_0^1 f^2 \, d\eta = 0.316$$

$$\int_0^1 (1 - f) \, d\eta = 0.55 \qquad \int_0^1 (1 - f)^2 \, d\eta = 0.416$$

Equation (4.10) can also be written as,

$$\frac{u}{u_1} = 1 - (1 - m)f \quad \text{where } m = \frac{u_2}{u_1}$$

Hence, $\int_0^1 \left(\frac{u}{u_1}\right)^2 d\eta = \int_0^1 [1 - (1 - m)f]^2 \, d\eta$

$$= \int_0^1 d\eta - 2(1 - m) \int_0^1 f \, d\eta + (1 - m)^2 \int_0^1 f^2 d\eta$$

$$= 1 - 2(1 - m) \cdot 0.45 + (1 - m)^2 \cdot 0.316$$

$$= 0.416 + 0.268\, m + 0.316\, m^2$$

$$\text{Also, } \int_0^1 \frac{u}{u_1}\, dn = \int_0^1 [1 - (1 - m)f]\, dn$$

$$= \int_0^1 dn - (1 - m) \int_0^1 f\, dn$$

$$= 1 - (1 - m) \cdot 0.45$$

$$= 0.55 + 0.45\, m$$

VITA

Atin Kumar Sinha was born in Calcutta, India on September 10, 1948. He received his high school education at St. Paul's School, Calcutta, from which he graduated in 1965. Afterwards he attended Jadavpur University, Calcutta, from where he obtained the degree of Bachelor of Mechanical Engineering with First Class (Honors) in 1970. After serving at a couple of companies for some time, he entered The Indian Institute of Science, Bangalore and graduated with the degree of Master of Engineering in Aeronautical Engineering in the summer of 1973. After working for a few months at The Indian Space Research Organization, Trivandrum as Engineer, in November 1973 he joined the Aerodynamics Division of The National Aeronautical Laboratory, Bangalore, as Scientist. At NAL, he worked in the field of Computer Aided Aircraft Design for configuration optimization against design requirements. In September 1979, he entered The University of Tennessee Space Institute for his doctoral studies. He received the Doctor of Philosophy degree in Aerospace Engineering in June 1984.

He is a Student Member of American Institute of Aeronautics and Astronautics and an Associate Member of Sigma Xi Research Society.

He is married to the former Shukla Ghosh of Calcutta.